NASA Contractor Report 187070

In-Space Experiment on Thermoacoustic Convection Heat Transfer Phenomenon-Experiment Definition

IN-34

M. Parang and D.S. Crocker
The University of Tennessee
Knoxville, Tennessee

February 1991

Prepared for
Lewis Research Center
Under Contract NAS3-25359

National Aeronautics and
Space Administration

ACKNOWLEDGEMENT

The authors are grateful for the financial support of the National Aeronautics and Space Administration under contract No. NAS3-25359 and the administration of the contract by the Lewis Research Center, Cleveland, Ohio, which made this work possible. The authors also wish to express their appreciation for the valuable comments and help of Dr. An-Ti Chai from the NASA-Lewis Research Center who served as the Contract Technical Director.

ABSTRACT

The definition phase of an in-space experiment in thermoacoustic convection (TAC) heat transfer phenomenon is completed and the results are presented and discussed in some detail in this report. Background information, application and potential importance of TAC in heat transfer processes are discussed with particular focus on application in cryogenic fluid handling and storage in microgravity space environment. This report also includes discussion on TAC space experiment objectives, results of ground support experiments, hardware information, and technical specifications and drawings. The future plans and a schedule for the development of experiment hardware (Phase B) and flight tests and post-flight analysis (Phase C/D) are also presented in the report.

The specific experimental objectives are rapid heating of a compressible fluid and the measurement of fluid temperature and pressure and the recording and analysis of the experimental data for the establishment of the importance of TAC heat transfer process. The ground experiments that were completed in support of the experiment definition included fluid temperature measurement by a modified shadowgraph method, surface temperature measurement by thermocouples, and fluid pressure measurements by strain-gage pressure transducers. These experiments verified the feasibility of the TAC in-space experiment, established the relevance and accuracy of the experimental results, and specified the nature of the analysis which will be carried out in the post-flight phase of the project.

TABLE OF CONTENTS

I. INTRODUCTION

The present report includes a comprehensive summary of the design of a space experiment. The goal of the experiment is to develop a sufficiently large experimental data base to permit investigation and evaluation of the effects of thermoacoustic, or thermoconvective, waves and to determine their importance in heat transfer processes in a microgravity environment.

The report is divided into several sections. In this chapter an introductory description of the phenomenon, the need and justification for the experimentation in space, and a discussion of previous analytical and experimental works are presented. In the second chapter the scope and limitations of the space experiment are discussed, and within that context the objectives of the experiment are elaborated. Chapter III includes the technical description of the flight hardware with appropriate functional drawings of the payload. A detailed discussion of the ground experiments which were carried out in support of the experiment design are included in Chapter IV. The numerical computation and the computer programs for data analysis and manipulation, which were developed and used in these experiments, are also discussed and described in that chapter. Finally, a tentative outline for flight hardware development is presented in Chapter V, and concluding remarks and a summary are found in Chapter VI.

A. Physics of the Thermoconvective Wave Phenomenon

The physical process of interest, and the focus of investigation in the space experiment, is the response of a compressible fluid that is subjected to a large heat flux at a boundary. As the fluid layer adjacent to the boundary is heated, the fluid experiences a volume expansion that results in local fluid pressure change. The ensuing pressure waves travel through the fluid medium and may introduce an added convective feature into an otherwise quiescent fluid. These pressure waves, which are of thermal origin, may be termed thermoacoustic or thermoconvective waves. The resulting induced fluid motion is of fundamental interest, especially in a microgravity environment where other thermally-induced motions (e.g., natural convection) are often absent or have negligible relative importance.

B. Justification and Potential for the Experimentation in Space

The role and importance of thermoacoustic convection (TAC) heat transfer in a microgravity environment remains unclear principally due to the paucity of experimental information. TAC heat transfer occurs in various processes and may produce effects which modify or alter the expected performance of a system in important ways. In general, this heat transfer process has several unique characteristics which are common to all technological processes which involve TAC. For Example:

(a) TAC requires a large imposed temperature gradient, and
(b) TAC is a transient heat transfer process and usually its effects dissipate with the disappearance of large driving temperature gradients, and
(c) TAC effects are significant only in compressible media and usually involve fluid motion including periodic motions.

These features occur in a variety of technological processes involving transient heat transfer. In a gravity environment TAC heat transfer is often in competition with the natural convection heat transfer mode. The latter is a gravity-induced heat transfer process which may involve substantial mass transfer and fluid motion. In a large number of technological applications in normal gravity environment, the natural convection heat transfer process is the dominant and controlling mode of heat transfer. It is also a much faster and more efficient process when compared with a molecular heat transfer process such as conduction.

TAC effects in a gravity environment have been observed in several applications. A sample of examples reported in the literature will be briefly discussed below. However, it is in the microgravity environment, and in the absence of natural convection, that TAC may acquire significance. This is primarily due to the fact that the only remaining mode of heat transfer is the slow molecular conduction heat transfer process. It is then possible for TAC to have significant heat transfer effects in various space processes while remaining insignificant in the same process in a gravity environment.

The number of space applications in which TAC may play a role is very large. A partial list includes:

(1) Spacecraft fluid handling and storage system: These include various cryogenic fluid transport processes that may involve large TAC

effects. For example, cool-down of transfer lines, pressurizing of liquid oxygen storage vessels to force the liquid through transfer lines, and filling storage vessels using siphons. These applications involve large temperature differences and high heat flux at the system boundary. For this reason this group of applications is used as the principal choice for the discussion and selection of design parameters in the space experiment.

(2) The stability of combustion systems: These applications involve TAC that is generated through large heat addition within the fluid body as opposed to heat addition at the boundary of the system, e.g., rocket combustion chambers.

(3) Space manufacturing processes: TAC heat transfer process may prove to be a useful mechanism of thermal control in transient heating of compressible fluids in space manufacturing processes. In such application the temperature and heat flux may be relatively smaller, and the importance of TAC in these processes remains unclear.

The study of TAC heat transfer phenomena in a gravity environment is made difficult by the interference of natural convection heat transfer and buoyancy-induced mass transfer. While some aspects of the flow can be qualitatively studied with the heat flux vector parallel to the gravity vector, the presence of the gravitational field may still mask important TAC-induced motion. For example, in heating a fluid from above the stabilizing role of gravity may dampen important features of TAC-induced motion.

The ground-based, zero-gravity experiments are also inadequate to provide a clear picture of TAC heat transfer phenomena. There are two time scales associated with the thermoconvective pressure waves. One is a fast time scale and is characterized by the characteristic length divided by the sound speed. A second time scale is associated with the motion induced by the expansion of the fluid. The latter motion is of the same order of magnitude as natural convection in enclosures and involves a relatively slower time scale. In the ground experiments with air that were carried out and will be discussed in conjunction with the design of the experiment, this motion involved average velocities and time scales that were found to be of the order of 1 in/min and 10 min, respectively. Therefore, to understand this aspect of the flow and compare with conduction heat transfer requires experimental times of the order of

conduction time, i.e., tens of minutes or more. This length of time is longer than the available time for earth-bound microgravity experiments.

For these reasons collection of experimental data on TAC effects in microgravity will require the design and fabrication of an in-space experiment. Here an apparatus capable of producing and measuring TAC heat transfer effects needs to be designed to take advantage of relatively longer experimental time available in microgravity space environment.

It is anticipated that the data obtained from the space experiment will help determine the importance of the TAC heat transfer characteristics. This will help provide design guidelines for space technologies where significant thermoconvective wave phenomena are expected. These may include cryogenic fuel storage and transport as well as space manufacturing processes that may require significant rates of heating of compressible fluids with negligible forced or natural convection effects present. The information on flow and temperature field obtained in these experiments also helps to improve thermal control and prediction of flow processes in which thermoconvective effects may be small relative to forced convection flows but yet may play an important role in near critical conditions.

As stated earlier and in order to focus on a set of requirements for the space experiment, the first group of applications discussed above was chosen as a basis for the selection of the range of design parameters. This selection was made mainly for two reasons. The first one is the importance of cryogenic fluid transport and storage in space operations and their use as fuel and coolants. The second reason is the large range of temperature and heat flux in this group of applications which may include, as a subset, temperature and heat flux ranges encountered in other applications.

Therefore, for the purpose of the experiment design, typical magnitudes of the temperature change can be considered by selecting the normal boiling point or critical temperature of the cryogen as the temperature of the cold source. The temperature of the hot source could vary widely and depends on application. For the purpose of estimating the overall temperature differential imposed on the system, the choice of an ambient condition (70°F) for the hot source seems reasonable. Selected temperatures of typical cryogenic fluids are presented in Table 1. The

TABLE 1

Selected Characteristic Properties of Cryogenic Fluids

	Normal Boiling Point at 1 atm, ^{o}F	Critical Temp, ^{o}F (Critical Pressure, Psia)	ΔT ^{o}F (Boiling Point relative to 70 ^{o}F)	$\frac{\Delta T}{T}$
Oxygen	-297.3	-181.8 (730)	367.3	2.26
Fluorine	-306..2	---- (808)	376.2	2.47
Nitrogen	-320.0	-232.8 (492)	390.0	2.79
Hydrogen	-423.0	-399.8 (188)	493.0	13.32
Helium	-452.1	-450.2 (33.2)	522.1	66.1

last column of the table represents the difference between the ambient condition of 70°F with that of the normal boiling point of the fluid. These temperature changes were used as a guide in the design of the heated wall in the test section.

Interrelationship of Flight Experiment with OAST, Industry and Universities

The proposed flight experiment is in consonance with the general goal of the NASA technology program to expand cooperation and assistance between NASA and the aerospace engineering community in developing and implementing in-space technology experiments. In particular, the proposed experiment satisfies the original goal of building a greater cooperation between NASA, universities, and aerospace industries. The proposed in-space experiment design was completed at the University of Tennessee, Knoxville, in cooperation with NASA and as part of the program to make greater use of space facilities for in-space research, technology, and engineering experiments. Furthermore, it is planned to propose the present experiment conceptual design for the development phase (Phase B) in cooperation with industry. Preliminary steps in this direction have already been completed, and it is anticipated that the proposed Phase B will be a joint industry-university cooperative proposal to NASA.

C. Previous Observations and Investigations of the TAC Phenomenon

Selected Ground Observations of TAC Heat Transfer:

Thermoacoustic convection heat transfer effects have been observed and reported in various situations involving cryogenic systems in a gravity environment. Large and intense oscillations were, for example, observed in transporting liquid helium by transfer siphons in a filling process [1]. It was found that the temperature distribution along the length of the oscillating device (tube) is the key parameter in the oscillation intensity. In these experiments, the temperature of the cold end of the siphon was reported to be at the boiling point of helium in the vented storage vessel and the hot end was at the room temperature.

It was noted that the oscillations occur in an annular space filled with helium vapor surrounding the inner siphon flow tube and they became

pronounced when the siphon tip was immersed in the helium liquid. Inversely, the oscillations diminished as the cold end was removed from the liquid and its temperature reached a minimum of 30 °K.

The typical frequency of oscillations was observed to depend on the position of the cold end and ranged between 60 Hz (farthest away from the liquid) and approximately 20 Hz several inches under the liquid surface. Furthermore, these oscillations were usually not audible and required sensitive microphones for detection. However, it was observed that the oscillations produce a positive over-pressure effect which warrants caution in gas or vapor pressure thermometer measurements.

Another area in which TAC may play a role is the transient behavior of the ullage pressure in cryogenic propellent tanks. The pressurization of propellent storage tanks generally involves large temperature changes and fluid oscillations. The temperature change imposed on the cryogenic vapor in these operations may be as large as that between the room temperature and boiling point of the cryogen. [2,3]

Boil-off and heat leak in storage tanks may also involve thermally-driven convection pressure waves. The cryogen vapor bubbles produced by uneven heating at the vessel surface may remain near the surface under microgravity conditions and serve as a compressible medium for TAC heat transfer. The heat fluxes through these "hot spots", which are larger than conduction heat fluxes at corresponding conditions, will alter the vessel pressure. The prediction of this pressure is often critical for vessel design and pressure control that is exercised through various means such as mixing.

In related heat transfer experiments [4] it was observed that sound levels between 70 db and 95 db generated by the flow can alter both the dynamic and thermal characteristics of the flow significantly but in a manner not obvious to the experimenter. The ratio of the induced velocity due to the sound field to that of the free stream velocity need not be large to produce important changes in the flow and were, in fact, limited to a range between 0.0001 and 0.002 in those experiments.

Another area in which significant thermally-induced flow oscillations may be observed is in superconducting power transmission lines. These lines are typically cooled by helium over the temperature range of 6 to

10 °K and at a pressure of 15 bars. [5] Localized high heat flux rates may prove sufficient to alter the conditions resulting in a non-superconducting configuration which would then result in a great deal of heat generation in the power line leading to the rupture of coolant lines.

Microgravity TAC Experiments

There is very limited experimental information on TAC heat transfer processes under microgravity conditions. The available information is limited to experiments that were carried out in drop tower facilities or KC-135 flights, which often severely limited experiment time and quality of experimental data.

Several experiments [6, 7, 8] were performed using the NASA-Lewis Drop Tower Facility in which air was used as the compressible medium. Air at atmospheric pressure was enclosed in a cylindrical geometry and was heated rapidly during the approximately two-second flight time. The air temperature during flight was measured along the axis of the cylinder using thermocouples. The unsteady spatial distribution of temperature was corrected for radiation-induced error and compared with numerically-calculated temperature history for conduction-only heat transfer through air. The results indicate that a significantly larger region of fluid is affected by the heating process in comparison with heating by pure conduction. However, the numerical results of several investigators had indicated much larger heat penetration depth than shown by the fluid temperature results obtained in these experiments.

The heated boundary in these experiments was a thin steel sheet which was heated electrically using dry cell batteries. The temperature of the surface could be raised to approximately 1400 °F in 2 seconds. This provided an overall temperature change of approximately 1300 °F. The choice of air as the experimental fluid seemed to work fairly well in providing a TAC medium.

The microgravity experiments reported in references 6, 7, and 8 were limited in several aspects. First, the only fluid property that could be measured was temperature. As a result no information on pressure or direct measurement of the heat flux at the boundary could be obtained. Also no flow visualization was attempted. The most important limitation of these experiments was the short experimental time. While the

pressure waves generated by the TAC are acoustic in nature and require short time scales (determined by the sound speed and the characteristic length of the enclosure), the time scale for the bulk fluid motion is similar in magnitude to the fluid motion observed in natural convection-dominated flow. Another limitation of these experiments was the use of thermocouples for temperature measurement. The major difficulty in the use of thermocouples is the measurement error associated with radiation absorption by thermocouples. The radiation shielding of the thermocouples interferes substantially with fluid temperature measurement and is not effective in reducing this error. Despite the limitations of the drop tower experiments, they provide useful guidelines for selecting the range of parameters appropriate for space experiments.

In another experimental study that was flown on a NASA KC 135 aircraft, a narrow strip of titanium was heated by an electrical pulse in a test cell containing Refrigerant-13[9]. The surface boundary temperature was measured electrically, and the temperature profiles of the fluid layers adjacent to the boundary were determined by measuring fluid refractive index using diffuse-light holography. The results were compared and discussed with the results of a one-dimensional, inviscid, numerical flow model. The experimentally-determined fluid temperature profiles at various times after the start of an electrical pulse were reported to be consistently lower than those predicted by a computer model at the corresponding times.

II. THE SCOPE AND SPECIFIC OBJECTIVES OF THE IN-SPACE EXPERIMENT

There are several experimental criteria that need to be considered in the design of the in-space experiment. These criteria help define the limitations and the scope of the flight experiment:

(a) The in-space experiment should provide sufficiently large and significant TAC effects for experimental detection and evaluation in spite of the constraints imposed on the space experiment, and
(b) The experiment design should obviously be compatible with the payload carrier requirements, and
(c) The design should be as simple as possible to reduce cost and technical risk.

Objectives of the In-Space Experiment:

There are several objectives in the design of the TAC flight experiment. These include sufficient heating of the compressible fluid and direct measurement of several fluid properties. These specific objectives have guided the design of the experiment that is proposed in the next chapter. These objectives include:

1. The experiment design shall provide a rapid and large temperature change between the enclosure boundary and the enclosed fluid. The selection of the magnitude of the imposed temperature is guided by the characteristic temperature change observed in cryogenic fluid transport and handling applications in space environment.
2. The design shall provide for measurement of transient fluid temperature. This objective is satisfied by incorporating a modified shadowgraph (Schmidt-schlieren) system[10] which measures fluid index of refraction gradient adjacent to the heated surface.
3. The design shall incorporate provisions for measurement of the heated surface temperature. This goal is achieved by direct instrumentation of the surface boundary using thermocouples. The output is measured and recorded in real time by a data logger.
4. The instrumentation shall include the means for measurement of transient fluid pressure. The pressure in the enclosed fluid is measured directly by a pressure transducer and the output is recorded similarly to the measured surface temperature.
5. The design provisions include video recording of the transient optical display. The change of the index of refraction is displayed on

a screen using the designed optical system. The display is recorded by a video recorder system that is incorporated into the experiment design. The recording is used in post-flight processing to determine the transient temperature profile near the heated surface. This information is also used to compute heat flux near the surface and compare that flux with data from ground experiments.

III. THE BASELINE FLIGHT EXPERIMENT DESIGN

A. Overview

The main objective of the In-Space Experiment is to measure the transient temperature of air versus distance from a rapidly heated wall. Knowledge of the temperature profile will allow an assessment of the relative importance of TAC, conduction and convection by bulk motion of the expanding gas. An isometric view of the experiment layout is shown in Figure III.1. Detailed descriptions of the flight hardware and the optical system layout are given in Appendices A and B.

The transient temperature profile of the air will be determined by measuring the deflection of a laser beam caused by refraction in the heated air. The transient deflection of the laser beam is to be recorded with a video camera. In the limited space available for the experiment, the deflection would be too small for accurate measurements, so the deflection is amplified by a series of right angle prisms.

The temperature of the walls of the test section, especially the heated wall, will be measured with thermocouples. The pressure in the sealed test section, which provides an indication of the total energy transfer from the heated wall to the air, will be measured with a pressure transducer. The wall temperature and fluid pressure measurements are recorded by the Data Logger and stored in the Data Storage Module.

B. Heated Cavity

The heated cavity apparatus will provide a surface that is capable of quickly reaching high temperatures and a test section in which one-dimensional heat transfer and fluid flow can be assumed. A schematic of the heated cavity apparatus is shown in Figures III.2 and III.3 (detailed drawings are in Appendix A). The heated cavity apparatus includes a heater element (heated wall) that consists of 0.001 inch thick stainless steel foil. Two copper busbars are clamped to the heater element on each end. One of the copper busbars is free to slide on a spring assembly which

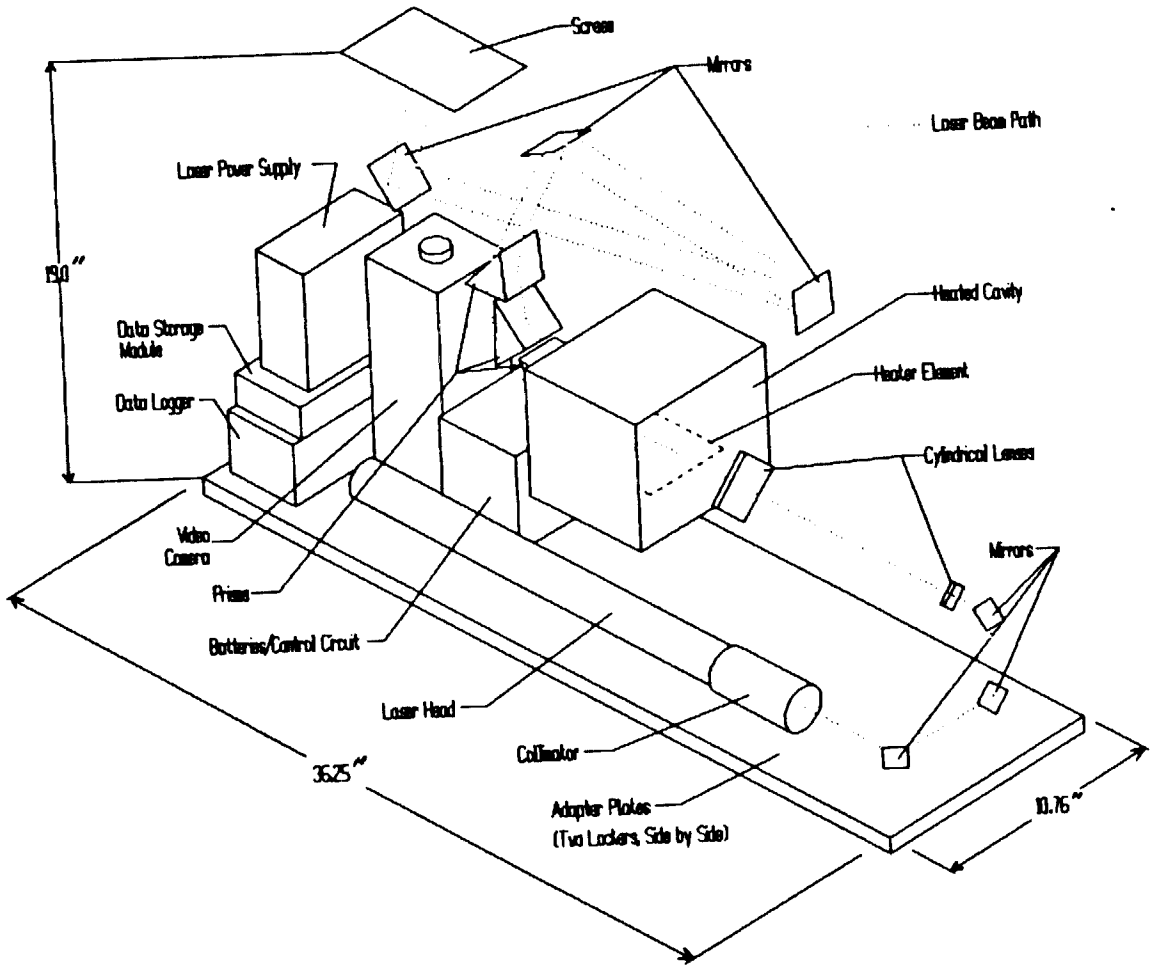

Figure III.1 - Isometric View of Flight Experiment Hardware Layout

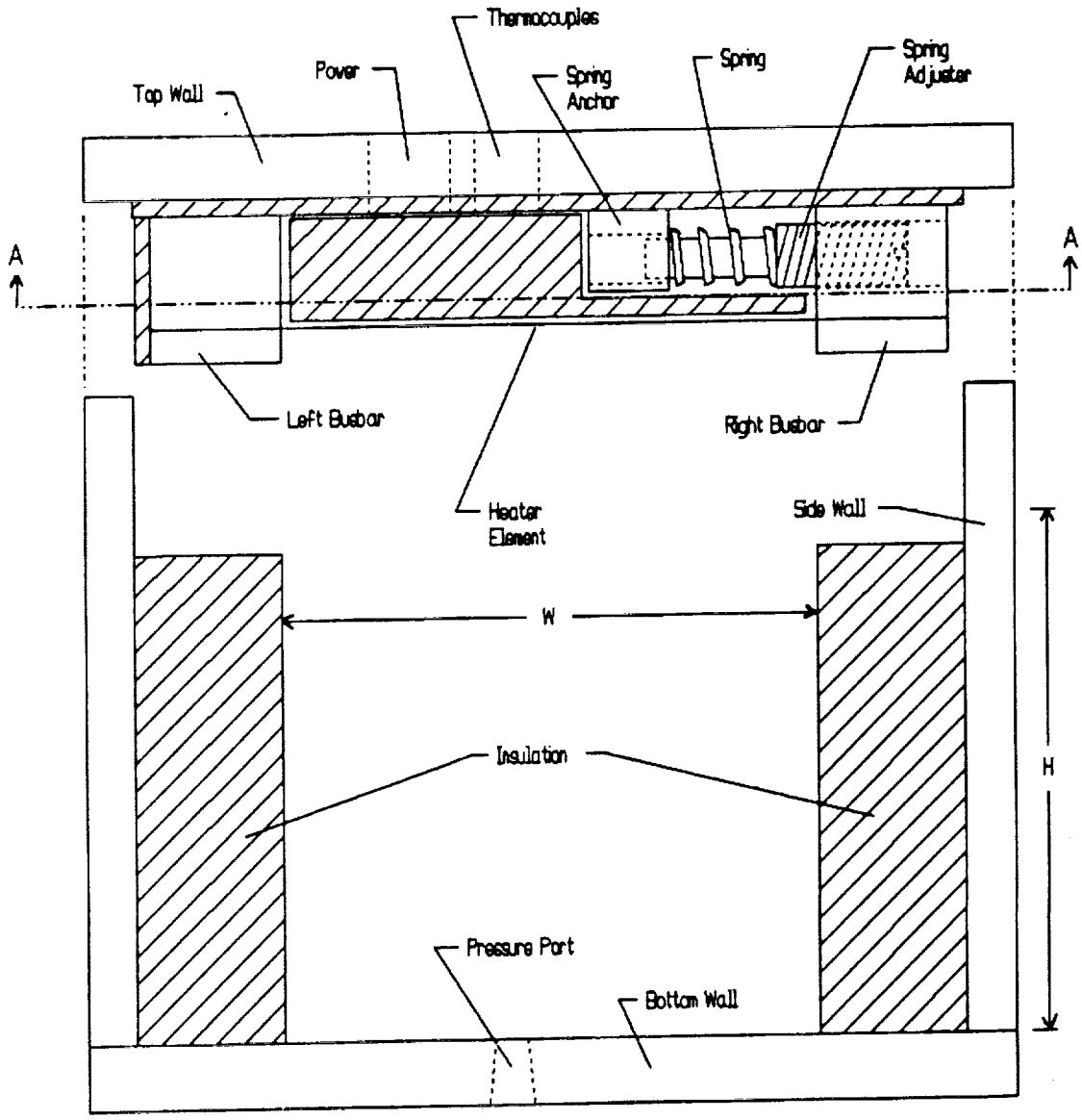

Figure III.2- Schematic of Heated Cavity Apparatus

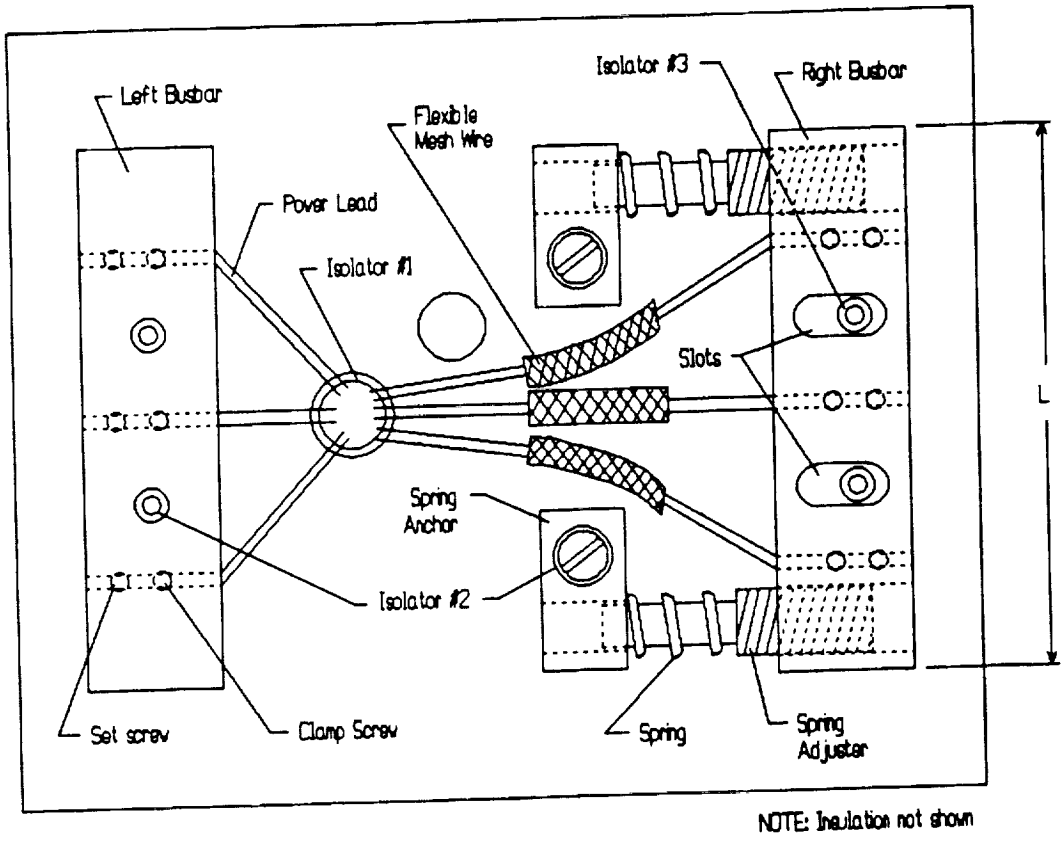

Figure III.3- Schematic of Heated Cavity Apparatus, Section A-A

pushes on the sliding busbar so that tension is maintained in the heater element. This is necessary to prevent deformation of the heater element caused by thermal expansion.

The dimensions of the baseline heated cavity volume (test section) adjacent to the heated wall are selected to be 4x4x4 inches. The top, bottom and two side walls are aluminum. The other two side walls are glass to provide parallel transparent surfaces for optical temperature measurement. The heater system is mounted to the top wall. The cavity provides a sealed environment to provide accurate pressure measurement.

The size of the test section is a critical variable in the experiment design. The test section volume is LWH where L is the laser path length, W is the distance between the busbars and H is the distance from the heated wall to the cold wall, as shown in Figures III.2 and III.3. The choice of the test section size should be based on the following considerations:

a) Power Dissipation -- the power dissipation of the heater element can be expressed as

$$\text{Power} = \frac{V^2 L t}{k W}$$

where V is the voltage drop across the heater element, t is the thickness of the heater element and k is the electrical resistance of the heater element material.

b) Heat Generation Rate in the Heater Element --

$$q''' = \frac{\text{Power}}{L W t}$$

and since $Power = VI = (V^2 Lt)/(kW)$, we have

$$q''' = \frac{V^2}{kW^2}$$

c) One-Dimensional Approximation -- Larger L and W clearly improves the one-dimensional approximation and $L = W$ maintains symmetry. The layout of the baseline design limits

W to about 5 inches.

d) Laser Deflection -- Laser deflection is proportional to L.

e) Space and Weight -- Smaller dimensions are obviously advantageous. H is flexible since it does not affect the above considerations.

f) Ease of Construction -- There may be difficulty if the test section is too small. A reasonable lower limit for the size of the test section is probably $L=W=2$ inches.

Another critical design element of the heated cavity apparatus is the heater element. An alternative to the stainless steel foil design is a very thin, vacuum-deposited layer of conductive material on an insulator[11]. This has the potential advantage of maintaining a very flat surface throughout heating, but reliability may be reduced because of the possibility of bubbling or peeling of the conductive layer.

C. Fluid Medium

The choice of fluid medium depends on the following:

a) Compressibility -- high compressibility is required to emphasize the effects of TAC.
b) Index of Refraction -- a high index of refraction is required to maximize the deflection of the laser beam (see following sections).
c) Ease of Handling -- the fluid must not be flammable, toxic or corrosive. Air is clearly the choice since leakage would not be a concern.
d) Near-Critical Condition -- Compressibility effects are greater near the critical point. Important space fluid heat transfer problems involve cryogenic fluids near the critical point.
e) Thermal Diffusivity -- A high thermal diffusivity results in a higher heat transfer rate which minimizes the required experiment run time and the power requirements.

Air is the logical choice to satisfy (a) and (c). The use of cryogenic fluids

will satisfy (d), however, their use would introduce complications (e.g. handling) that are difficult to control or resolve in this experiment. Table 2 shows the refractive properties and thermal diffusivity of several gases. CO_2 is slightly better than air for refraction, but has thermal diffusivity less than half that of air. Helium has a very high thermal diffusivity, but it has very low refractive ability. Since there is no clear winner considering refractive and thermal properties, air is chosen for the baseline design because of its clear superiority in satisfing (c).

D. Optical Temperature Measurement Method

1. Justification of Optical Temperature Measurement

An optical temperature measurement method is selected in this experiment for the measurement of fluid temperature. This method is preferred over temperature measurement by thermocouples. Issues concerning this selection include:

a) Radiation Error -- Thermocouples with a view of the heated wall will absorb a significant amount of radiative energy. Previous experimental work[12] has shown that thermocouples may be heated by radiation to such an extent that they may achieve a higher temperature than the surrounding air. Therefore large errors may be introduced in the measurement of fluid temperature. Thermocouples could be shielded from incoming radiation. This, however, would severely interfere with the induced flow convection. Also, shielding would alter the thermal features of the flow around the thermocouples.

b) Time Response -- The time response of even very small thermocouples (0.0005 inch bead) in the relative low velocity air flow may introduce large errors in the acoustic time scales of the experiment. Also, very small thermocouples are generally difficult to install and handle in a fluid environment. The time response of optical methods is essentially instantaneous when compared with the convective time scales of the experiment.

c) Interference -- thermocouples and thermocouple wiring are, of course, intrusive.

d) Simplicity -- Thermocouples are easier to use except for possible difficulties with mounting very small thermocouples.

Table 2. Refractive and Thermal Properties of Gases

Gas	$\frac{(n_o - 1)}{\rho_o R}$ $\frac{(R - ft^3)}{Btu}$	Thermal Diffusivity $\frac{ft^2}{hr}$
Air	0.060	1.28
CO_2	0.078	0.59
Helium	0.0074	12.09
Argon	0.058	1.44

e) Cost -- Thermocouples are less expensive.

2. The Laser Sheet

The light beam used in the optical system is a wide laser beam, or sheet, which approaches the test section at a pre-set angle. The other components of the optical system include an expander/collimator lens assembly and a screen for displaying the laser sheet deflections. The relationship of the laser deflection and the air temperature are discussed below.

Orientation of Laser Sheet - The laser sheet is slanted at an angle θ and passes through the test section as shown in Figure III.4. (Detailed drawings of the entire optical system are shown in Appendix A.) With this incident angle and orientation, the beam deflection can be measured at any distance from the heated wall. Assuming that the temperature gradients parallel to the heated wall are zero, the deflection of the beam will be away from and perpendicular to the heated wall.

The angle, θ, of the laser sheet, measured from a perpendicular to the heated wall, must be chosen based on the following considerations:

a) The resolution of distance from heated wall is proportional to $\tan\theta$. (If $\theta = 0$, it would not be possible to determine the amount of deflection at a given distance from the wall at all.)
b) The maximum range of distance from the heated wall that can be measured is $w(\cos\theta)$, where w is the expanded width of the laser sheet.
c) Minimizing three dimensional (wall) effects requires the laser to be at a distance of $w(\sin\theta)/2$ from the centerline or at $(w - w\sin\theta)/2$ from the side walls (W is defined in Figures III.2 and III.4).

Clearly, (a) improves with larger θ and (b) and (c) improve with smaller θ. The actual size of θ must be determined by balancing the above considerations with regard to the size of the test section and the width, w, of the laser sheet. For a 4x4 inch test section and w=2.0 inches, an

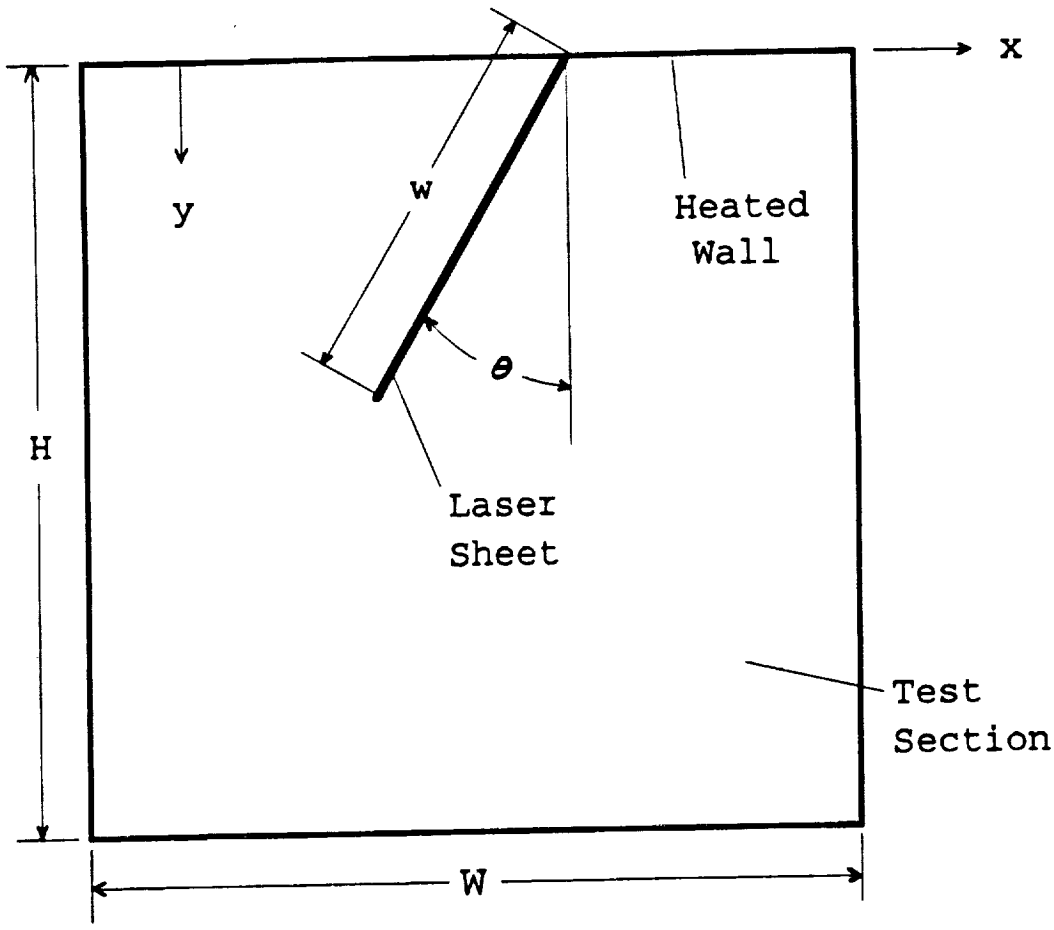

Figure III.4- Laser Sheet Orientation in Test Section

angle of $\theta=30^\circ$ is selected.

Generation of Laser Sheet - The laser sheet is produced as shown in Figure III.5. The He-Ne laser produces a 632.8 nm wavelength (red) beam with a 0.68 mm diameter and a divergence of 1.2 mrad. The laser must have sufficient power to provide a bright image on the screen after expansion and losses from reflections at numerous glass-air interfaces. A 10 mW laser is found to provide adequate brightness.

The beam expander/collimator provides a well-collimated beam at a slightly larger diameter of 3.4 mm. The larger diameter provides for less beam divergence since diffraction effects (which limit the minimum beam divergence) decrease with increasing beam diameter.

The collimated, circular beam passes through a negative (concave) cylindrical lens with a focal length of -19 mm. This lens causes the beam to diverge in one direction only so that an expanding laser sheet is created. This expanding sheet then passes through a positive (convex) cylindrical lens with a focal length of 300 mm. This lens is placed so that its focal point is at the same location as the focal point of the negative cylindrical lens. The result is a parallel sheet with width

$$w = d\left|\frac{f_{c2}}{f_{c1}}\right|$$

where d, is the diameter before the cylindrical lenses and f_{c1} and f_{c2} are the focal lengths of the first and second lenses, respectively. The thickness t of the sheet is simply $t=d$. The selected values of w and t for the baseline design are w=53.7 mm and t=3.4 mm, respectively. Both of the cylindrical lenses are tilted at the angle θ to produce the laser sheet oriented as shown in Figure III.4.

3. The Relationship between Laser Deflection and Temperature

If measuring the deflection of the laser sheet is to be useful, its relationship to the temperature of the air must be known. The deflection of the beam is the result of refraction, so it is the index of refraction (or its derivative) that is actually measured. For a homogeneous transparent

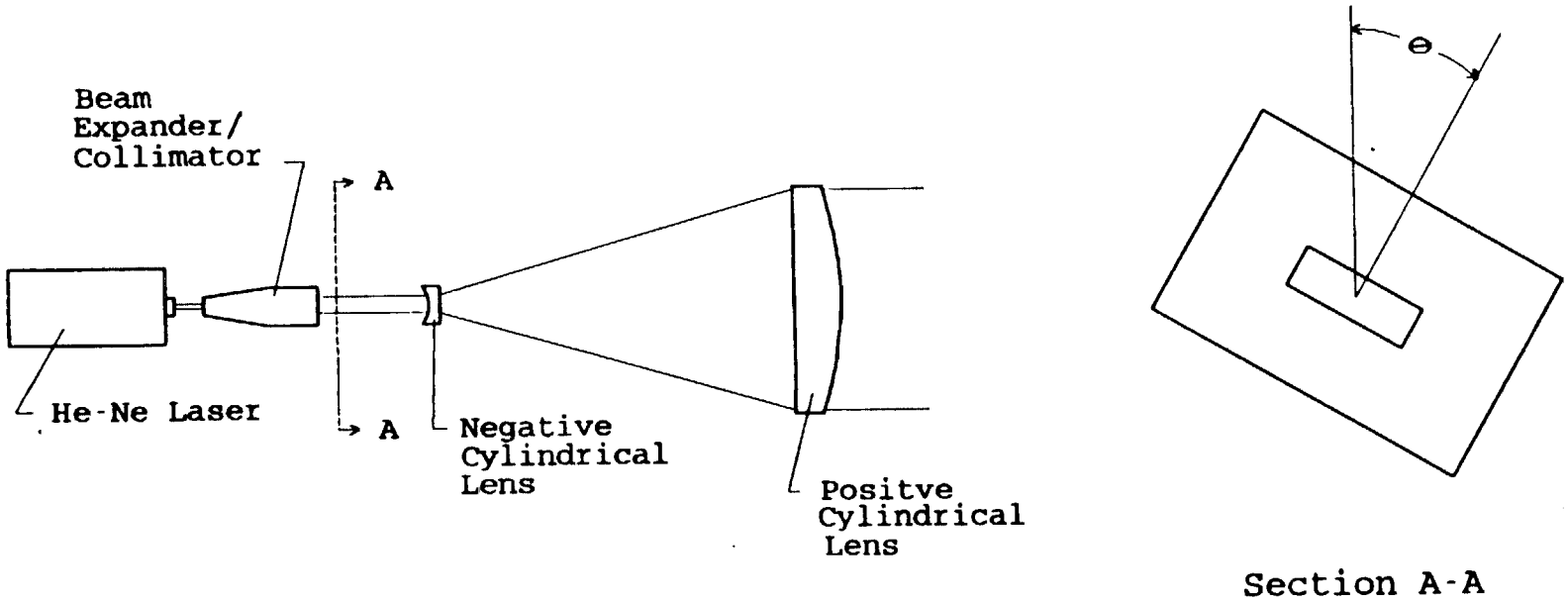

Figure III.5- Schematic of Optical System for Generating Laser Sheet

medium, the index of refraction n is primarily a function of density as given by the Lorenz-Lorentz relation:

$$\frac{1}{\rho}\left(\frac{n^2-1}{n^2+2}\right)=C \qquad (1)$$

where C is a constant. When n is close to 1 (which is true for air), this reduces to the Gladstone-Dale equation

$$C=\frac{n-1}{\rho}=\frac{n_0-1}{\rho_0} \qquad (2)$$

where n_o and ρ_o are the index of refraction and density, respectively, at standard temperature. The value of the Gladstone-Dale constant C depends on the particular gas and the wavelength of the light source used in the optical system. The wavelength dependence is, however, small.

The refraction of light is actually a result of changes in the index of refraction, so from Equation (2)

$$\frac{\partial n}{\partial y}=\frac{(n_0-1)}{\rho_0}\frac{\partial \rho}{\partial y} \qquad (3)$$

where y is in the direction perpendicular to the light source as shown in Figure III.6. For an ideal gas $\rho = P/RT$, and if P is not a function of y (note that acoustic pressure disturbances can be shown to be much smaller compared to the mean pressure)

$$\frac{\partial \rho}{\partial y}=-\frac{P}{R\,T^2}\frac{\partial T}{\partial y} \qquad (4)$$

Combining (3) and (4) gives

$$\frac{\partial n}{\partial y}=-\frac{(n_0-1)}{\rho_0}\frac{P}{R\,T^2}\frac{\partial T}{\partial y} \qquad (5)$$

The path of a light ray through the test section is given by[10]

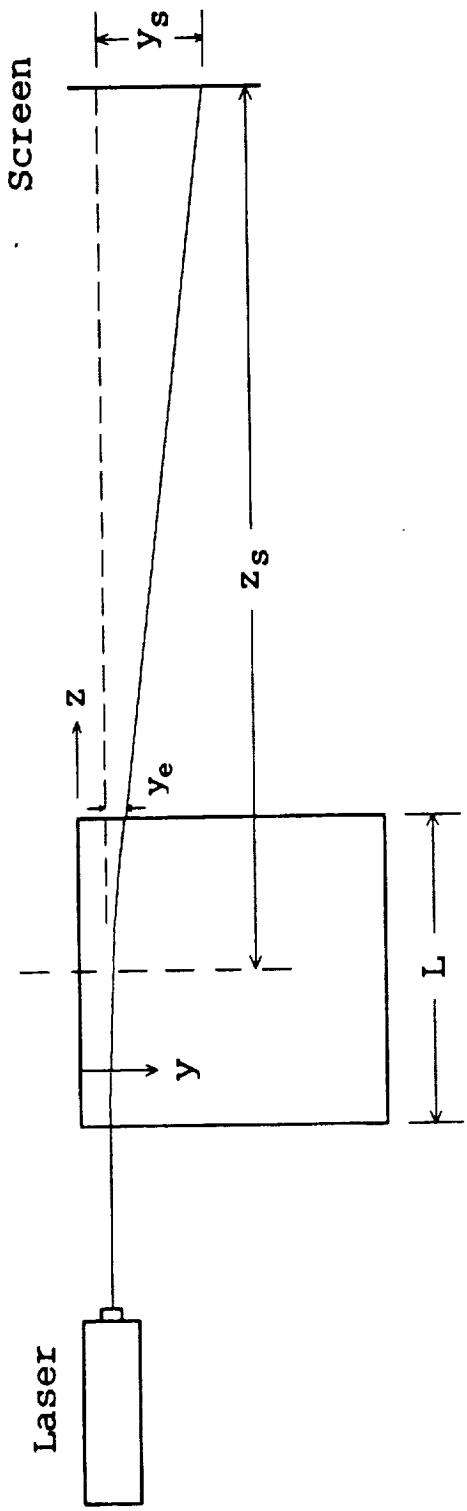

Figure III.6- Schematic of Laser Ray Passing Through Test Section

$$\frac{\partial^2 y}{\partial z^2} = \frac{\partial n}{\partial y} \qquad (6)$$

if the deflections are small and $\partial n/\partial z = \partial n/\partial x = 0$ and $n \approx 1$. These assumptions can be easily justified for air with the length L of the test section in the z direction equal to 4 inches. If in addition the deflection is small, $\partial n/\partial y$ is not a function of z, so integration over the length of the test section gives the slope of the beam at the exit of the test section:

$$\frac{\partial y}{\partial z_e} = \frac{\partial n}{\partial y} L \qquad (7)$$

Integrating again gives

$$y_e = \frac{\partial n}{\partial y} \frac{L^2}{2} \qquad (8)$$

After exiting the test section the light travels in a straight line, so with the slope given in Equation (7) one obtains

$$y_s = y_e + \frac{\partial n}{\partial y} L \left(z_s - \frac{L}{2} \right) \qquad (9)$$

where z_s is the length of the path to the screen and y_s is the deflection at the screen as shown in Figure III.6. Equations (5), (8), and (9) can now be combined to give

$$y_s = -\frac{(n_0 - 1)}{\rho_0} \frac{PLz_s}{RT^2} \frac{\partial T}{\partial y} \qquad (10)$$

or

$$\frac{\partial T}{\partial y} = -\frac{\rho_0}{(n_0 - 1)} \frac{RT^2 y_s}{PLz_s} \qquad (11)$$

Equation (11) relates the temperature and its derivative to the deflection at the screen in terms of other known quantities (recall that the mean pressure P is directly measured as a function of time). With the wall temperature known from thermocouple measurements, Equation (11) can be used along with measured laser deflection varying with y to determine temperature as a function of y at any given time. The numerical integration of Equation (11) is discussed in Section (IV.B.4).

4. Amplification of Laser Deflection

The deflection of the laser beam is proportional to the distance from the test section to the screen, and in the limited space available (approximately 3 feet) for the In-Space Experiment, some means of amplifying the deflection is required to get deflections large enough for accurate measurement. One possibility is to use a series of mirrors to reflect the beam several times thereby effectively increasing z_s. However, since z_s must be about 70 feet to get a maximum deflection of about 1 inch, this method is not practical.

One or more right angle prisms can be used to amplify the laser beam deflection. A wide range of deflection angle amplification can be achieved by varying the number of prisms in series and the initial (undeflected) angle of incidence of the laser beam. Figure III.7 is a schematic that shows the path of a laser ray through a series of three prisms.

The incidence angle α_i of the laser ray entering and the exiting angle α_e for each prism can be found by applying Snell's law

$$\frac{\sin \alpha_a}{n_a} = \frac{\sin \alpha_p}{n_p} \qquad (12)$$

where the subscript *a* indicates the air side and the subscript *p* indicates the prism side of the air-prism interface. Since $n_a \approx 1$, then,

$$\alpha_{e_k} = \sin^{-1}\left[n_p \sin\left(45^\circ - \sin^{-1}\left(\frac{\sin \alpha_{i_k}}{n_p} \right) \right) \right] \qquad (13)$$

where k indicates the k^{th} prism in a series of prisms. The prisms are oriented relative to each other by

$$\gamma_k = \gamma_{k-1} + \alpha_{e_{k-1}} + \alpha_{i_k} - 45^\circ \qquad (14)$$

where the angle γ_k is defined in Figure III.7.

The above equations describe the path of an undeflected laser ray where

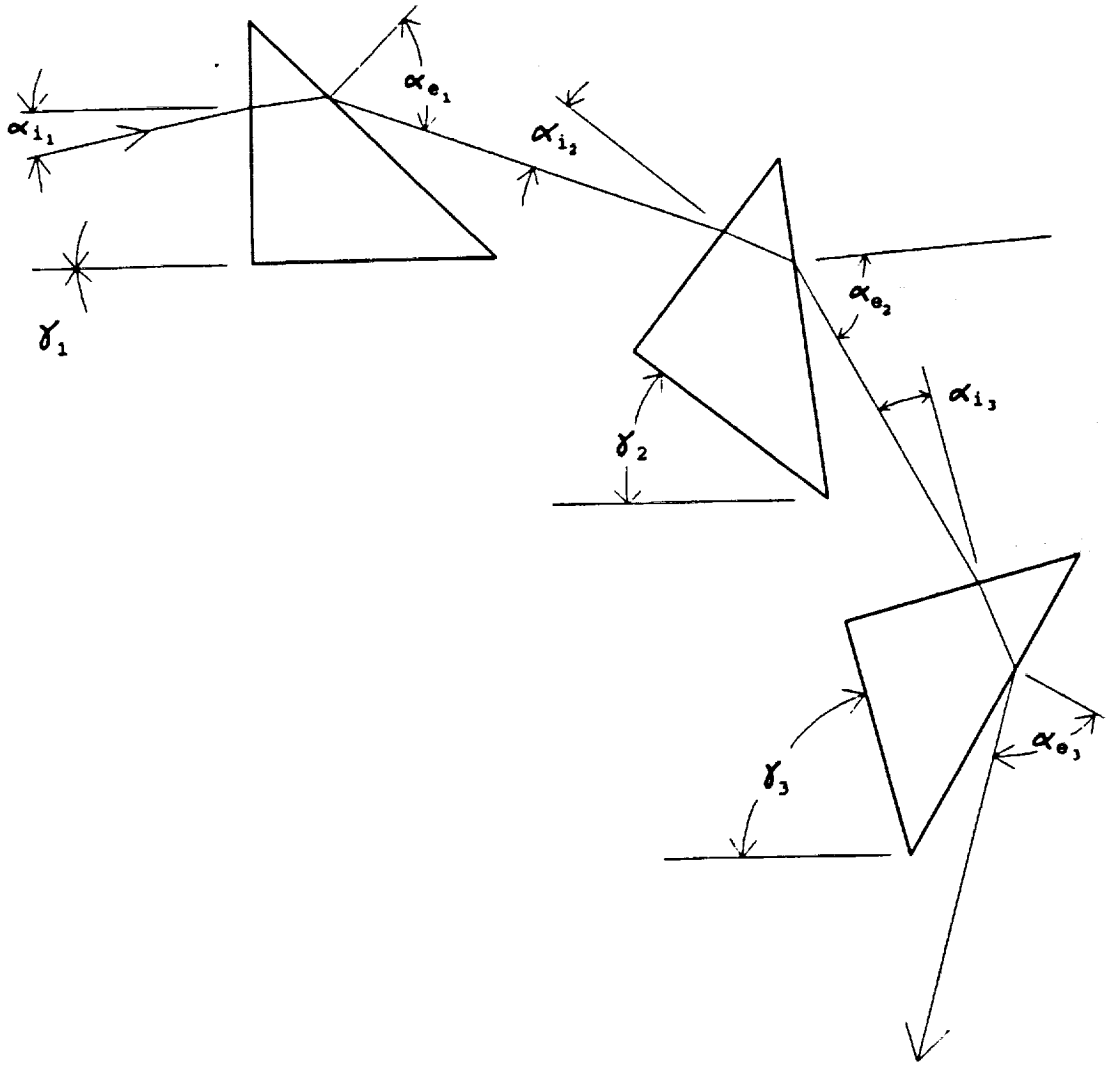

Figure III.7- Schematic of a Laser Ray Path Through a Series of Three Prisms

α_{i_k} is predetermined. Given this fixed arrangement of the prisms, it is necessary to determine incidence angles for a deflected ray. This can easily be done using the above equations and the relation

$$\alpha'_{i_k} = \alpha_{i_k} + (\alpha_{e_{k-1}} - \alpha'_{e_{k-1}}) \qquad (15)$$

where primes indicate incidence angles for a deflected ray. Figure III.8 shows the ratio of the change in exit angle to the change in entrance angle as a function of the change in the entrance angle, that is, $(\alpha_{e3} - \alpha'_{e3})/(\alpha_{i_1} - \alpha'_{i_1})$ as a function of $(\alpha_{i_1} - \alpha'_{i_1})$, for a series of three prisms. The relationship is nonlinear but for the small angle changes considered (maximum change in entrance angle expected is 0.1°), the deviation from linearity is small for $\alpha_{i_k} > 7°$. The flight experiment has been designed for $\alpha_{i_k} = 8°$ which provides an angle change ratio of approximately 25. Thus, using only three prisms and locating the screen just 4 feet past the prism array provides an effective z_s of approximately 100 feet.

Unfortunately, amplification of laser beam deflections is not the only effect of the prism array. Also, because the experiment requires a laser sheet rather than a narrow beam, the following additional comments should be considered:

a) The laser sheet will be constricted in the direction of deflection. The prisms must be oriented so that deflections are perpendicular to the prism base as shown in Figure III.9. (Refer also to Figure III.4 for comparison of the laser sheet orientation in the test section.) This constriction is simply a result of the turning of each parallel ray of the laser sheet as shown in Figure III.10. The effect is compounded by each prism. The constriction is not a problem, however, because $w(\sin\theta)$ remains constant, and there is still a linear relationship between the distance along the laser sheet profile and the distance from the heated wall.

b) The above constriction effect also results in a thin image on the screen if the incoming rays are parallel and remain parallel after the prism array. If they are not perfectly parallel, however, the divergence will be amplified. The prism system is, of course, designed to amplify angle changes. Even

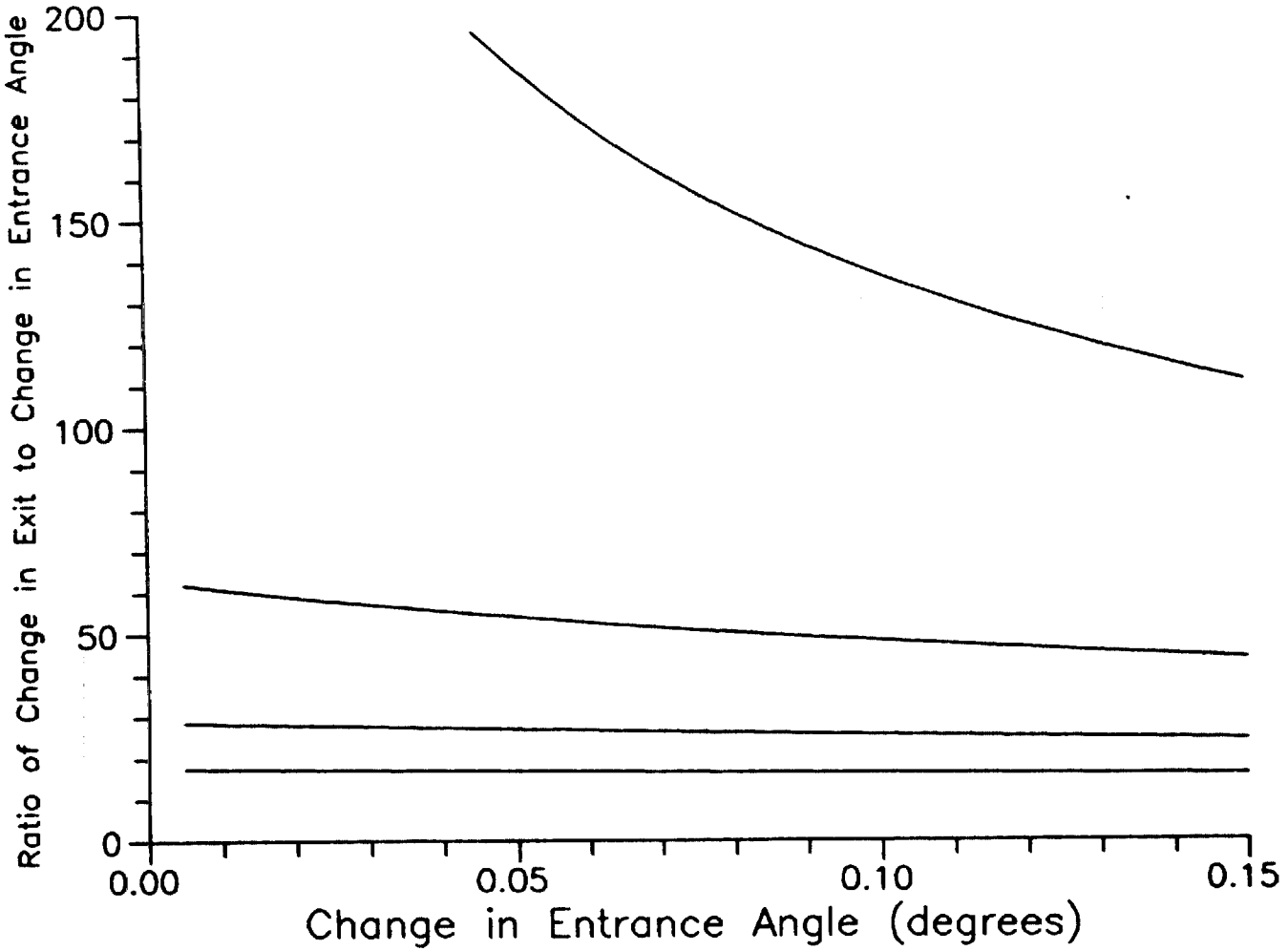

Figure III.8 - Ratio of Change in Exit Angle to Change in Entrance Angle as a Function of Change in Entrance Angle.

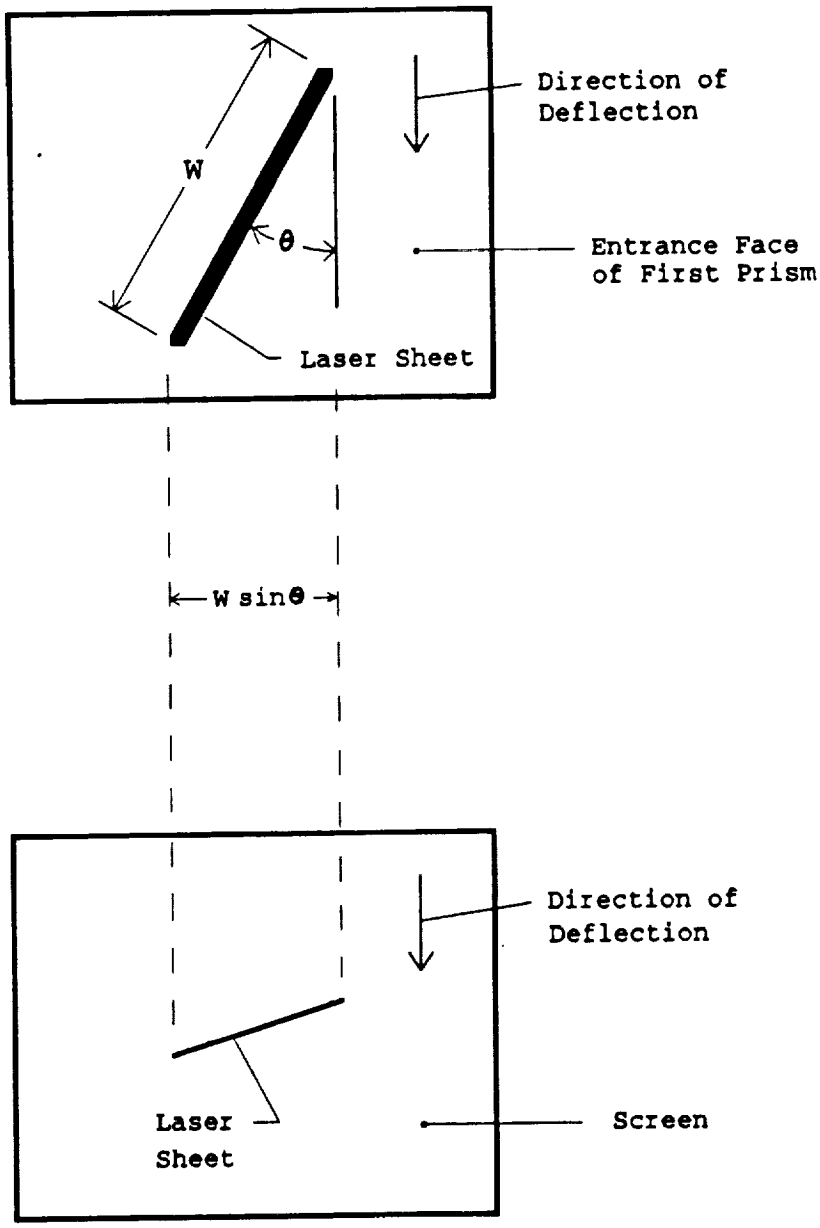

Figure III.9 - Undeflected Laser Sheet Orientation at the Entrance Face of the First Prism and at the Screen

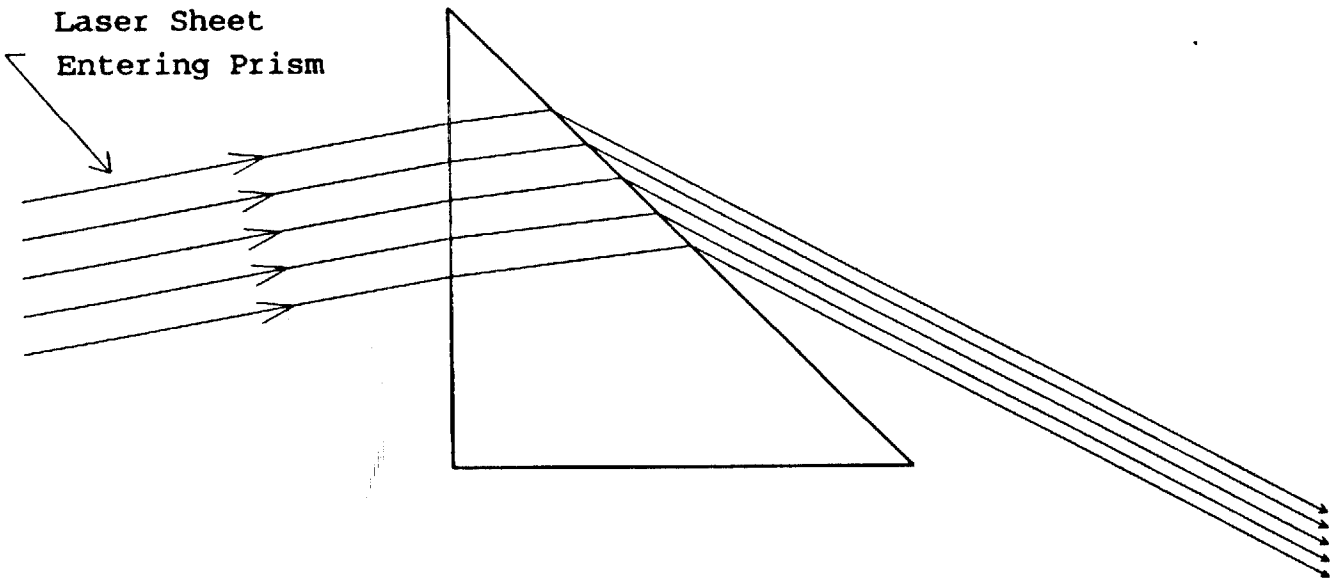

Figure III.10 - Constriction of Laser Sheet by One Prism

if the incoming rays are perfectly parallel, divergence due to diffraction effects on the very thin sheet is unavoidable. The result is a thicker line at the screen. A well-collimated beam should minimize this effect, and furthermore, even a relatively thick image at the screen will influence the accuracy of deflection measurements only minimally since only beam displacement from a reference position (e.g., the edge of the beam) is measured.

c) Reflections of the beam at each glass/air interface will reduce the intensity of the beam at the screen. The relatively high incidence angle as the beam exits each prism results in high reflection. Preliminary calculations indicate that approximately 39% of the original beam intensity would be transmitted for the present design with no anti-reflection coating. This lower bound is sufficient for a 10 milliwatt He-Ne laser, and a MgF_2 coating will significantly improve transmittance.

5. Analysis of Laser Deflection Data

The data collected during the experiment run time includes the deflection of the laser sheet recorded by video camera, the heated wall temperature measured by thermocouples and the test section pressure determined by a pressure transducer. The thermocouple and pressure transducer voltage data can be easily converted to temperature and pressure data from known calibration curves. Generating a temperature profile from a video image of the laser sheet deflection requires more effort.

Equation (11) provides the relationship between the temperature gradient and the deflection. This equation, however, does not consider the amplification of the deflection by the prism system, so an effective length, z'_s past the test section must be determined. z'_s can be approximated, assuming small angle deflections, by

$$z'_s = z_b + r_p z_a \qquad (16)$$

where z_b and z_a are the laser path distances before and after the prism system, respectively, and r_p is the angle ratio as shown in Figure III.8. This equation neglects the deflection that occurs within the prism system. The accuracy of the equation is also limited because r_p is highly

sensitive to the orientation of the prism system and is a function of the deflection angle. Therefore, z'_s probably needs to be determined in terms of y_s by calibration. This is accomplished by turning the incoming beam by a known angle ß and noting y_s, then

$$z'_s = \frac{y_s}{\sin \beta} \qquad (17)$$

Equation (11) can now be used (with z'_s rather than z_s) to determine the temperature gradient, $\partial T/\partial y$. The gradient can then be used with the heated wall boundary condition measured with thermocouples to determine the temperature profile, $T(y)$. This process is described in detail in the next section on Ground Experiment Results.

E. Power Supply

The main power for the heater element can be supplied in either of two ways. One way is to use rechargeable batteries. The batteries supply the large power requirement for the relatively short duration of each experiment run and are recharged between experiment runs by STS Orbiter power. Each battery is size D (about 2.5 inches high by 1.25 inches in diameter) with 4 amp-hrs and 1.2 volts and weighs about 0.29 pounds. The baseline design provides space for 18 batteries, but more could easily be added if necessary. The batteries must be configured in a combination of series and parallel so that sufficient power can be supplied at various voltage levels. The voltage level determines the heating rate of the heater element. A simple circuit diagram corresponding to the battery power supply method is shown in Figure III.11.

Another way to supply power is to directly use Orbiter power. The elimination of batteries has several advantages including improved safety, reduction of weight, more available space and simplification of the design. The disadvantage is the limitation of the power supply. The current limitation of 115 W for middeck experiments would require much smaller heated wall dimensions to achieve a high heating rate. It may be possible to use the Middeck Utility Panel (MUP) with a power supply of 1 kW to resolve this problem. However, the limited availability of the MUP would probably delay manifesting the payload for flight.

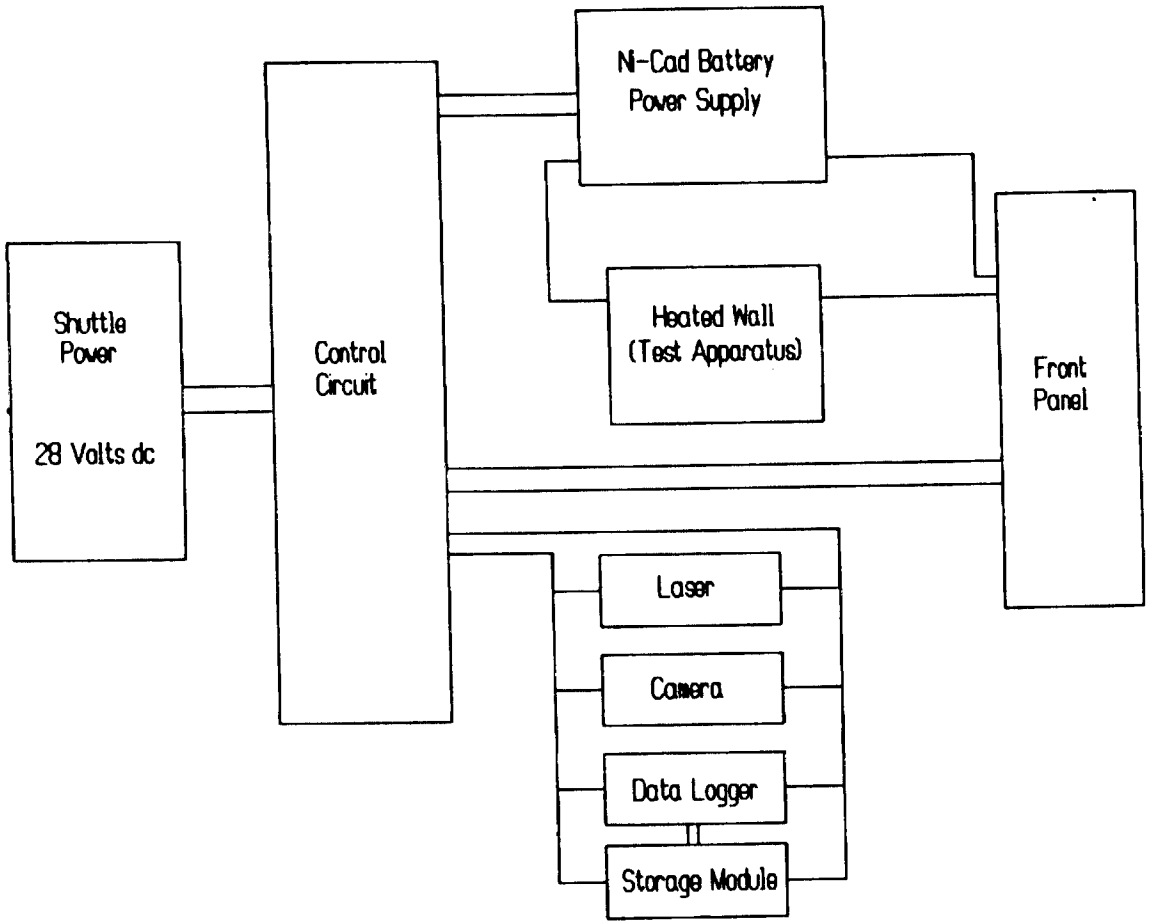

Figure III.11 - Flight Experiment Circuit Diagram

F. Procedure

Most of the experimental steps can be executed automatically so that crew interaction with the experiment is minimized. The basic steps required to perform one run are as follows:

a) Turn on front panel switch to begin run.
b) Turn on laser, video camera, data logger and storage module.
c) Adjust voltage level to be applied to heated wall.
d) Turn on power to heated wall for duration of run.
e) Turn off power to heated wall.
f) Turn off laser, video camera, data logger and storage module.
g) Turn off front panel switch to end run.
h) Begin recharge of battery.
i) End recharge of battery.

It is probably necessary for the crew to perform steps (d) and (e) since the relatively high current to the heated wall would require a large, heavy relay for automatic switching. The duration of each run depends on available power supply.

IV. GROUND EXPERIMENT RESULTS AND ANALYSIS

A. Description of Ground Experiment

An experimental apparatus similar to the flight experiment was designed, fabricated and tested to perform a series of ground experiments. These experiments were carried out to gain insight into the physics of TAC phenomena and to establish the feasibility of the flight experiment design. This section describes the ground experiment and its results. The analysis required to obtain temperature profiles from raw deflection data and an error analysis is also included.

1. Ground Experiment Apparatus and Instrumentation

The ground experiment design is similar to the flight experiment design except that prisms were not used to amplify the deflection. Details of the ground experiment are given below, but elements that are in common with the flight experiment and were described in the previous section are not repeated here.

A schematic of the ground experiment optical system is shown in Figure IV.1. A 5 milliwatt red He-Ne laser with a beam diameter of 0.83 mm and divergence of 0.97 mrad was used as the light source. The beam was expanded in the ground experiment with two spherical lenses with focal lengths of 36 mm and 125 mm rather than a beam expander/collimator as in the flight experiment design. The focal point of each lens was at the same location, so the resulting beam was parallel with a diameter of

$$d_2 = d_1 \left| \frac{f_{s2}}{f_{s1}} \right| \qquad (18)$$

where d_1 is the original laser beam diameter and d_2 is the diameter after the lenses. Here f_{s1} and f_{s2} are the focal lengths of the first and second spherical lens, respectively. This results in d_2=2.88 mm.

The laser sheet was generated by a negative cylindrical lens with focal length of -6.35 mm followed by a positive cylindrical lens with focal length of 300 mm. The focal point of the second (positive) cylindrical

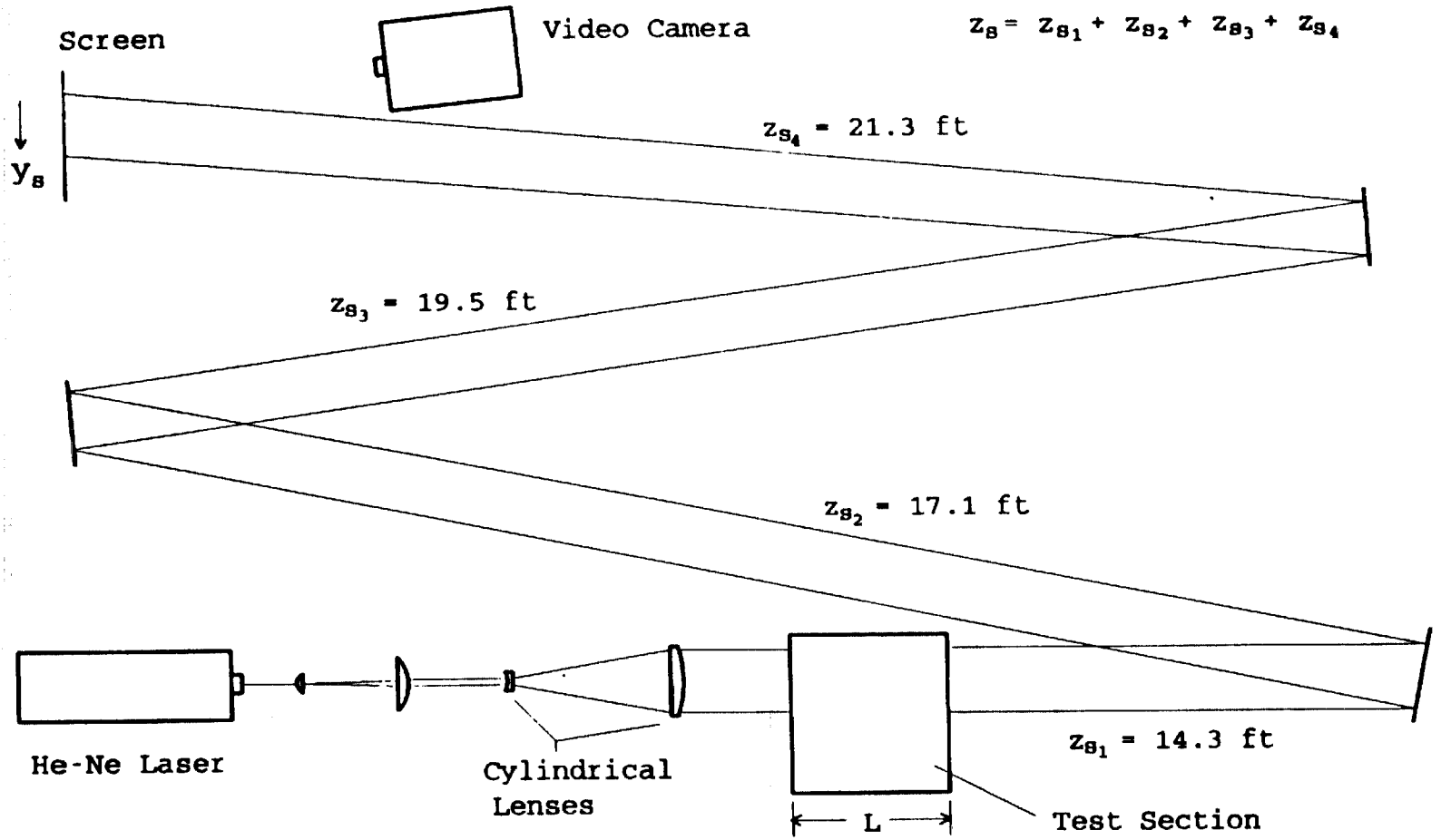

Figure IV.1 - Schematic of Ground Experiment Optical System

lens was slightly farther from the test section than that of the first (negative) cylindrical lens so that the resulting laser sheet expanded slightly after exiting the lens system with a width, w, given by

$$w = d_2 \left| \frac{f_{c4}}{f_{c3}} \right| \qquad (19)$$

where f_{c3} and f_{c4} are the focal lengths of the third and fourth (the two cylindrical) lenses, respectively. This results in w=136 mm, however, since the height of the second cylindrical lens was only 50 mm, effectively, w=50 mm. The thickness t of the laser sheet is $t=d_2$=2.88 mm. The slight expansion of the width of the sheet had a negligible effect on w at the test section but provided an elongated image at the screen for better resolution of the distance from the heated wall. Both of the cylindrical lenses were tilted to an angle of about θ=37° relative to the test section.

After the test section the beam was reflected off a series of three plane mirrors, as shown in Figure IV.1, so that the total length, Z_s from the test section to the screen was 72.2 feet. A video camera was used to record the image of the laser sheet on a white screen. The video camera took 30 images per second for a time least count of 0.033 seconds. Fixed reference markers were used on the screen to make it easier to identify the undeflected position of the laser image during video image processing.

Power to the heated wall was supplied with two 12-volt automotive batteries connected in parallel. Variable resistance was added in the power circuit as a means of varying the voltage drop across the heated wall. A detailed description of the test section and heated wall apparatus is given in Section III.B.

Two chromel-alumel (Type K) thermocouples with a 0.015 inch bead on 0.005 inch diameter leads were spot-welded to the heated wall approximately 3/4 inch away from and on opposite sides of the center of the heated wall. It is important that a single bead be attached to the heated wall rather than two separate leads because of the voltage potential across the heated wall. An unbonded strain gauge pressure transducer was also connected to the test section on the wall opposite the heated wall. The thermocouples and pressure transducer were connected

to a Hewlett Packard 3497A Data Acquisition and Control unit which was connected in series with a Hewlett Packard 9826 computer. The computer was programmed to read the voltage outputs from the thermocouples and pressure transducer and record the elapsed time. The temperatures and pressure were then calculated from calibration curves.

In separate experimental runs, temperature boundary conditions were measured. The temperature of the heated wall was measured at various locations with six thermocouples as shown in Figure IV.2. The 12 thermocouple leads were not insulated because of the high temperature environment. It was, therefore, quite difficult to spot-weld them to the surface so that none of the leads touched each other.

The temperatures of the side walls and bottom wall were measured with fifteen 0.002-inch chromel-alumel thermocouples; nine on the glass side wall, five on the insulated side wall and one on the bottom wall. The locations of the side wall thermocouples are shown in Figure IV.3. The thermocouples on the glass wall were attached with a very small amount of epoxy and shielded from radiation by a thin piece of insulation. The insulation wall thermocouples were slightly imbedded in the insulation and also shielded by a thin piece of insulation. The thermocouple on the bottom wall was spot-welded near the center of the wall.

2. Ground Experiment Procedure

Experiments were run with four different levels of power applied to the heated wall which will be referred to as low, medium low, medium high, and high power. Three runs were made for each power level, and the results were averaged before presentation. Quantitative data for the power and heated wall temperatures are presented in Sections IV.B.1-2.

The computer program provided a printed copy of the thermocouple temperatures, the pressure and the elapsed time since the beginning of data acquisition. The actual start time of the run could be determined from the beginning of the rise in temperature. The video camera also provided an on-tape elapsed time from the instant the camera was turned on. Again, the actual start time could easily be determined from the initiation of the deflection of the laser.

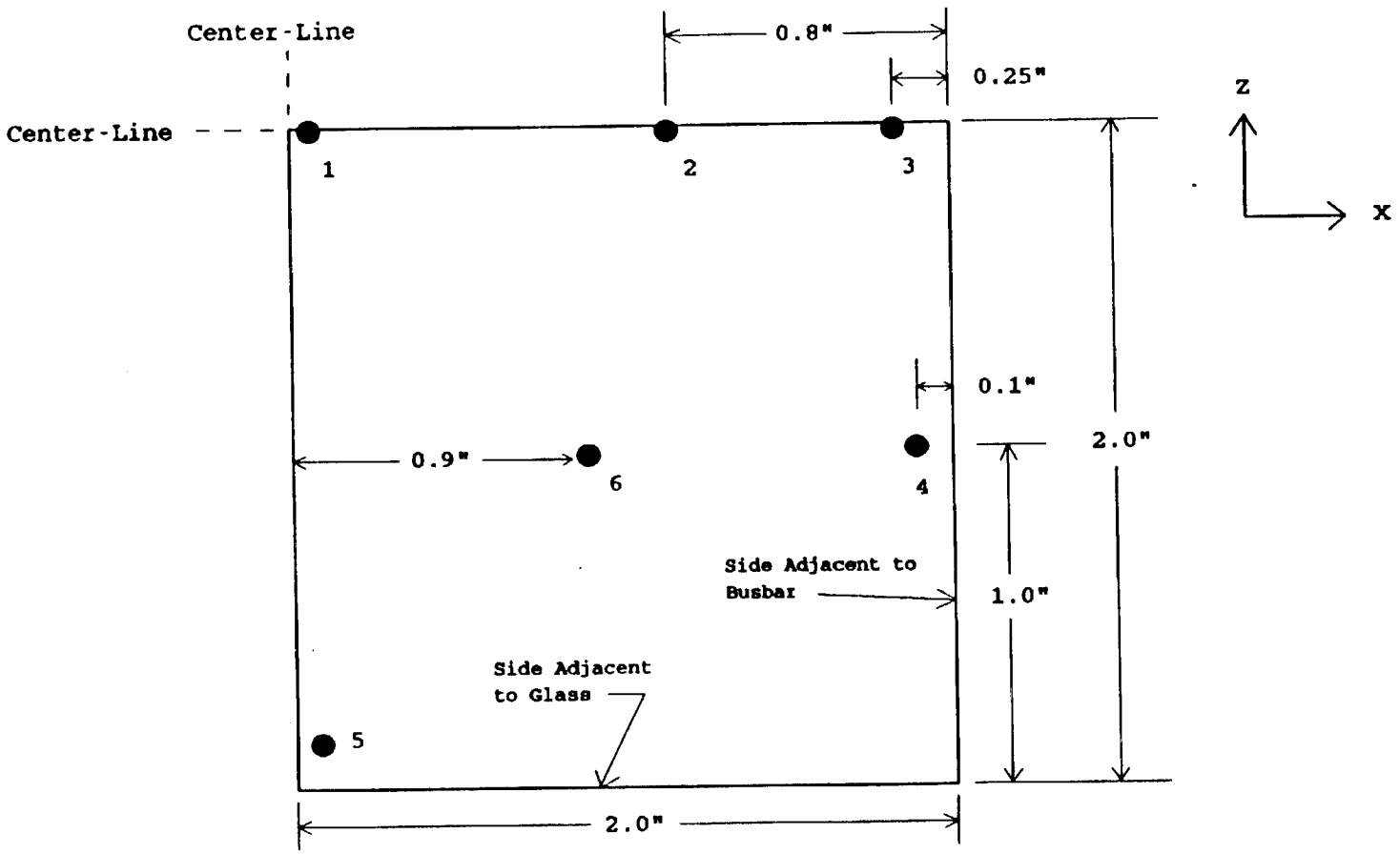

Figure IV.2 - Location of Thermocouples on Heated Wall

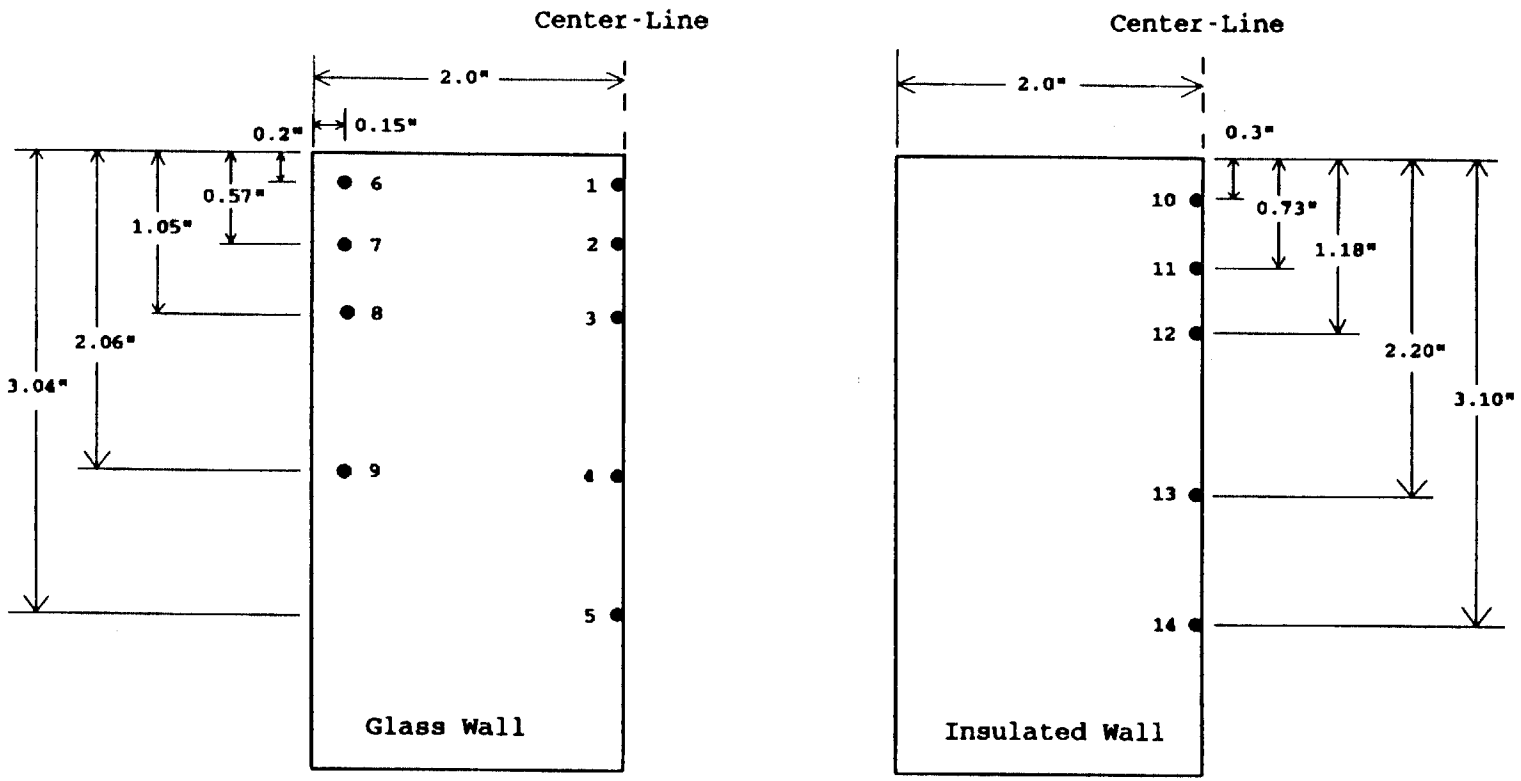

Figure IV.3 - Location of Thermocouples on Side Walls

The next task was to determine the laser deflection from the video tape. Using an IBM AT compatible PC with a PCVision Plus image processing card and Werner Frei Associates image processing software along with a high resolution television monitor, it was possible to obtain a series of digitized images at various selected times from the video tape. These images were then enhanced to improve the visibility of the laser sheet image, and the location of the laser sheet was then measured with a mouse pointer. Deflection measurements were taken at times of 0.5, 1.0, 2.0, 5.0, and 10.0 seconds after initiation of heating. The following steps were taken to obtain the detailed measurements:

a) The number of pixels per length in each direction was determined directly from marks on the screen that were spaced six inches apart.

b) The image was zoomed to include only the deflected beam. With the ratio of the original to the zoomed image known, the number of pixels per length was determined in each direction. There were approximately 80 pixels/inch in the z direction (perpendicular to the deflection direction) and approximately 60 pixels/inch in the y direction (along the deflection direction).

c) The coordinates of the top edge of the undeflected laser sheet image was established before heating. The top edge of the image is the edge adjacent to the heated wall.

d) The frames were counted at 30 frames/second to locate the frame at the selected time of interest.

e) The y and z pixel location of the top edge of the deflected laser sheet was recorded for each selected time of interest.

From this recorded set of information, the deflection versus distance from the heated wall for a given time was determined as described in the next section.

Separate runs were made to get transient temperature boundary conditions. One run at each power level was made to measure the temperature of the heated wall at various locations. These runs also measured the voltage drop across the heated wall and the current to obtain the power dissipation of the heated wall. Another run at each power level was made to measure the side wall temperatures at various locations. These runs, of course, did not involve the laser or video camera.

Flow visualization experiments were performed using the heated cavity apparatus previously described. The wall opposite the heated wall included an open hole, so the test section was not pressurized. Tobacco smoke was injected into the test section to allow visualization. The results, recorded on movie film, indicate a uniform flow, or expansion, of the air away from the heated wall. Flow visualization was not included in the flight design because of the added complexity.

The velocity of the air during expansion away from the heated wall was measured as a function of time. The measurements were made with a hot-film velocity meter.

B. Ground Experiment Results

1. Power Consumption

The voltage drop and current were measured for each power level. The current was highest at the beginning of each run before leveling off after about 1 second. This is the result of increasing resistance of the heated wall and external resistor with temperature. Figure IV.4 shows a plot of current as a function of time for each power level. The voltage fluctuated only slightly (±5%) with time. The nominal voltage for each power level was

- Low power 3.7 volts
- Medium low power 5.7 volts
- Medium high power 7.0 volts
- High power 10.4 volts.

The resulting power consumption at each level is shown in Figure IV.5.

2. Heated Wall Temperature and Measured Pressure

Output from the HP computer consisted of two temperatures, pressure and the time for each reading. Each reading, however, required approximately 0.15 seconds, so the actual time associated with each value varied slightly from the recorded time. The actual time for each value was determined by linear interpolation between the recorded times. The data for each run at a given power level and for a given thermocouple were very repeatable (maximum difference in temperature rise less than 2%), however, one of the thermocouples consistently read a temperature 50 to

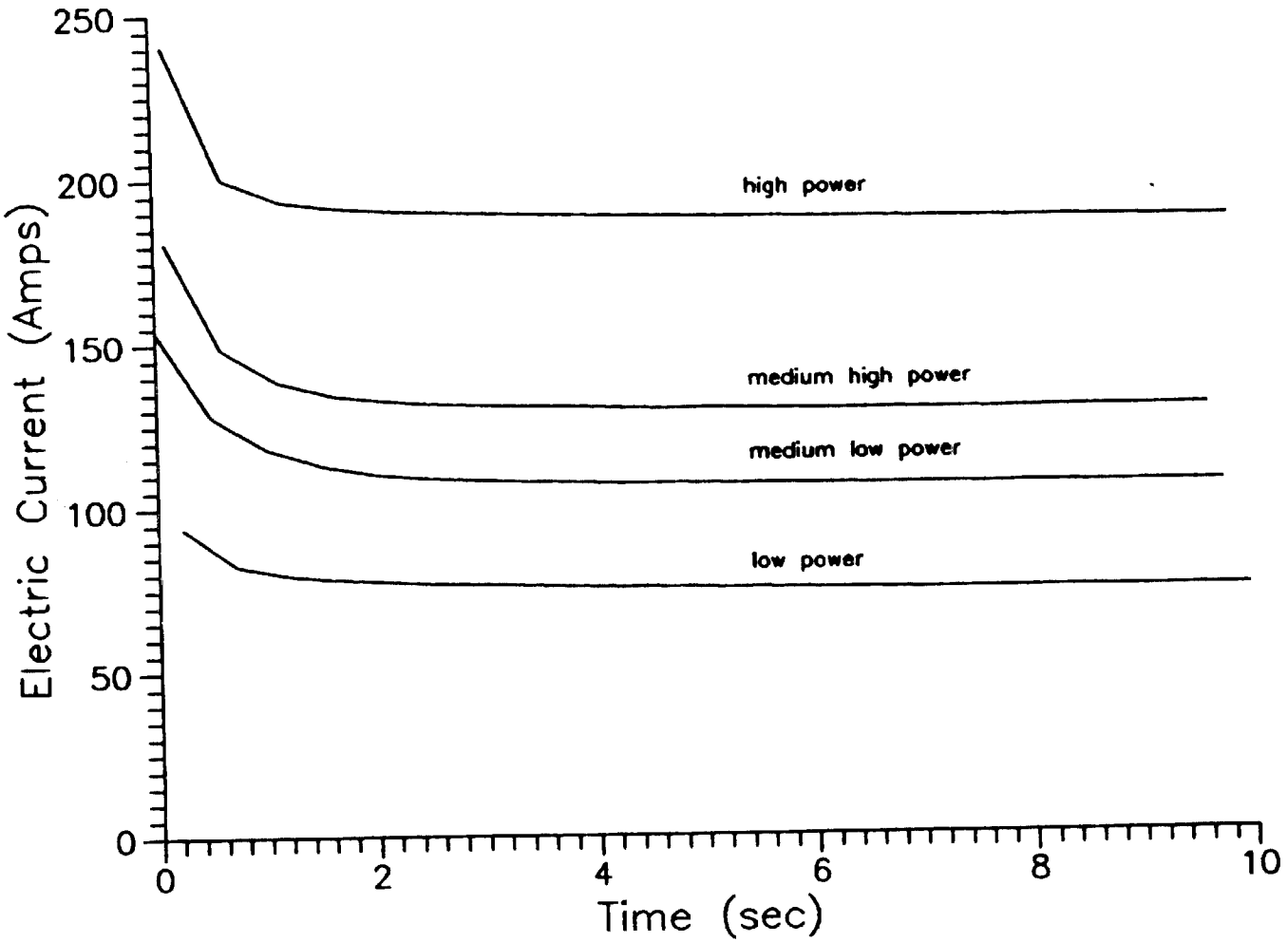

Figure IV.4 - Current as a Function of Time for Each Power Level

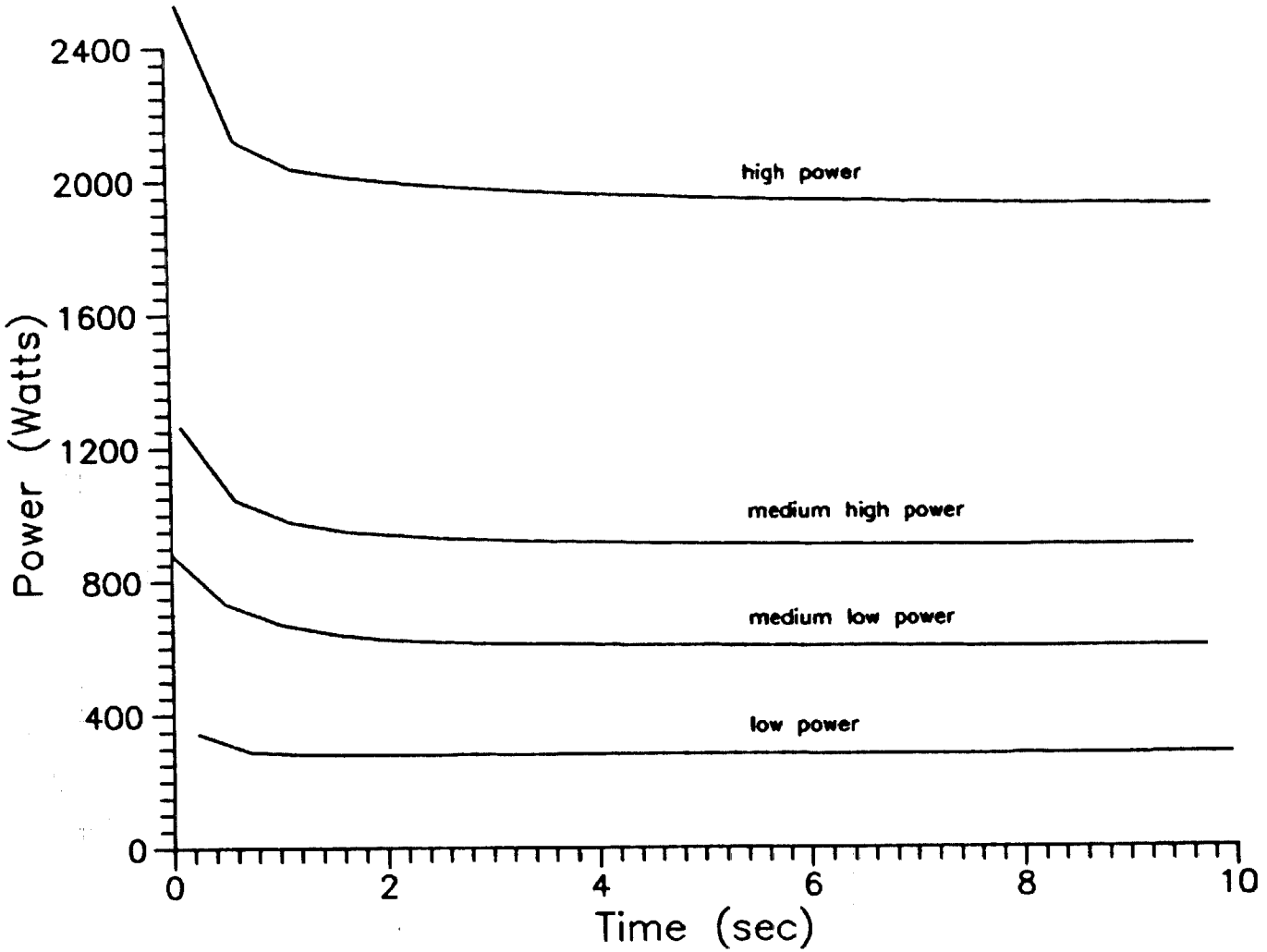

Figure IV.5 - Power Consumption as a Function of Time for Each Power Level

60°F above the other after 2 or 3 seconds. This is less than 9% of the total temperature rise for the low power case and a smaller percentage for higher power levels. The average of the two thermocouple readings was taken as the temperature of the center of the heated wall.

Since the laser sheet passes through the length of the test section between the glass side walls, it essentially averages conditions along its path. Therefore, it is necessary to determine the average temperature of the heated wall between the glass walls. Figures IV.6 through IV.9 show the temperatures of the heated wall at each power level in the locations shown in Figure IV.2. These temperatures were normalized by dividing by the center point temperature and fit to a two dimensional quadratic curve. The average temperature along the centerline between the glass side walls was then determined and is shown in Figure IV.10.

The measured pressure for each run at a given power level varied by less than 1% of the maximum pressure rise. The measured pressure for each power level is shown in Figure IV.11.

3. Laser Deflection

The raw data taken manually from the image processor consists of the coordinate (y,z) of pixels that form the contour of the laser sheet profile on the screen. The coordinate data are first converted from number of pixels to inches before any further manipulations.

The shape of the undeflected beam is saved for comparison with the deflected beam shapes at the selected time slices. Though the undeflected beam would ideally be a straight line, some curvature is present due to errors in lens alignment and imperfect mirrors. This is, however, not a problem if the actual shape of the undeflected beam is used. The deflection at a given point is simply (y_d - y_u), where y_d and y_u are the deflected and undeflected points, respectively, for a given z. The distance from the heated wall associated with each point is

$$y = \frac{w}{w_s}\sqrt{(y-y_0)^2+(z-z_0)^2}\,\cos\theta \qquad (21)$$

where w and w_s are the laser sheet width at the test section and at the screen, respectively, and θ is the angle of inclination of the laser sheet

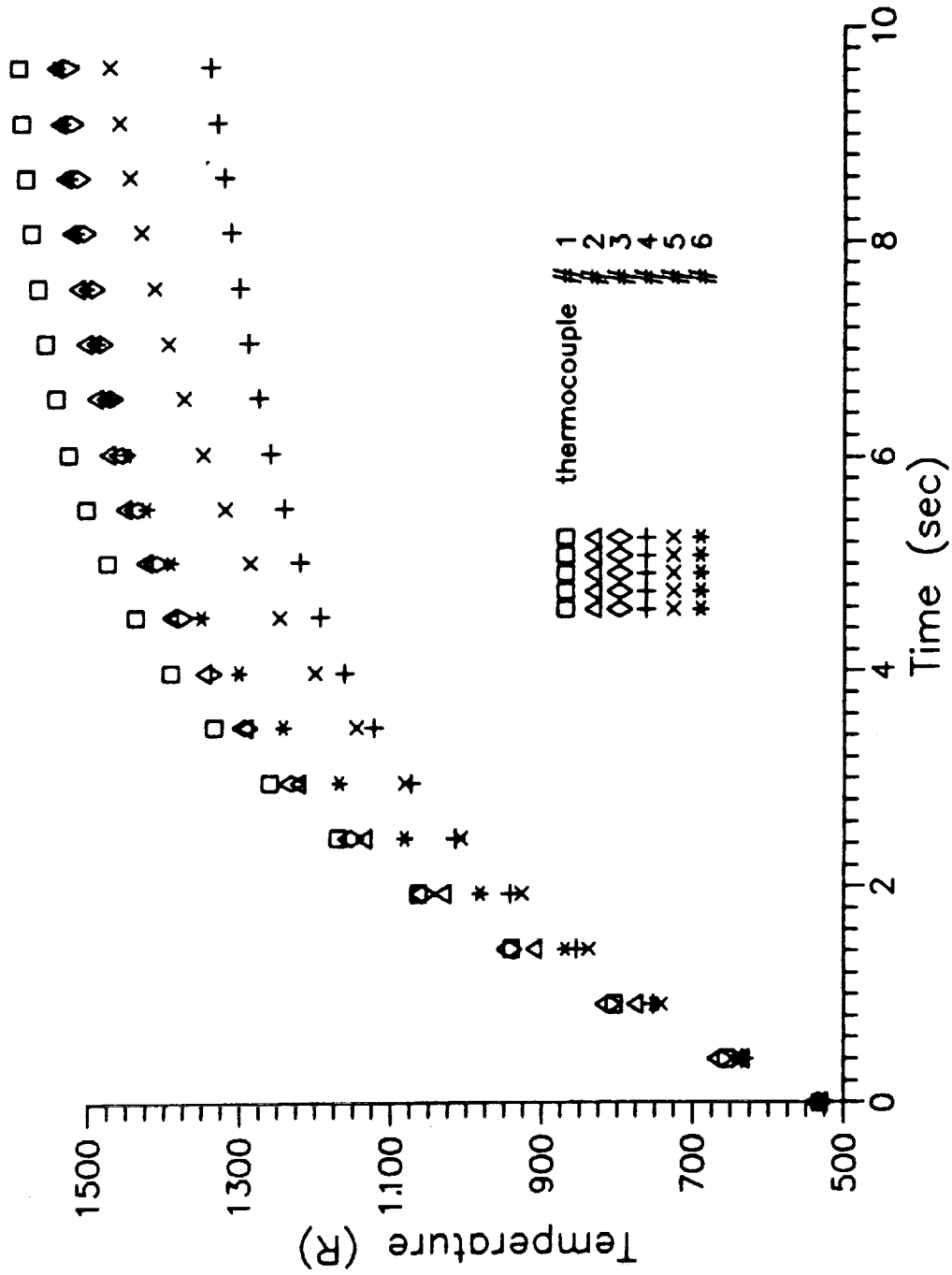

Figure IV.6 - Heated Wall Temperature at Various Locations as a Function of Time for Low Power

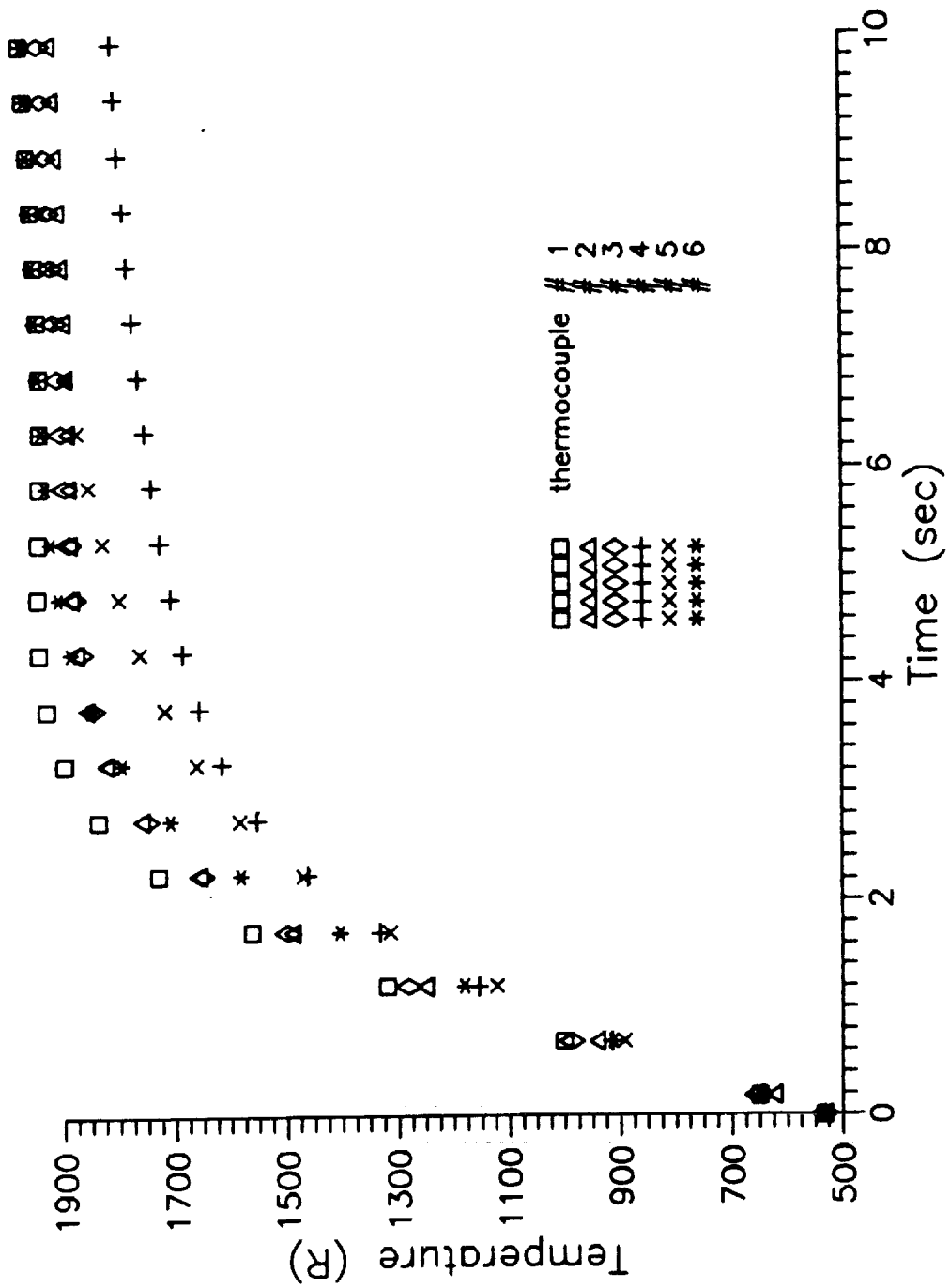

Figure IV.7 - Heated Wall Temperature at Various Locations as a Function of Time for Medium Low Power

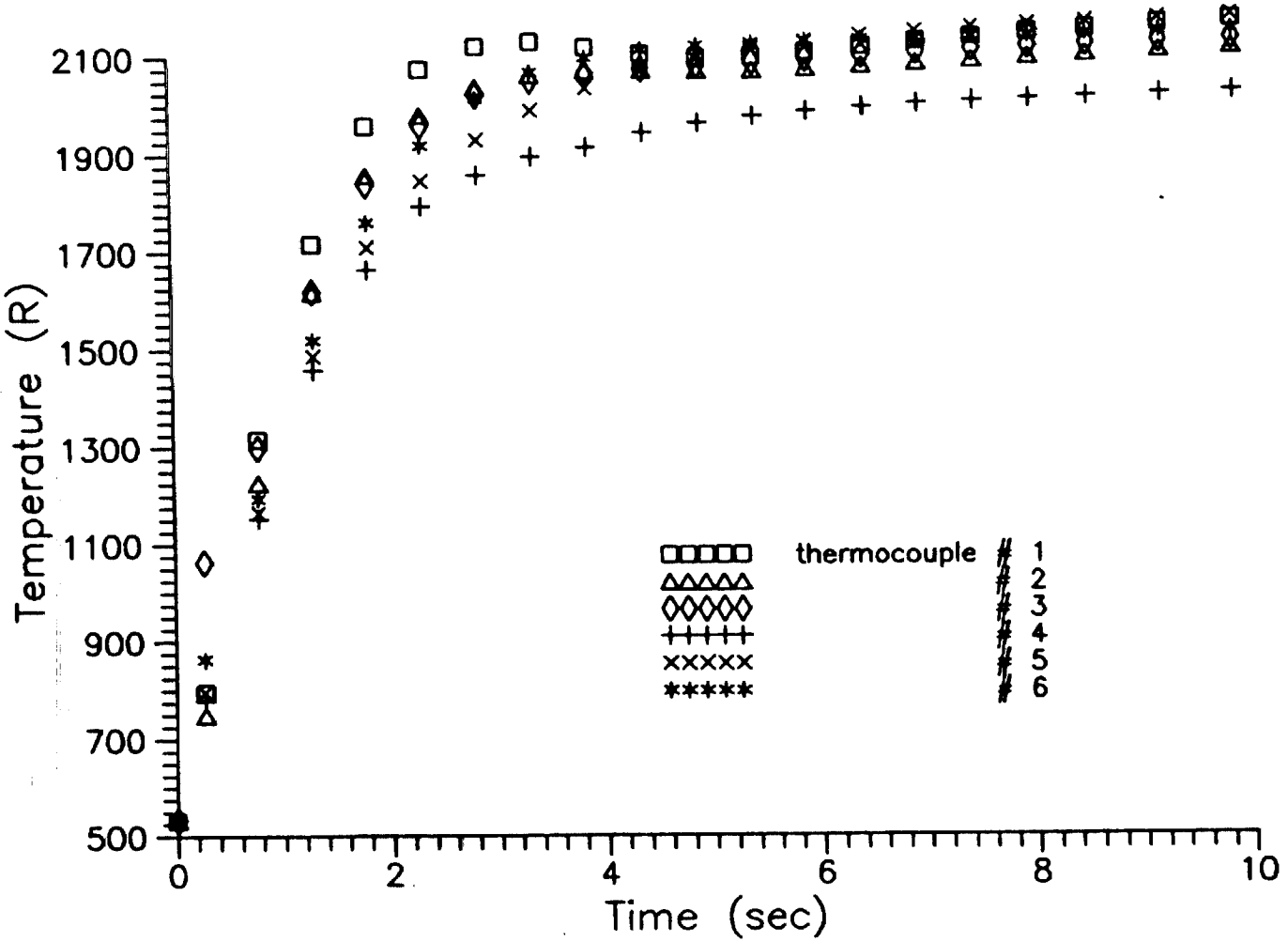

Figure IV.8 - Heated Wall Temperature at Various Locations as a Function of Time for Medium High Power

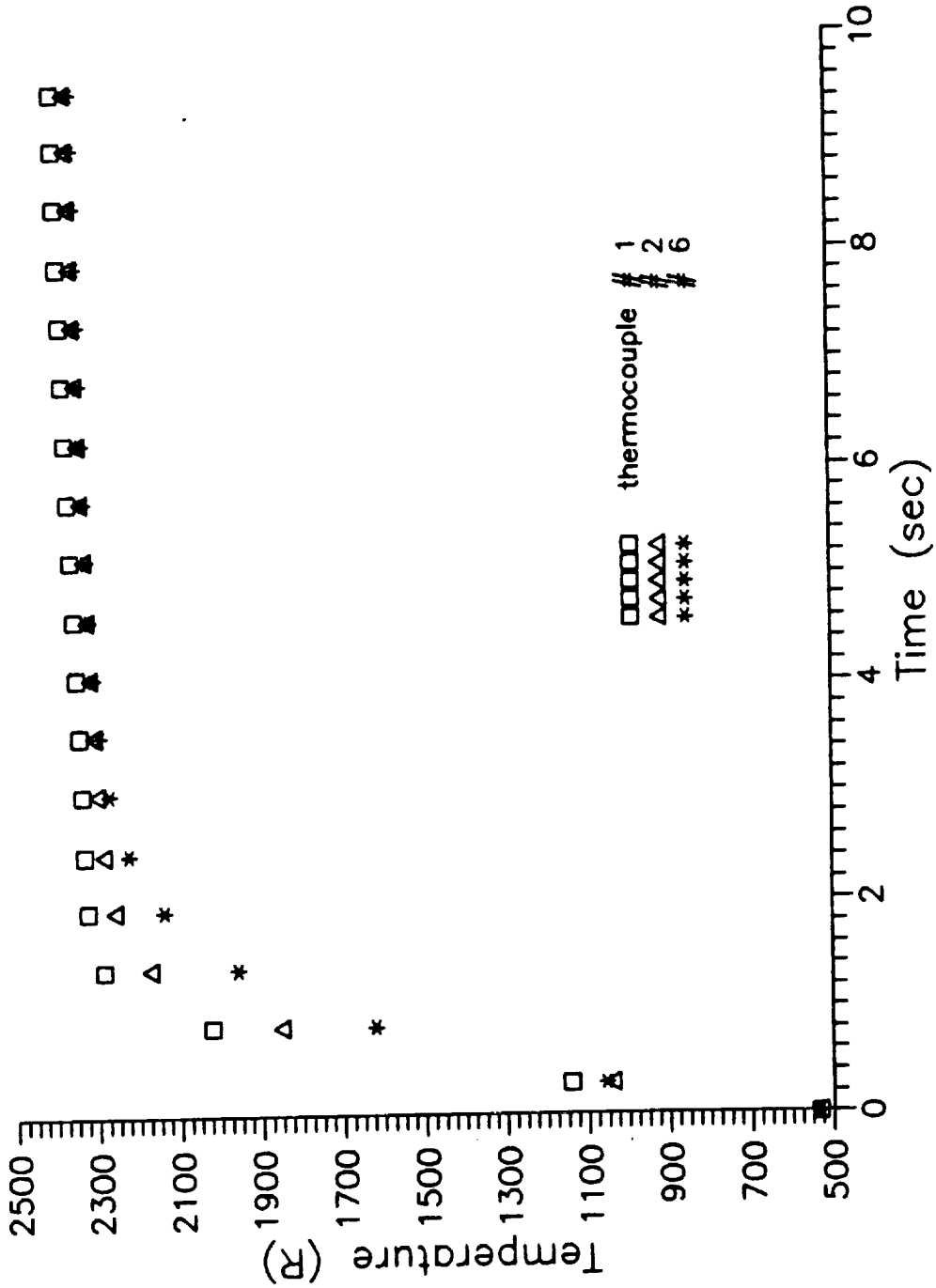

Figure IV.9 - Heated Wall Temperature at Various Locations as a Function of Time for High Power

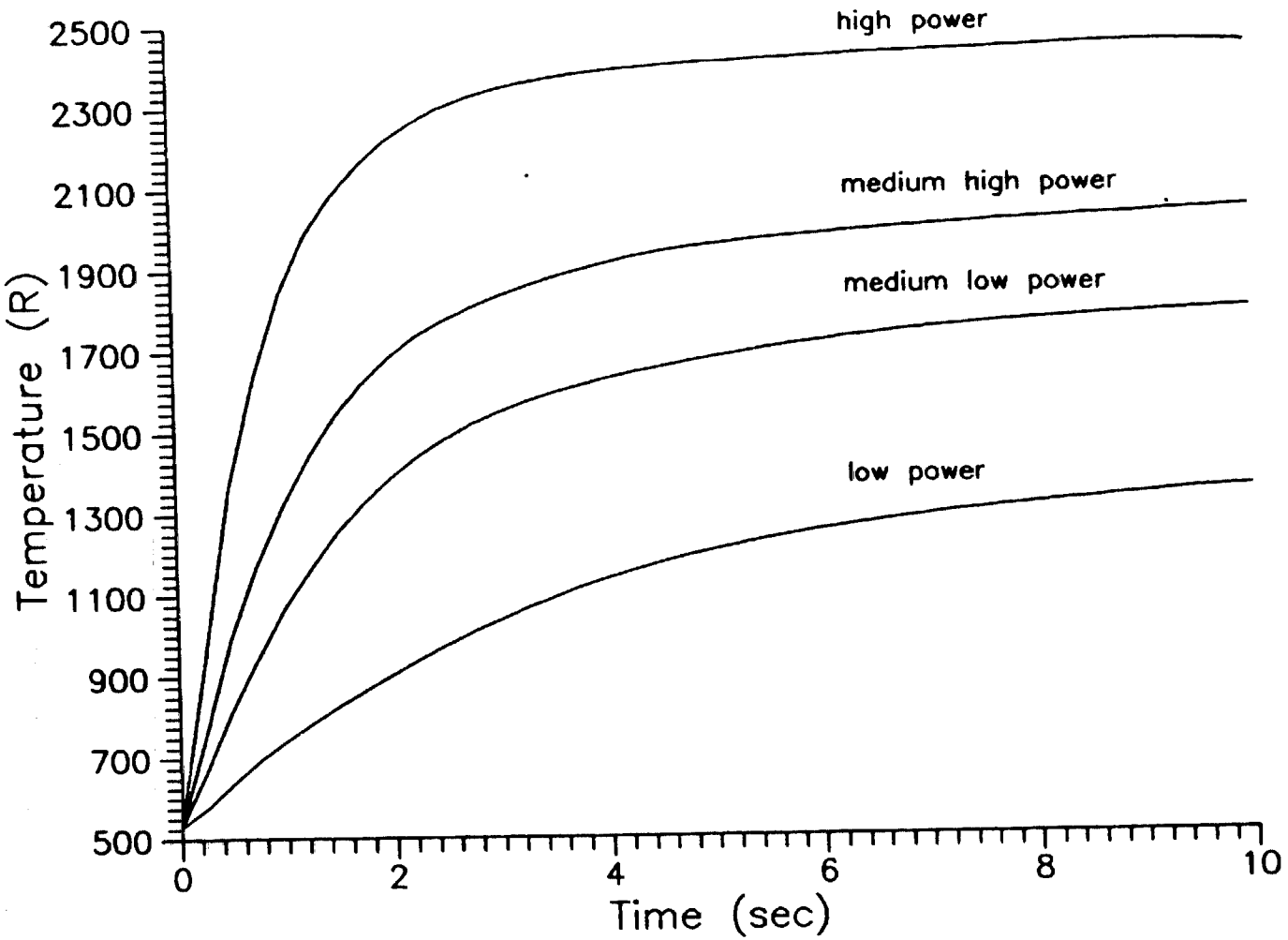

Figure IV.10 - Heated Wall Temperature Averaged Along the Center Line for Each Power Level

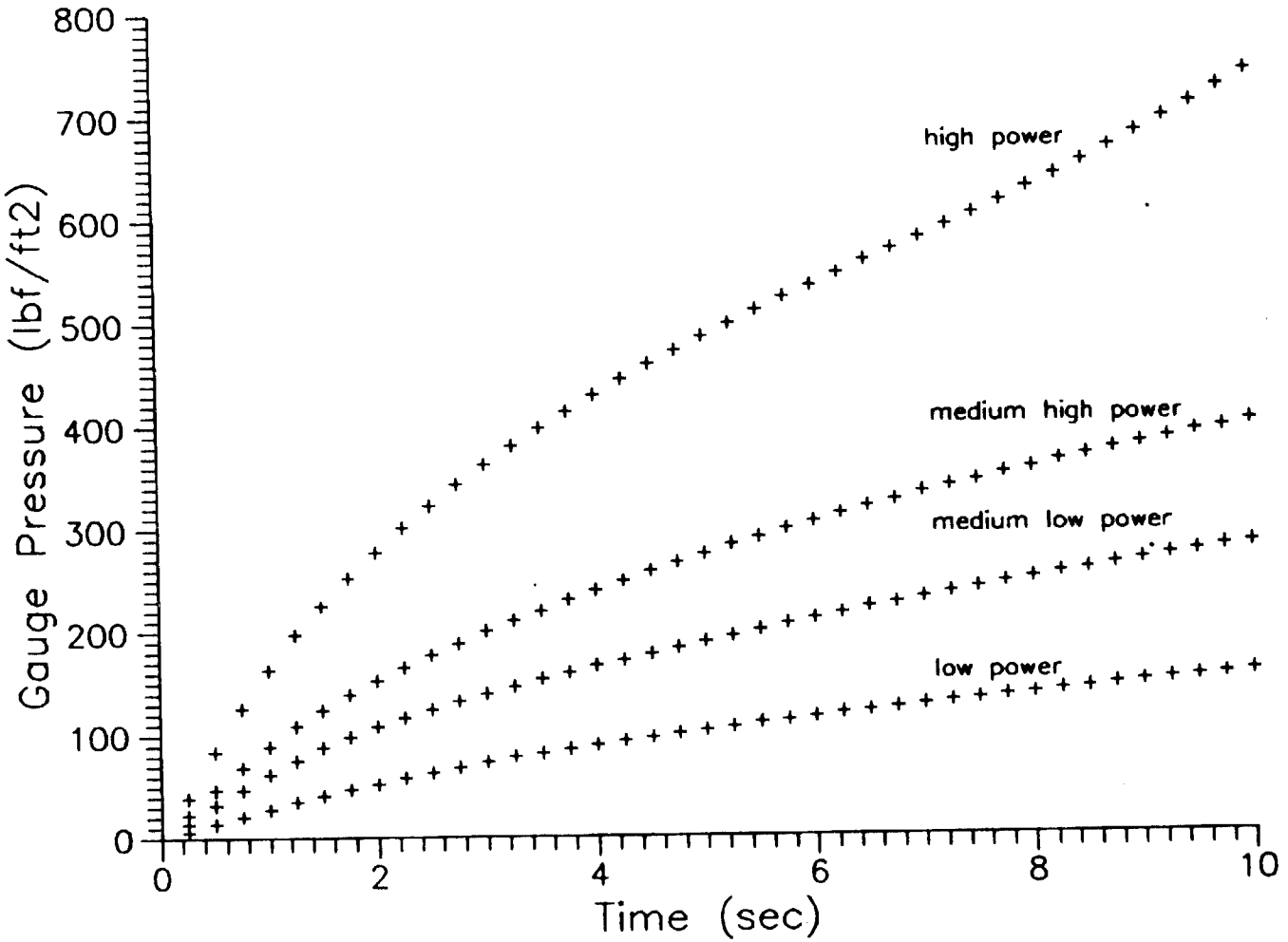

Figure IV.11 - Measured Pressure as a Function of Time for Each Power Level

(see Figure III.4). The square-root quantity represents the distance along the undeflected beam image on the screen. The laser deflection at times 0.5, 1.0, 2.0, 5.0, and 10.0 seconds are presented in Figures IV.12 through IV.15 as a function of the distance from the heated wall at each power level.

4. Temperature Profile

Equation (11) can be used to relate the laser deflection to the temperature of the air. All factors in Equation (11), except T and $\partial T/\partial y$, are known quantities, including the pressure which has been measured as a function of time and the laser deflection which has been measured as a function of time and y. The temperature T_w of the heated wall is required as a boundary condition for Equation (11) and has been measured as a function of time. Equation (11) can be written as

$$\frac{dT}{dy} = K T^2 y_s \qquad (22)$$

since, for a given time, T is assumed to be only a function of y. From Equation (11), K is

$$K = -\frac{\rho_0 R}{(n_0 - 1) P L z_s} \qquad (23)$$

The temperature can be found from a Taylor series expansion of the temperature profile. The following equations can be written directly

$$\begin{aligned}
T_i &= T_{i-1} + \Delta x_i T'_{i-1} + \frac{\Delta x_i^2}{2} T''_{i-1} + \ldots \\
T_{i-1} &= T_i - \Delta x_i T'_i + \frac{\Delta x_i^2}{2} T''_i + \ldots \\
T_i &= T_{i+1} - \Delta x_{i+1} T'_{i+1} + \frac{\Delta x_{i+1}^2}{2} T''_{i+1} + \ldots \\
T_{i+1} &= T_i + \Delta x_{i+1} T'_i + \frac{\Delta x_{i+1}^2}{2} T''_i + \ldots
\end{aligned} \qquad (24)$$

where each i represents a discrete location along y, and primes indicate derivatives with respect to y. Equations (24) can be combined to give

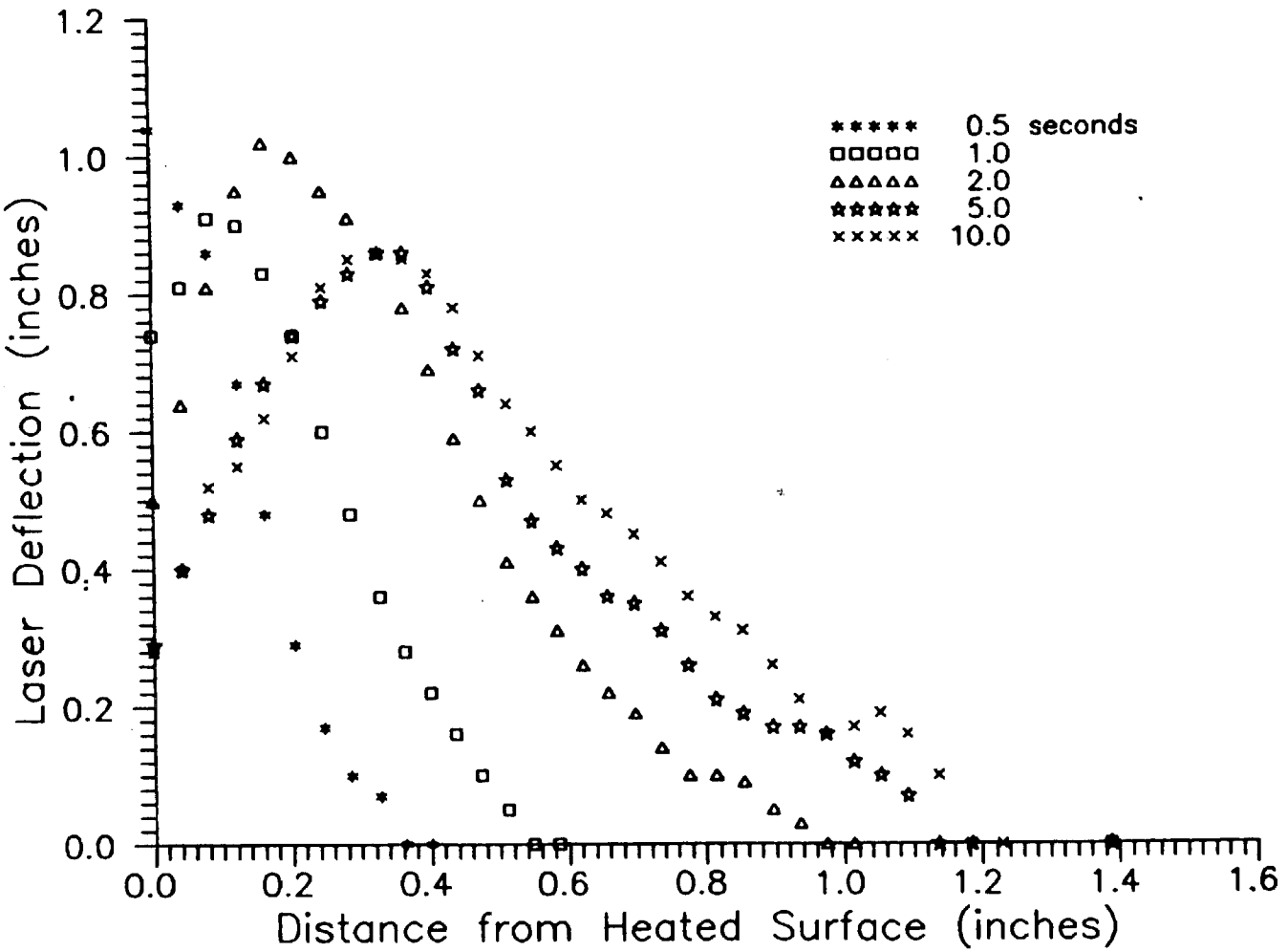

Figure IV.12 - Laser Deflection as a Function of Distance from the Heated Wall for Low Power

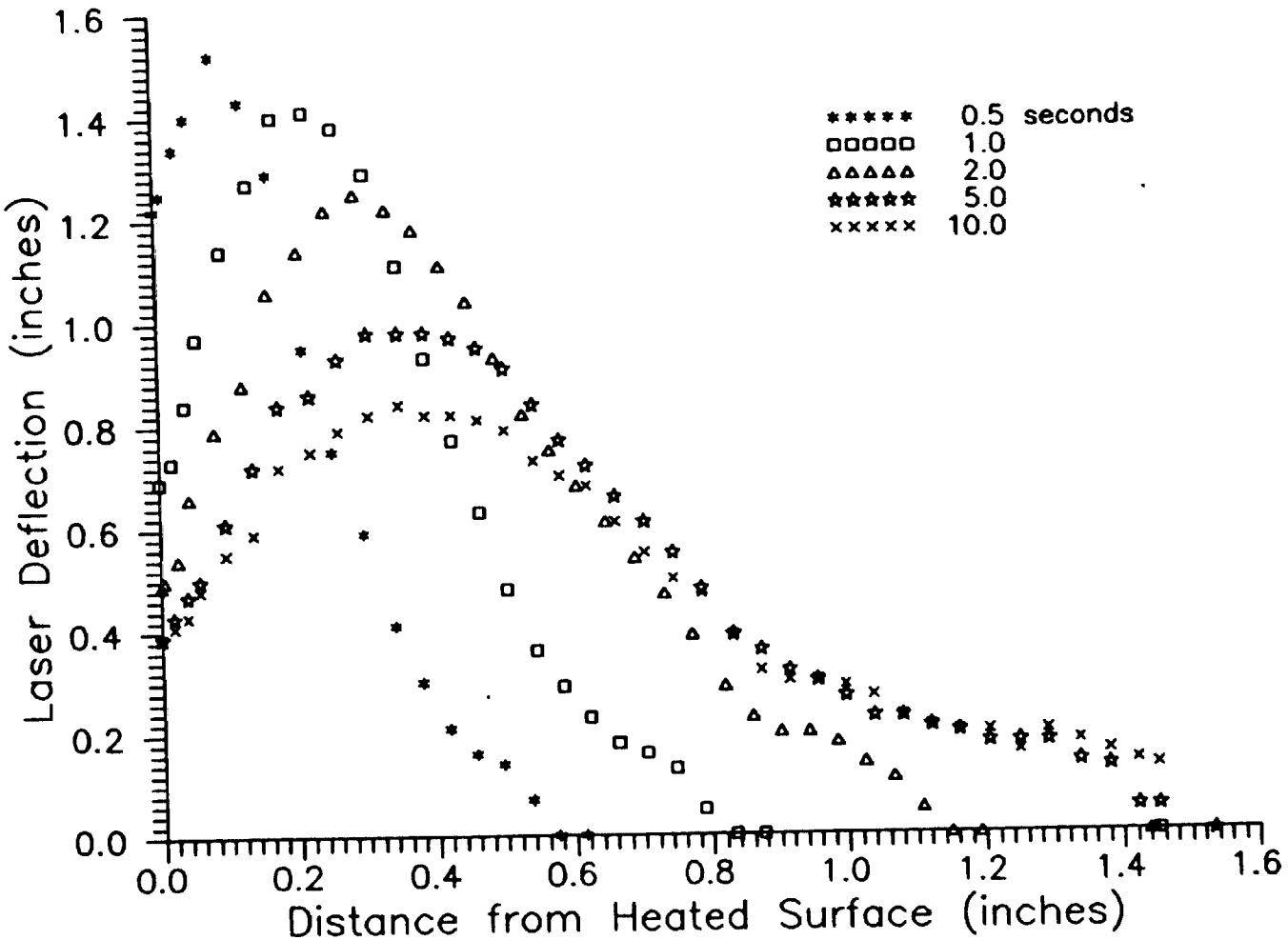

Figure IV.13 - Laser Deflection as a Function of Distance from the Heated Wall for Medium Low Power

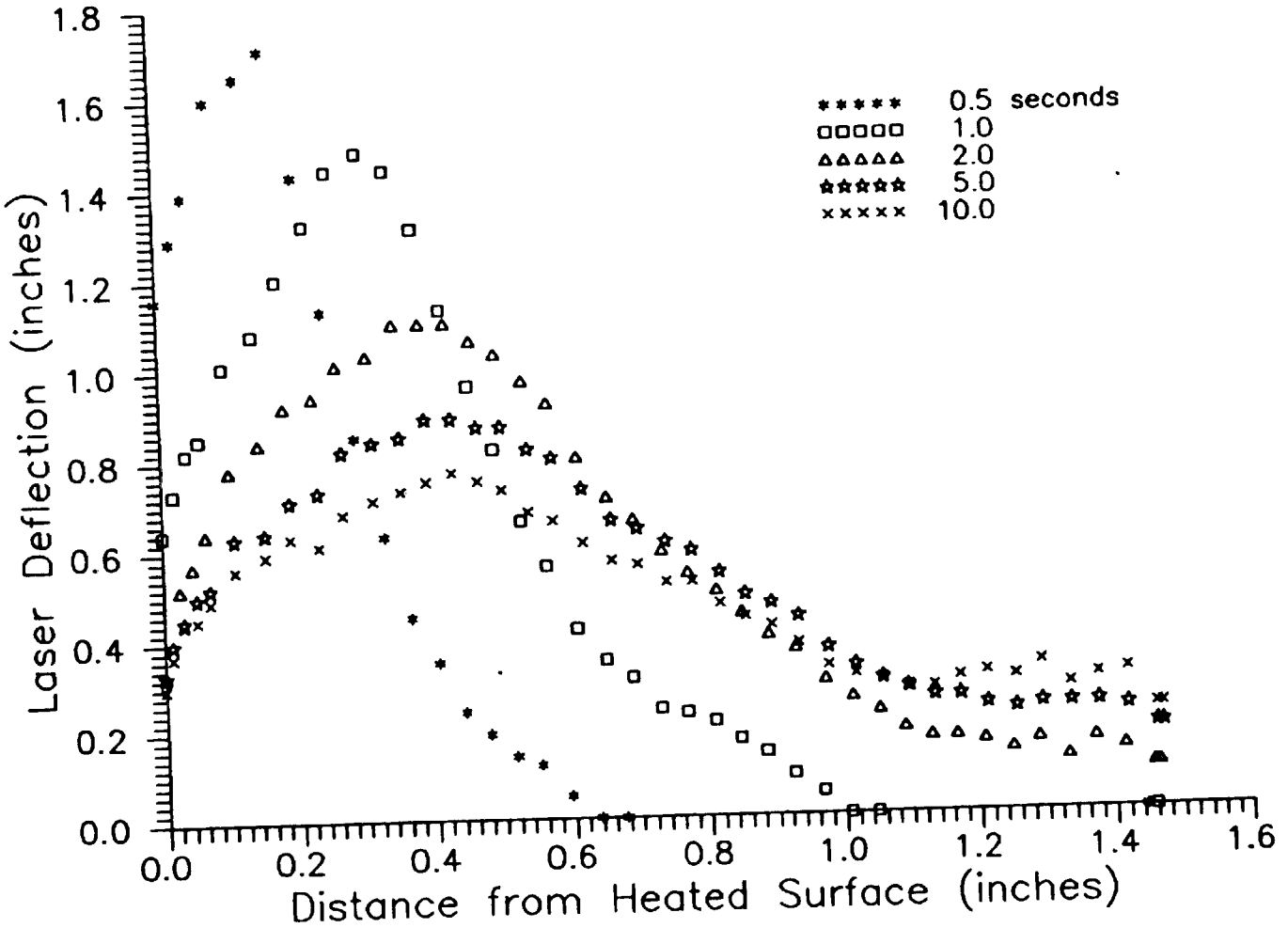

Figure IV.14 - Laser Deflection as a Function of Distance from the Heated Wall for Medium High Power

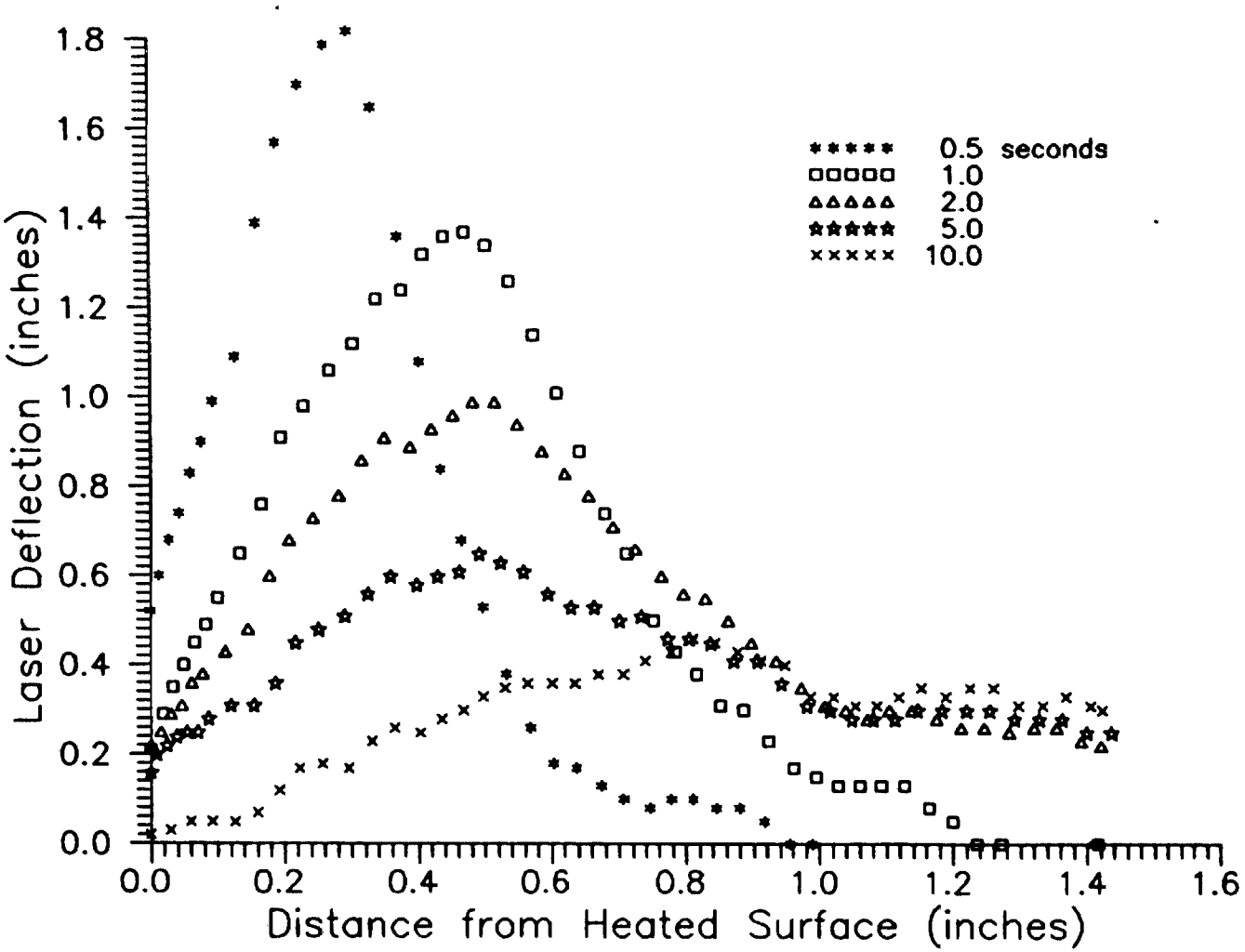

Figure IV.15 - Laser Deflection as a Function of Distance from the Heated Wall for High Power

$$T_i = \frac{1}{2}(T_{i-1} + T_{i+1}) + \frac{\Delta x_i}{4}(T'_{i-1} + T'_i) \qquad (25)$$

$$- \frac{\Delta x_{i+1}}{4}(T'_i + T'_{i+1}) + O(\Delta x^2)$$

Equation (25), along with Equations (22) and (23), can be solved for each T_i. Since T' = f(T^2), the solution must be found iteratively. The O (Δx^2) terms were found to be negligibly small and were dropped from the expansion. The above formulation (Equation (24)), which includes derivative approximations from both sides of T_i, prevents accumulated error which may occur with a solution that marches in one direction from the known derivative at the wall.

The measured temperature profile extends only as far from the wall as the laser beam which was approximately 1.4 inches for the ground experiment. If dT/dy was not zero at the "end" of the measured temperature profile, the profile was extended. The point where dT/dy=0 is

$$y_b = y_e + \left[\frac{dT/dy}{d^2T/dy^2}\right]_e \qquad (26)$$

where the subscript b indicates the edge of the temperature boundary and the subscript e indicates the end of the laser beam. The temperature is extended linearly so that

$$T_b = T(y_b) = T_e + (y_b - y_e)\left(\frac{1}{2}\right)\frac{dT}{dy} \qquad (27)$$

The temperature profiles at various times are shown for each power level in Figures IV.16 through IV.19. It is important to note that neither T_e nor T_b are specified in the solution of the temperature profile. The temperature T_c far from the wall, or core temperature will be the initial temperature T_o plus a small temperature rise due to pressure work. The proximity of T_b to T_c is an indication of the accuracy of the results.

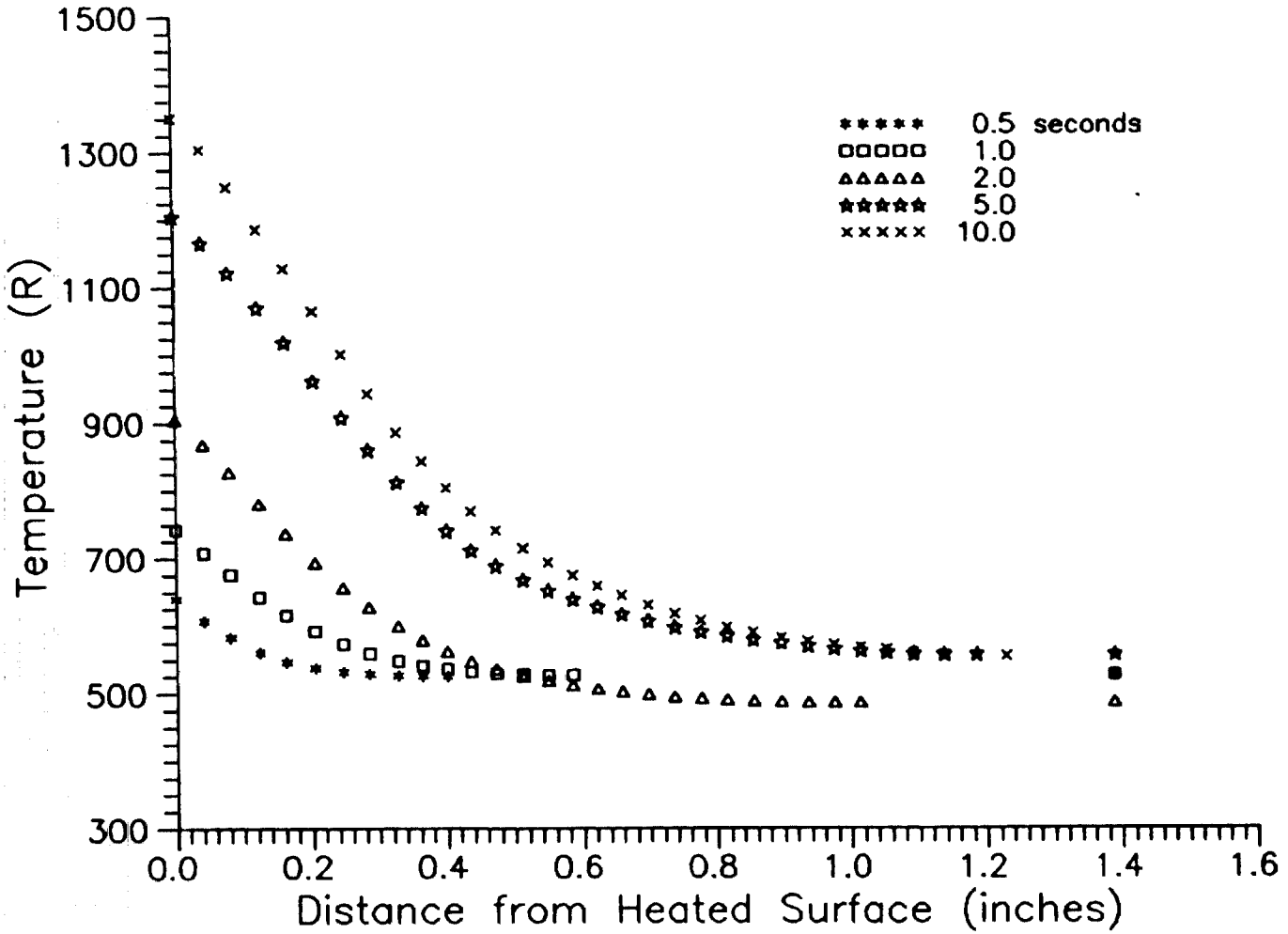

Figure IV.16 - Temperature as a Function of Distance from the Heated Wall for Low Power

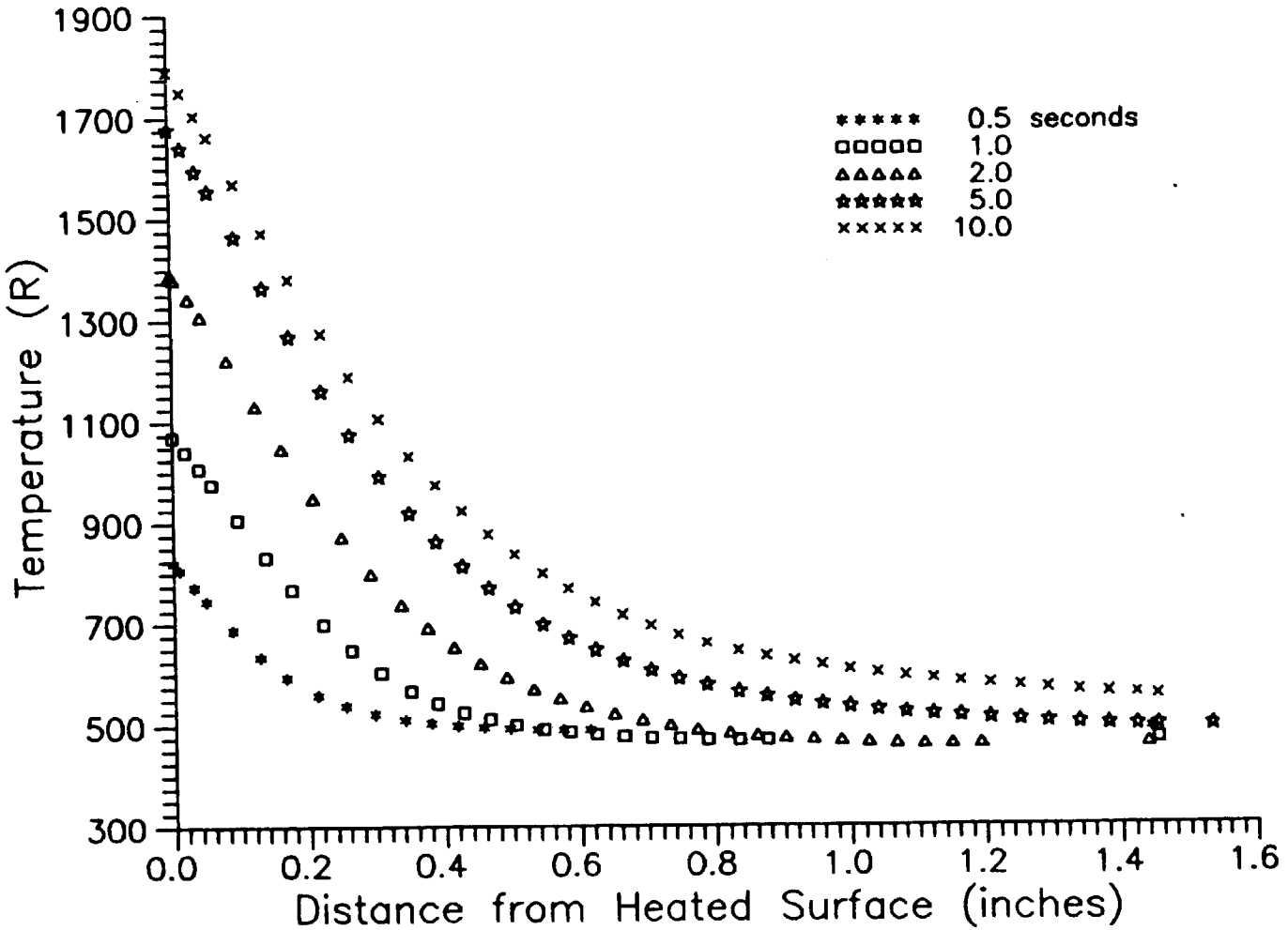

Figure IV.17 - Temperature as a Function of Distance from the Heated Wall for Medium Low Power

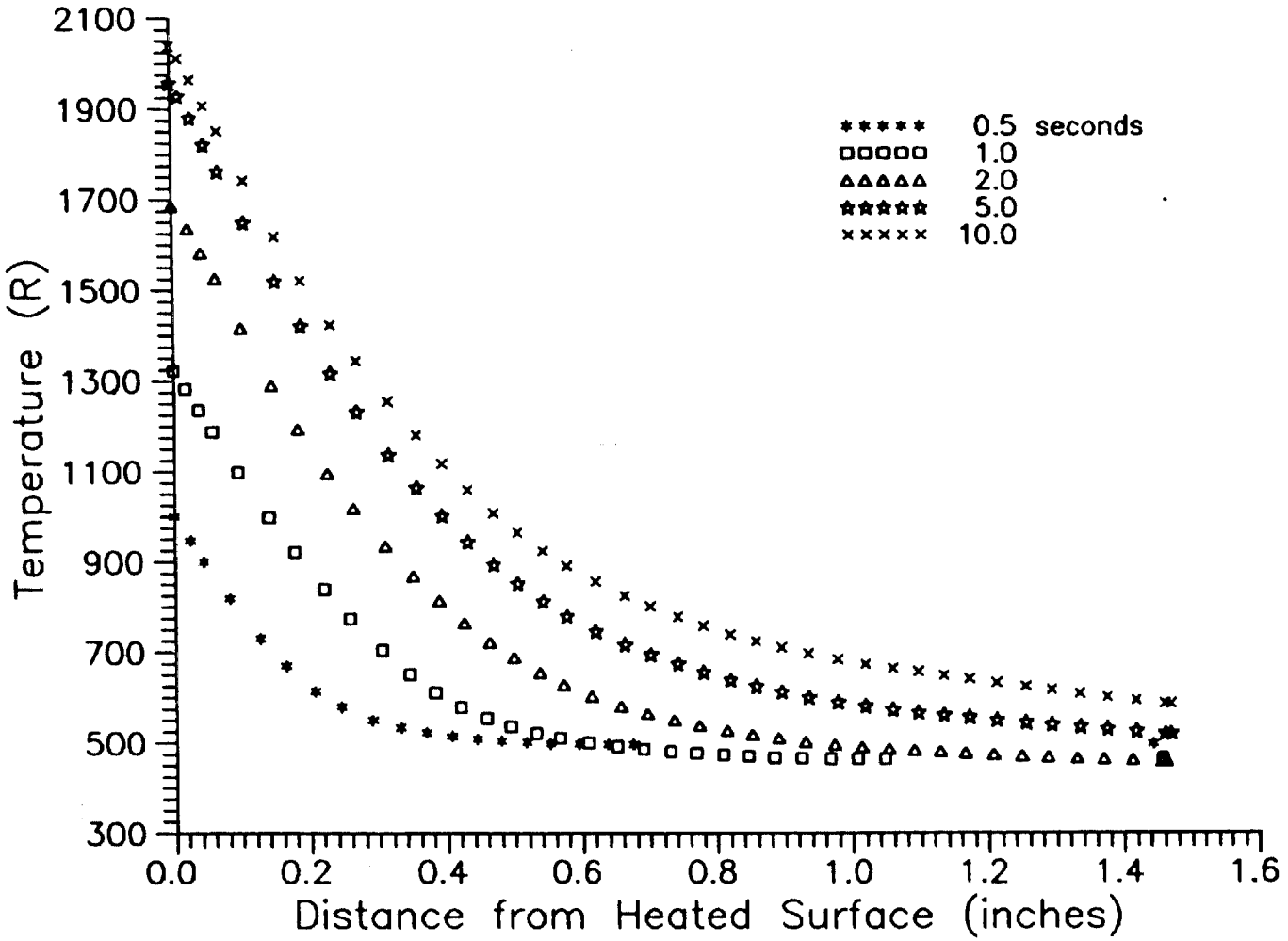

Figure IV.18 - Temperature as a Function of Distance from the Heated Wall for Medium High Power

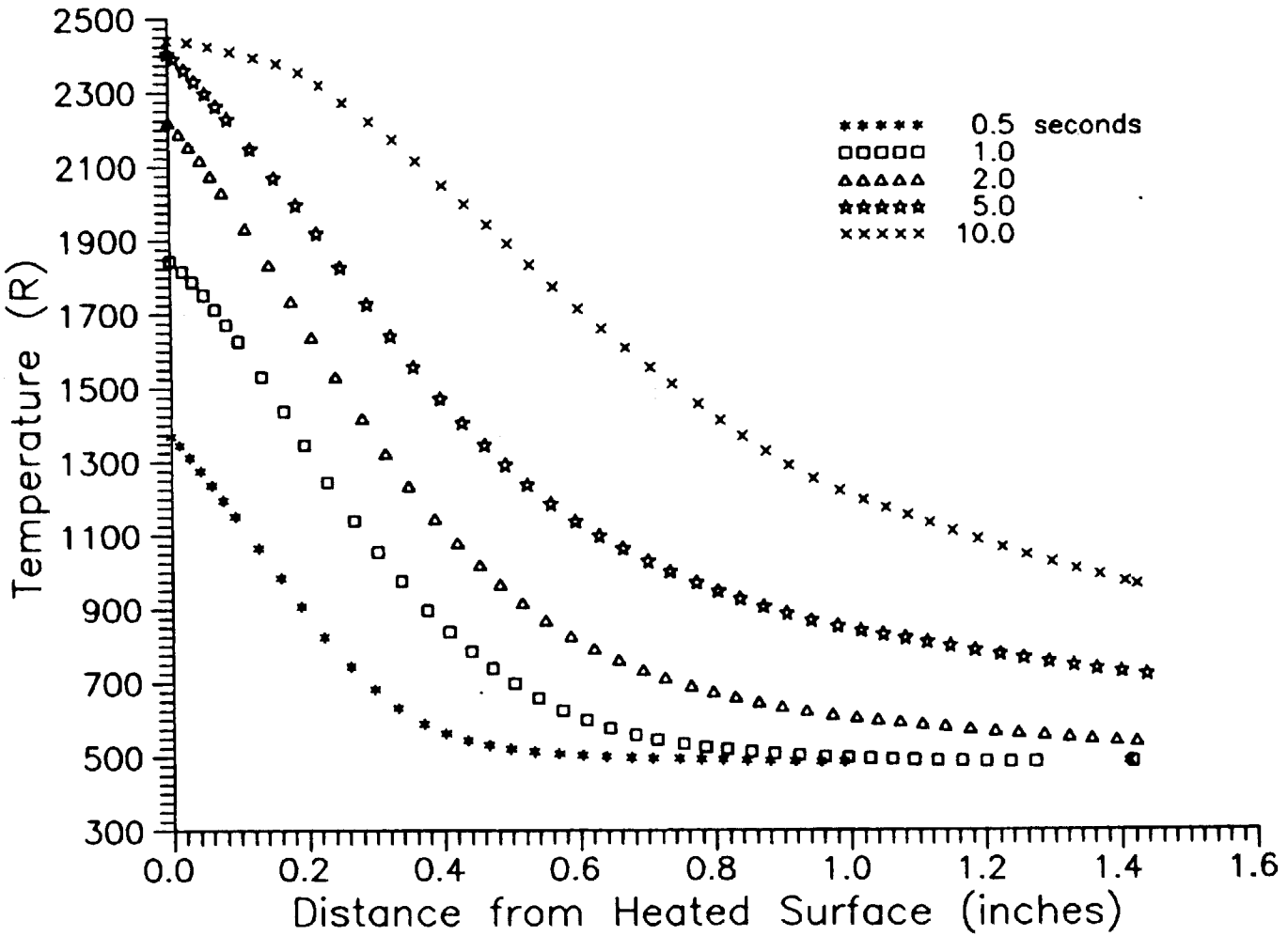

Figure IV.19 - Temperature as a Function of Distance from the Heated Wall for High Power

5. Temperature Correction

Since T_b cannot be expected to be exactly equal to T_c, the temperature profile is adjusted as follows

$$T_{a_i} = T_i - (T_b - T_c)\left[\frac{(T_w - T_i)}{(T_w - T_b)}\right] \qquad (28)$$

where T_a is the adjusted temperature. The core temperature can be chosen such that the measured gauge pressure equals the gauge pressure calculated from the temperature profile.

The absolute pressure can be determined from the temperature profile as

$$P = \frac{R}{(H + H_{ex})} \int_0^{(H+H_{ex})} \rho\, T\, dy \qquad (29)$$

Equation (29) includes the height H of the test section which has been modified to include an "extra" volume enclosed in the heated cavity apparatus but not part of the actual test section (a 4x4x4 inch cube). The total free volume in the heated cavity apparatus was measured by measuring the volume of water it would hold. This volume was 114.6 in^3 which is 1.79 times the test section volume. The extra volume is represented by an equivalent height, H_{ex} = 0.79H. The density in Equation (29) is found from ρ = P/RT after assuming an initial value for pressure. Iteration is performed until continuity is satisfied, i.e.,

$$\frac{1}{(H + H_{ex})} \int_0^{(H+H_{ex})} \rho\, dy = 1 \qquad (30)$$

The adjusted temperature T_{ai} and the core temperature T_c can be determined by iteration of Equations (28), (29) and (30). The adjusted temperature profiles are shown in Figures IV.20 through IV.23.

Another way to correct the temperature profile is to determine T_c by performing an energy balance between the thermal boundary layer and the core region. This is discussed in Appendix C.

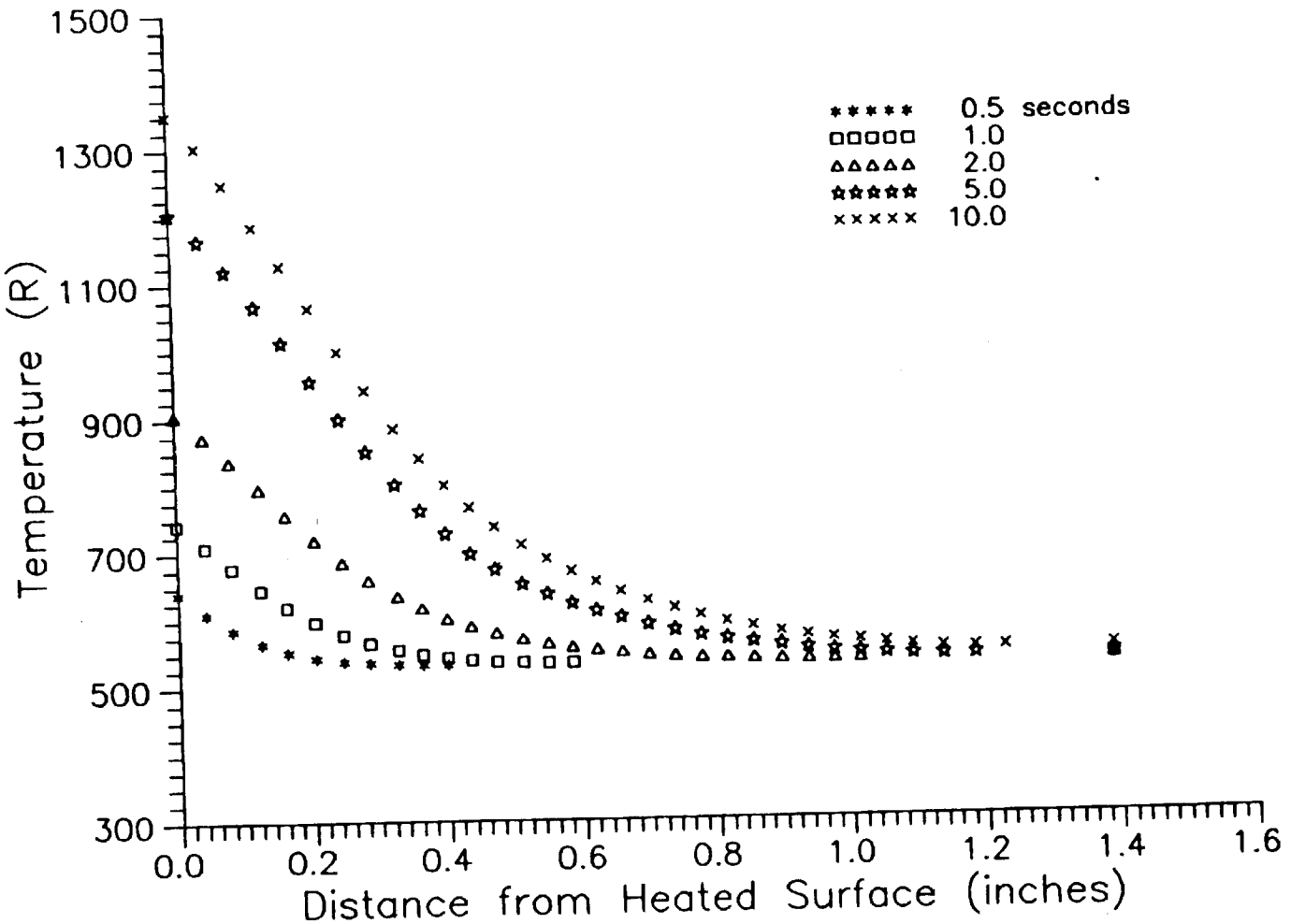

Figure IV.20 - Corrected Temperature as a Function of Distance from the Heated Wall for Low Power

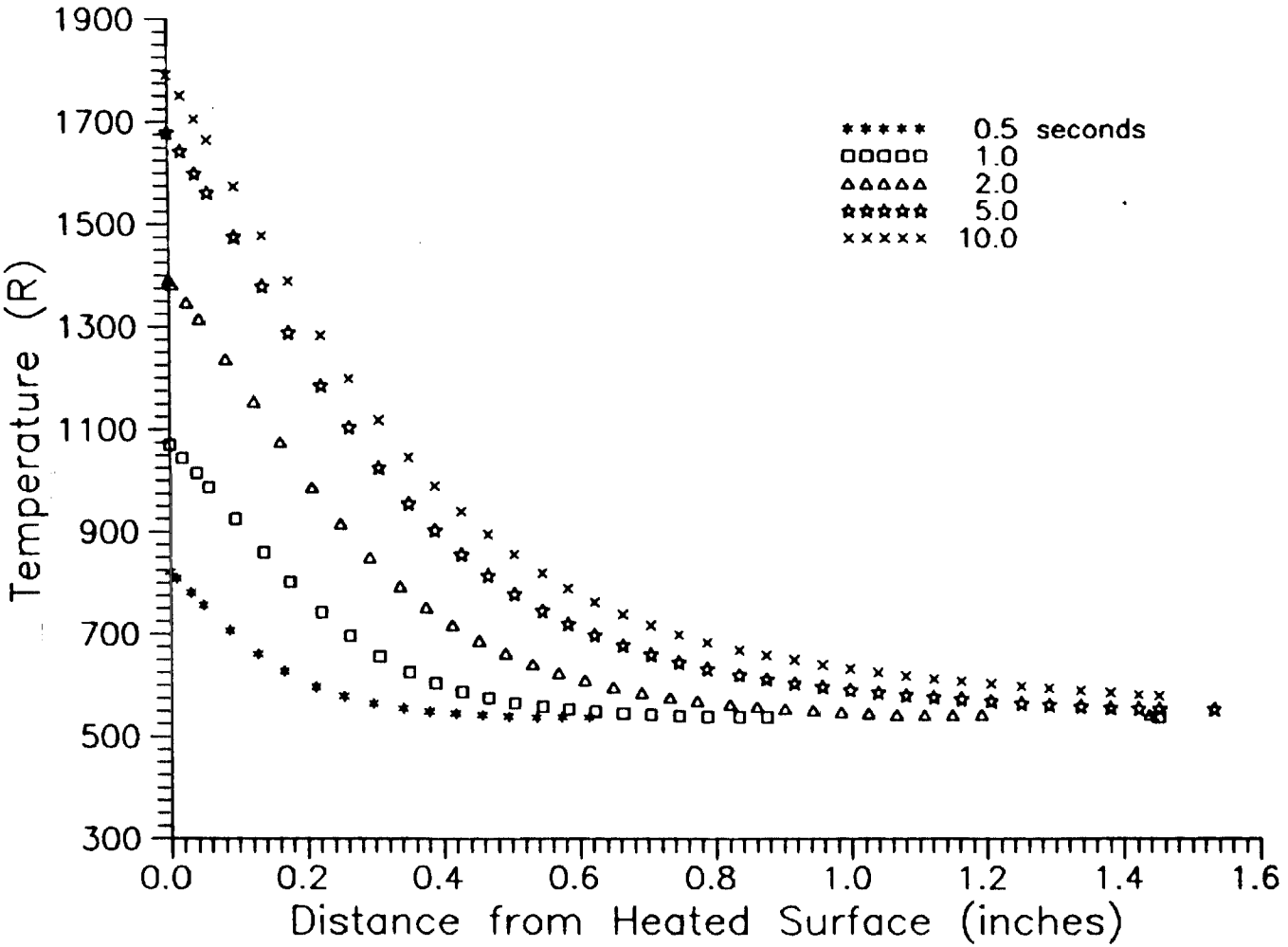

Figure IV.21 - Corrected Temperature as a Function of Distance from the Heated Wall for Medium Low Power

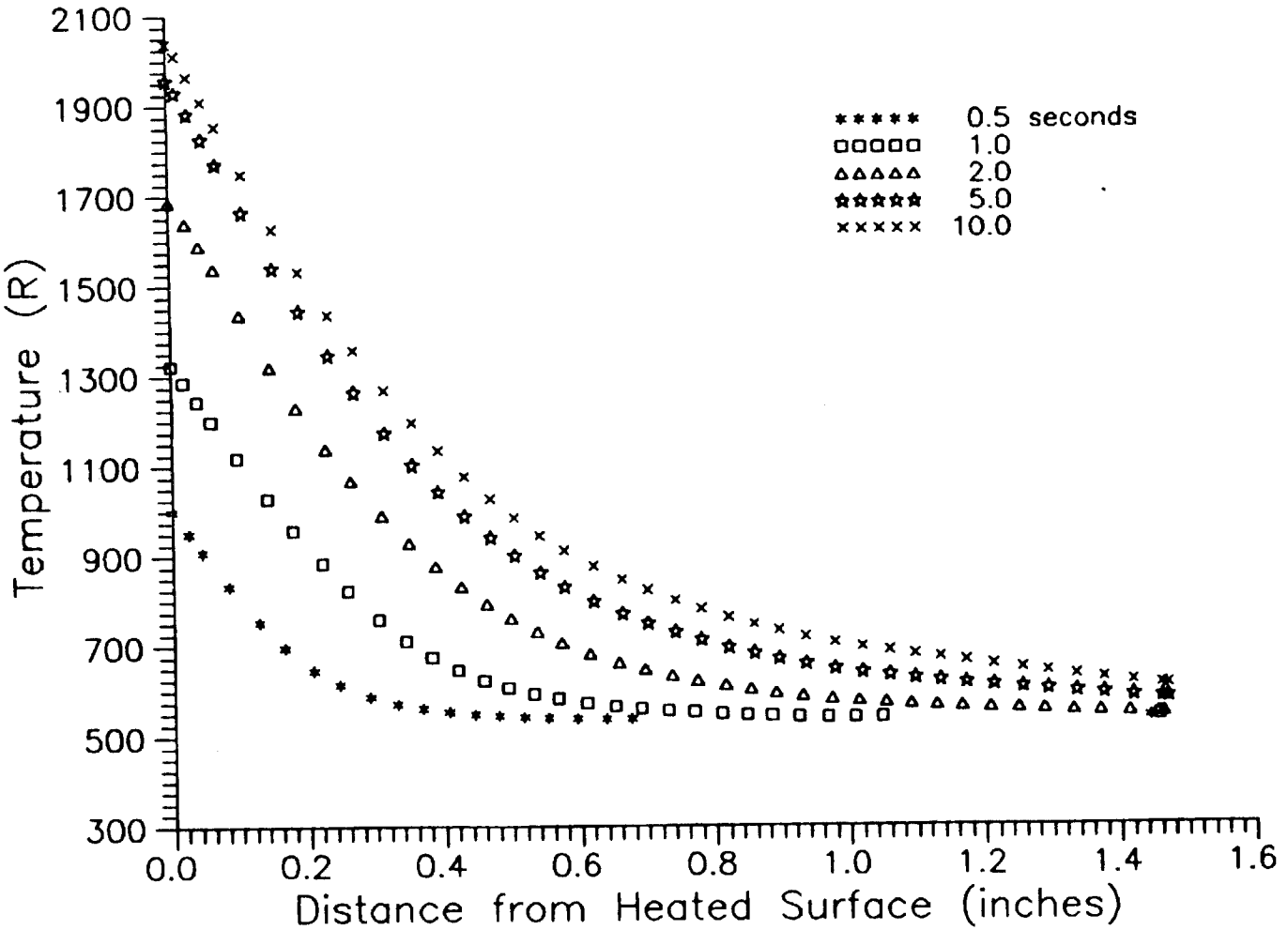

Figure IV.22 - Corrected Temperature as a Function of Distance from the Heated Wall for Medium High Power

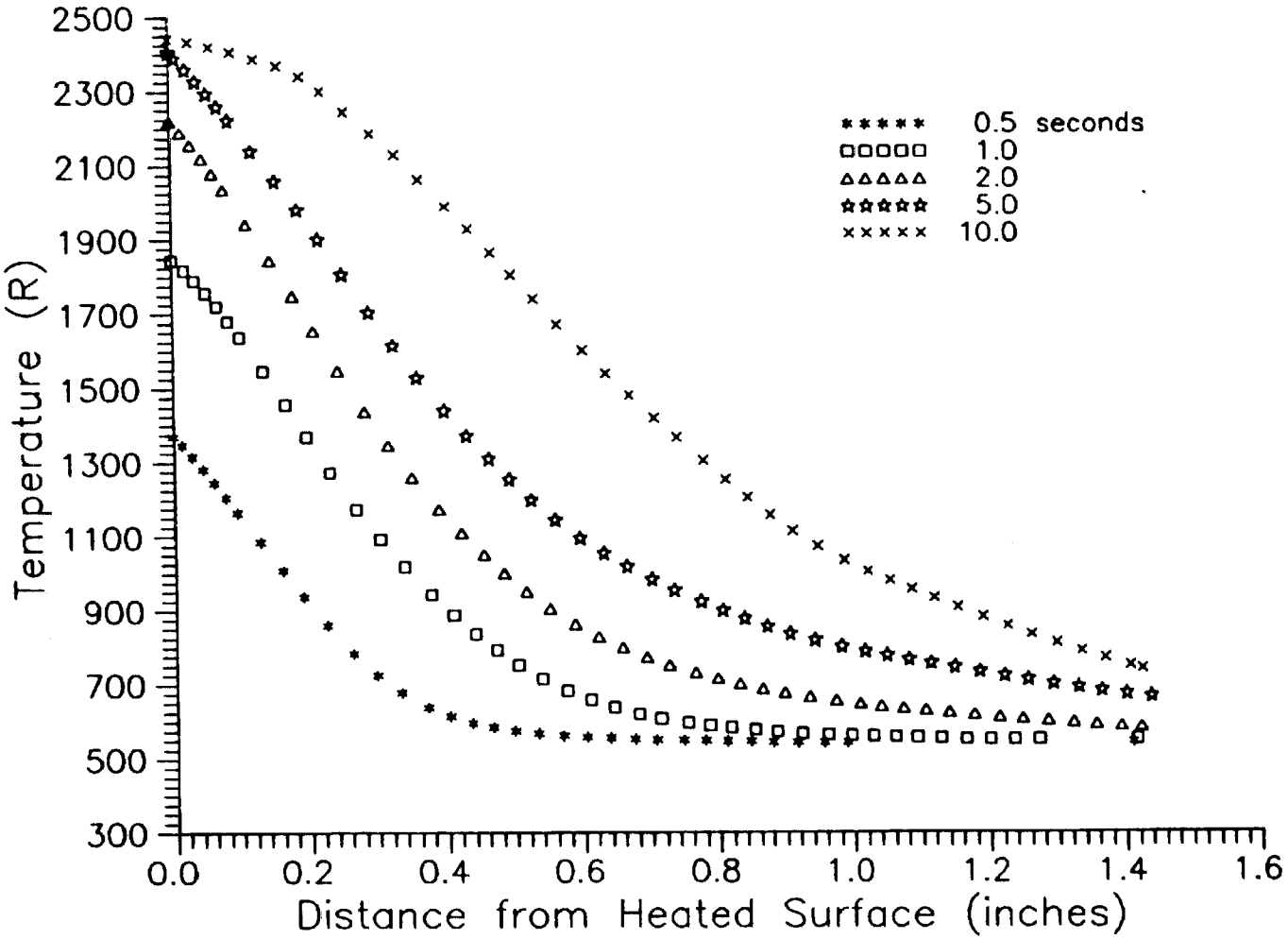

Figure IV.23 - Corrected Temperature as a Function of Distance from the Heated Wall for High Power

6. Core Air Velocity

The velocity of the air in the core was measured with a hot-film velocity meter. The air velocity as a function of time for high power is shown in Figure IV.24.

C. Error Analysis

An analysis to determine the maximum error in the measured temperature profile has been performed. Several sources of error have been identified and are discussed below:

a) Laser Sheet Deflection - The least count measurement of the video image is one pixel, however, imperfect sharpness of the laser sheet at the screen can increase the uncertainty.

b) Heated Wall Flatness Correction - If the heated wall is not perfectly flat and parallel to the laser beam direction, the end of the laser sheet nearest the heated wall will not be exactly adjacent to the heated wall. The end of the laser sheet will actually pass an average distance h away from the wall. This distance may change with time if the heated wall deforms as it is heated. This changing distance, Δf, can be estimated by the change in the location of the end of the laser sheet on the screen. The corrected temperature profile is obtained by assuming that $\partial T/\partial y$ at the wall is equal to $\partial T/\partial y$ at h.

c) Wall Temperature - Although thermocouple measurements should be accurate within $\pm$ 2°R, ground experimental measurements indicate larger uncertainty even near the center where the end effects are minimal. Heated wall temperature variations were probably caused by a varying level of contact pressure with insulation behind the heated wall. This problem can be minimized by providing a small gap between the heated wall and insulation.

d) Test Section Length, L - A significant source of error in L (see Figure III.6) is the gaps between the edges of the heated wall and the glass side walls. These gaps is necessary to avoid heat damage to the glass. The error in L will not be as large as the gaps, however, since the gap space is not directly heated.

e) Other Dimensions - There is uncertainty in the measurement of the following quantities: the laser path length z_s to the screen,

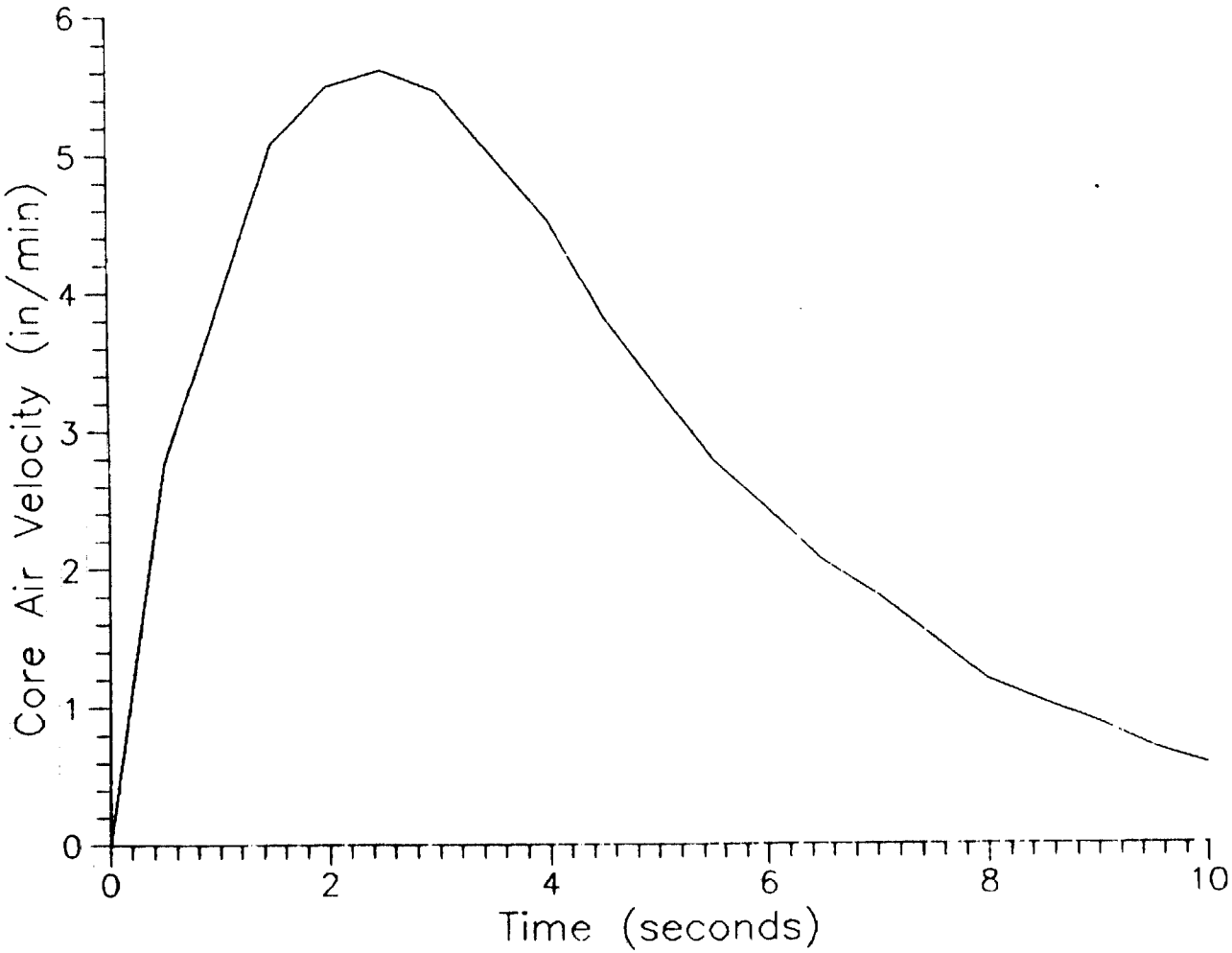

Figure IV.24 - Average Air Velocity in the Test Section Core as a Function of Time for High Power

the angle θ and width w of the laser sheet in the test section (see Figure III.4).

f) Three-Dimensional Effects - The temperature of both the heated wall and the air will be affected by the side walls. This effect has been measured and accounted for. Effects on the air temperature were estimated by numerical approximation since their experimental measurement was difficult.

The uncertainty for the above sources of error has been estimated and the effects on the temperature profile determined. The results for the temperature profile for medium high power at 5.0 seconds are given in Table 3 and Figure IV.25. Table 3 gives the sign and magnitude of the maximum temperature error as a percent of the heated wall temperature rise for each source of error. Note that the wall flatness correction is always positive, but results in increased temperature near the wall and decreased temperature at the edge of the temperature profile. The worst-case high and low percent error is also given. Figure IV.25 shows a plot of the temperature profile with a worst case high and low band. The error band is biased toward higher temperatures because of the effects of the wall flatness correction and the uncertainty in the test section length.

Table 3. Temperature for Medium High Power, Time = 5.0 seconds

Uncertain Quantity	Amount of Uncertainty	Maximum Temperature Error as a percent of Wall Temperature Increase
Laser Sheet Deflection	+1 pixel - 1	-2.8 +3.0
Heated Wall Flatness Correction	0.05 + Δf inches	+4.8 -0.5
Wall Temperature, T_w	+40^{o}R - 40	+2.8 -2.8
Test Section Length, L	+0.0167 feet - 0.0	+3.6 0.0
Laser Path Length to Screen, z_s	+0.1667 feet - 0.1667	+0.2 -0.2
Laser Sheet Angle, θ	+1.0^o - 1.0^o	+1.0 -1.0
Width of Laser Sheet, w	+0.025 inches - 0.025	-1.0 +1.0
Worst Case High	-	8.5
Worst Case Low	-	-2.8

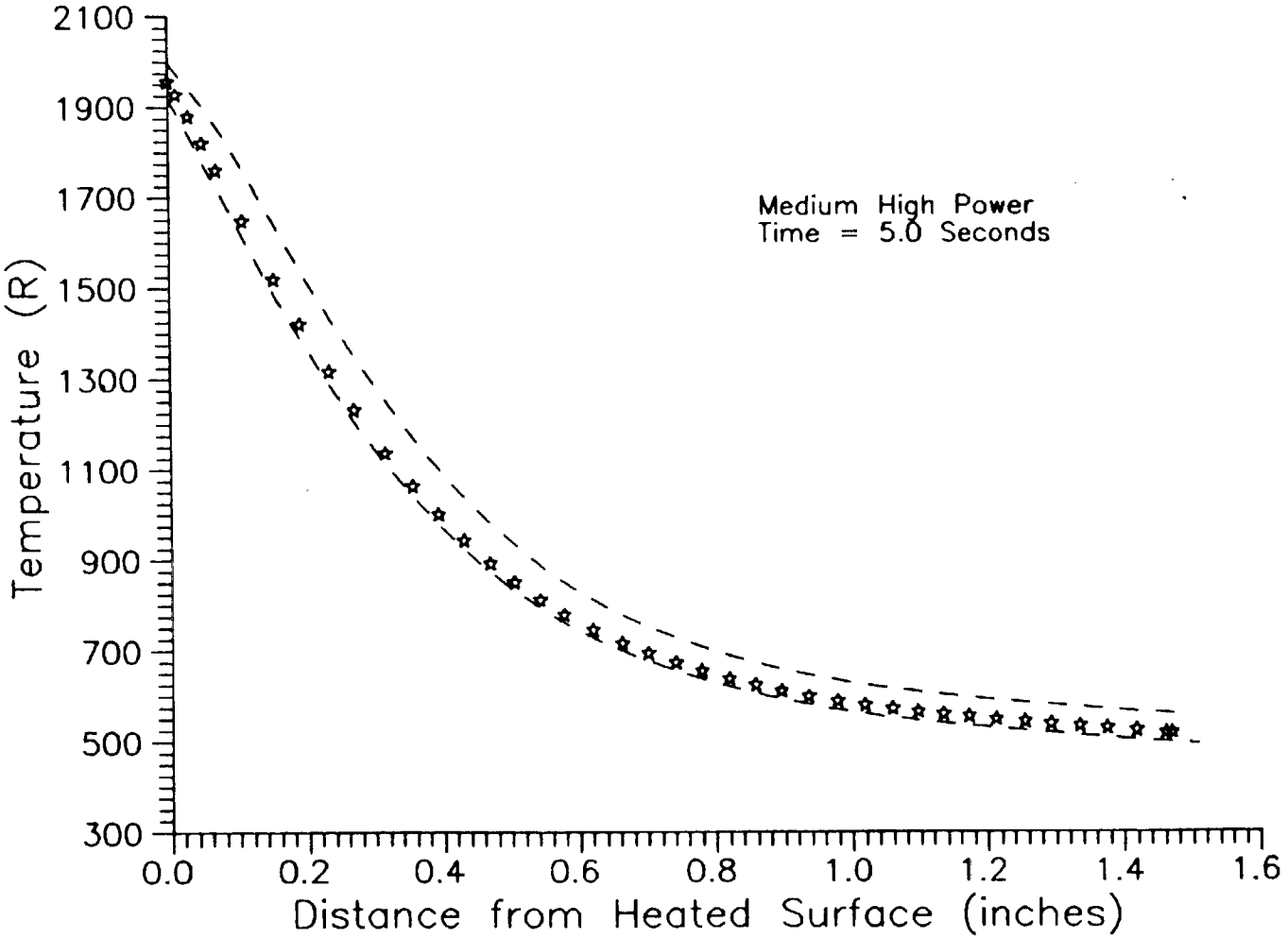

Figure IV.25 - Temperature as a Function of Distance from the Heated Wall with Worst-Case Error Band

V. OUTLINE FOR THE DEVELOPMENT OF FLIGHT EXPERIMENT

The development of the flight experiment and its conclusion includes two major phases. In Phase B the preliminary requirements of the experiment, conceptual design, and project definition and plan are completed. This phase will also require safety documentation, interim review, and final report and review. The required time for the completion of Phase B is 12 months.

In Phase C/D the hardware design and fabrication, assembly and ground testing, development of flight test procedure, flight operations, and data analysis with appropriate documentations are completed. This phase is anticipated to last 24 months.

A schedule for these two phases are shown in Table 4.

Table 4. Thermoacoustic Convection Heat Transfer Experiment

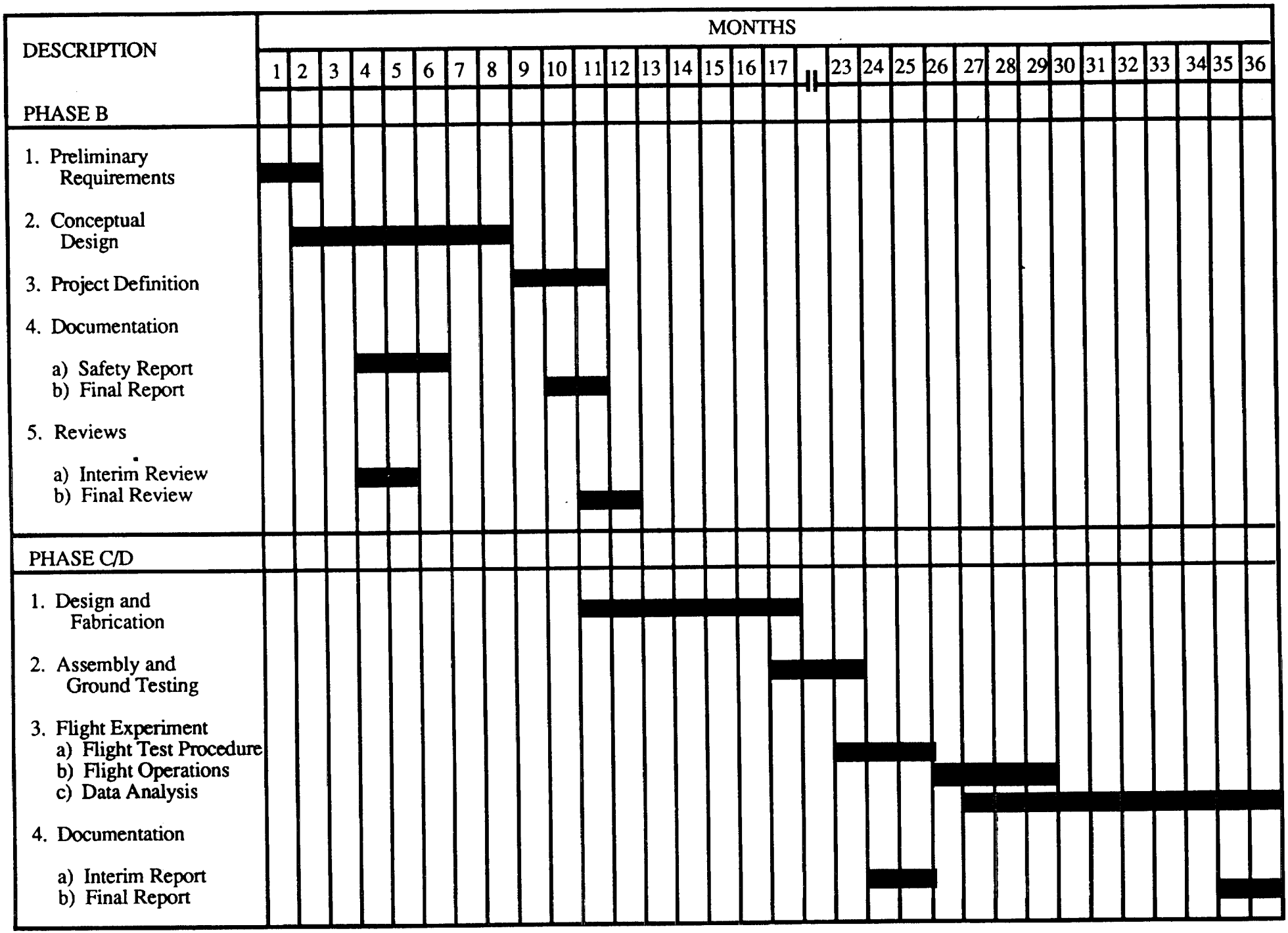

VI. SUMMARY AND CONCLUSION

The potential importance of TAC heat transfer process in space technologies, in particular in cryogenic fluid systems in space environment, were discussed and with background information and previous earth-bound microgravity experimental results are presented in Section I of this report. The specific objectives of the space experiment that included the method to generate TAC process and the measurement of the associated transient fluid temperature and pressure were enumerated in Section II.

The design parameters, the selection criteria and background analysis of the experiment were discussed in some detail in Section III. The description of the ground experiments and a discussion of the experimental results are in Section IV. These results establish the feasibility of the in-space experiment and provide the basis for the post-flight data analysis of the proposed experiment. Finally, Section V includes a plan and schedule for the phases B and C/D for the hardware development and flight tests of the TAC in-space experiment. In Appendix A the technical drawings for the experiment design are presented. Also a detailed description of few selected off-the-shelf hardware items that could potentially be used directly in the space experiment are included in Appendix B.

VII. REFERENCES

1. Clement, J.R., Gaffney, J. "Thermal Oscillations in Low-Temperature Apparatus," Adv. in Cryogenic Eng., Vol. 1, 1960, pp. 302-306.

2. Spradley, L., Bourgeois, S., Fan, C., and Grodzka, P., "A Numerical Solution for Thermoacoustic Convection of Fluids in Low Gravity," NASA CR-22269, May 1973.

3. Larkin, B.K., "Heat Flow to a Confined Fluid in Zero Gravity," Progress in Astronautics and Aeronautics: Planetary Bodies, Vol. 20, 1967, pp. 819-833.

4. Shah, R.K., Ganic, E.N., and Yang, K.T., (editors), "Acoustic and Experimental Methods: The Influence of Sound on Flow and Heat Transfer," Experimental Heat Transfer, Fluid Mechanics, and Thermodynamics, Elservier Science Publishing Co., Inc., New York, 1988.

5. Daney, D.E., Ludtke, P.R., and Jones, M.C., "An Experimental Study of Thermally-Induced Flow Oscillations in Supercritical Helium," J. of Heat Transfer, Vol. 101, pp. 9-14, 1979.

6. Parang, M., "An Experimental and Analytical Investigation of Thermoacoustic Convection Heat Transfer in Gravity and Zero-Gravity Environment," NASA GR-17957, April 1986.

7. Parang, M., and Salah-Eddine, A., "Thermoacoustic Convection Heat Transfer Phenomenon," AIAA Journal, Vol. 22, No. 7, July 1984.

8. Parang, M., and Salah-Eddine, A. "Experiments on Thermoacoutic Convection Heat Transfer in Gravity and Low Gravity Environment," AIAA 22nd Thermophysics Conference, Honolulu, Hawaii, AIAA-87-1651, June 8-10, 1987.

9. Giarrantano, P.J., Kumakawa, A., Arp, V.D., Owen, R.B., "Transient Heat Transfer Studies in Low Gravity Using Optical Measurement Techniques," J. Thermophysics and Heat Transfer, Vol. 4, No. 1, January 1990.

10. Eckert, E.R.G., and Goldstein, R.J., Measurements in Heat Transfer, Second Edition, Hemisphere Publishing Corp., Washington, 1976.

11. Robben, R., Schefer, R., Agrawal, V., Namer, I., "Catalyzed Combustion in a Flat Plate Boundary Layer I . Experimental Measurements and Comparison with Numerical Calculations," Western States Section, Combustion Institute, Paper No. 77-37, Sept. 1977.

12. Parang, M., and Catt, J.A., "Convective Air Motion Generated by Rapid Heating in an Enclosure," AIAA 28th Aerospace Sciences Meeting, Jan. 8-11, 1990, Reno, Nevada, AIAA 90-0412.

APPENDIX A

1) Experiment Component Layout

Detailed drawings of the experiment layout are shown in Figures A-1, A-2 and A-3.

2) Optical System Layout

Detailed drawings of the optical system layout are shown in Figures A-4 through A-7.

3) Heated Cavity

Detailed drawings of the heated cavity apparatus parts are shown in Figures A-8 through A-15.

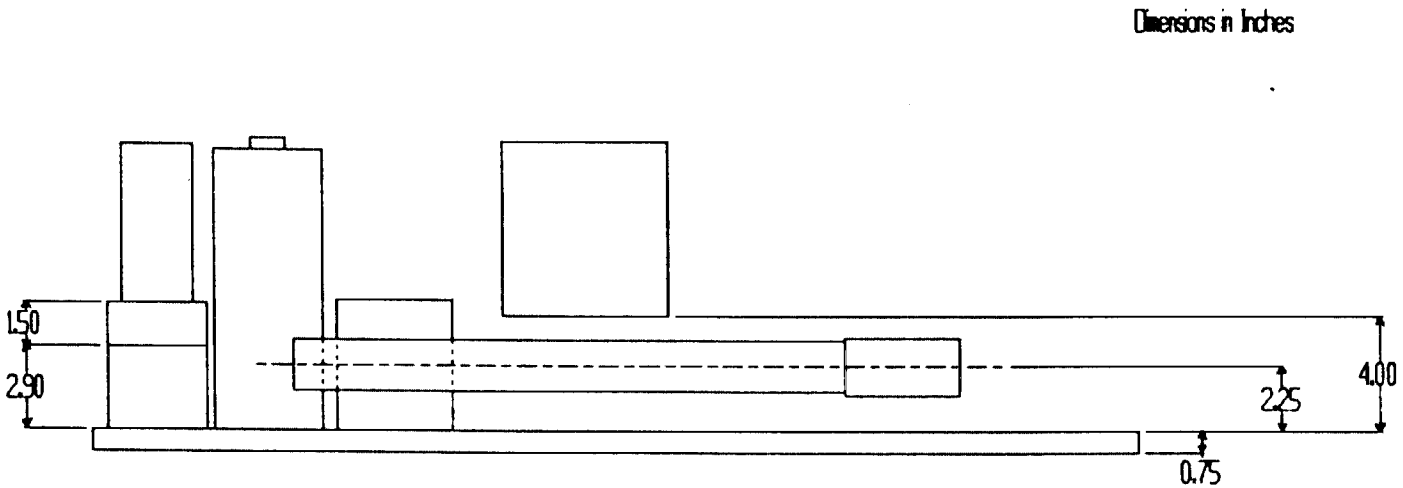

Figure A.1 - Flight Experiment Hardware Layout, Front View

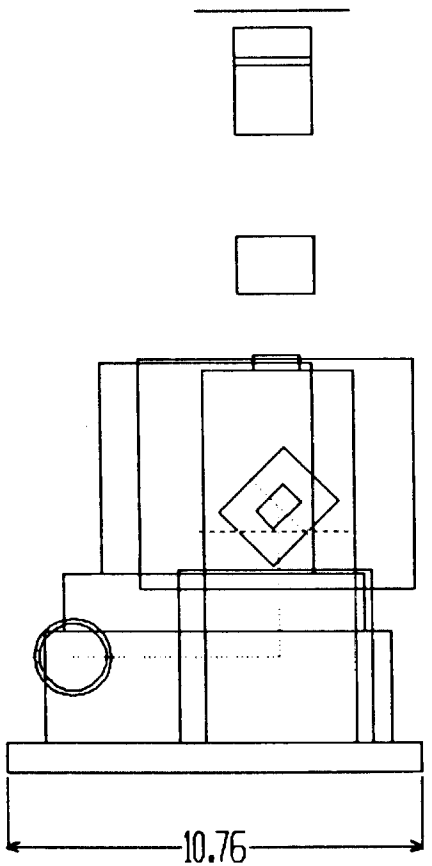

Figure A.2 - Flight Experiment Hardware Layout, Side View

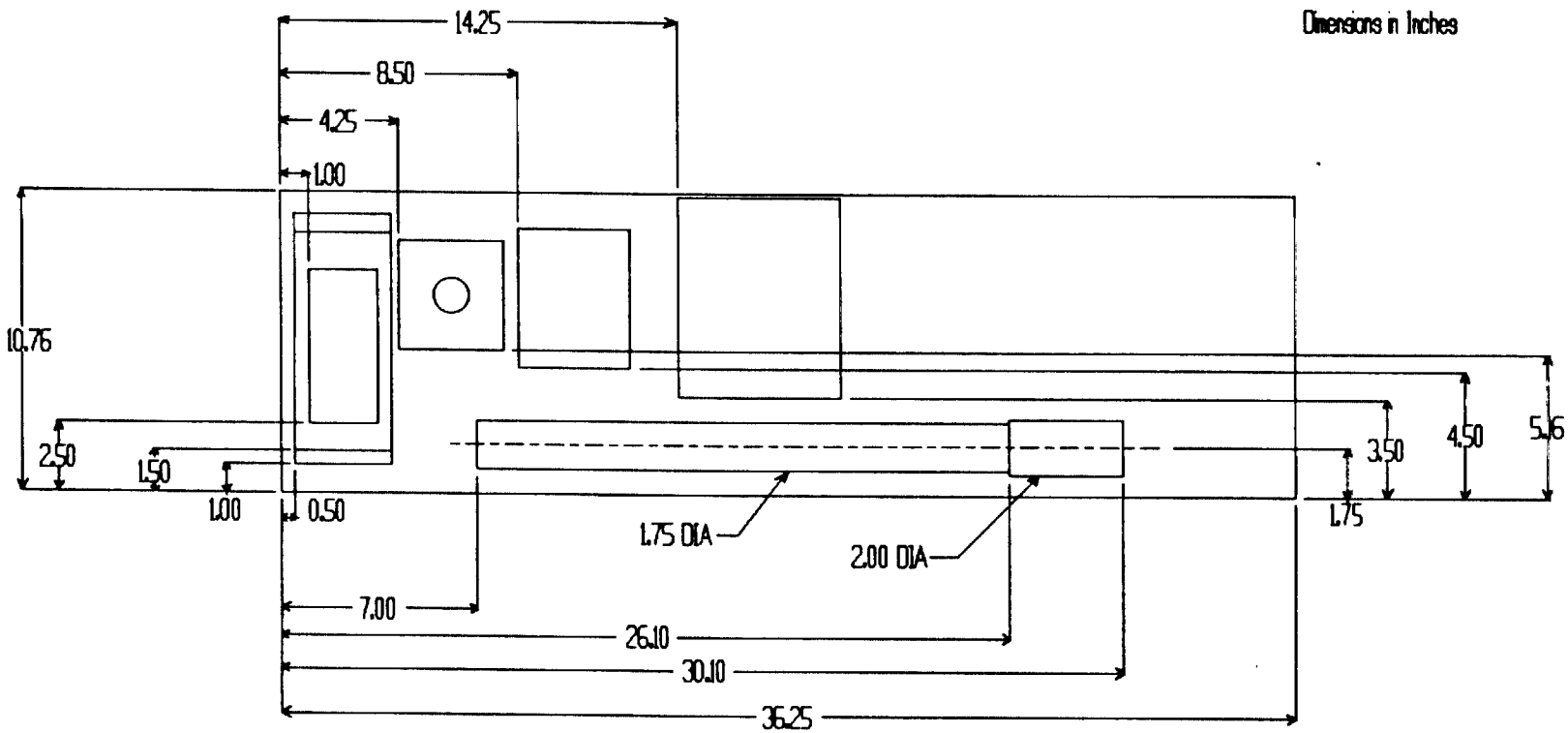

Figure A.3 - Flight Experiment Hardware Layout, Top View

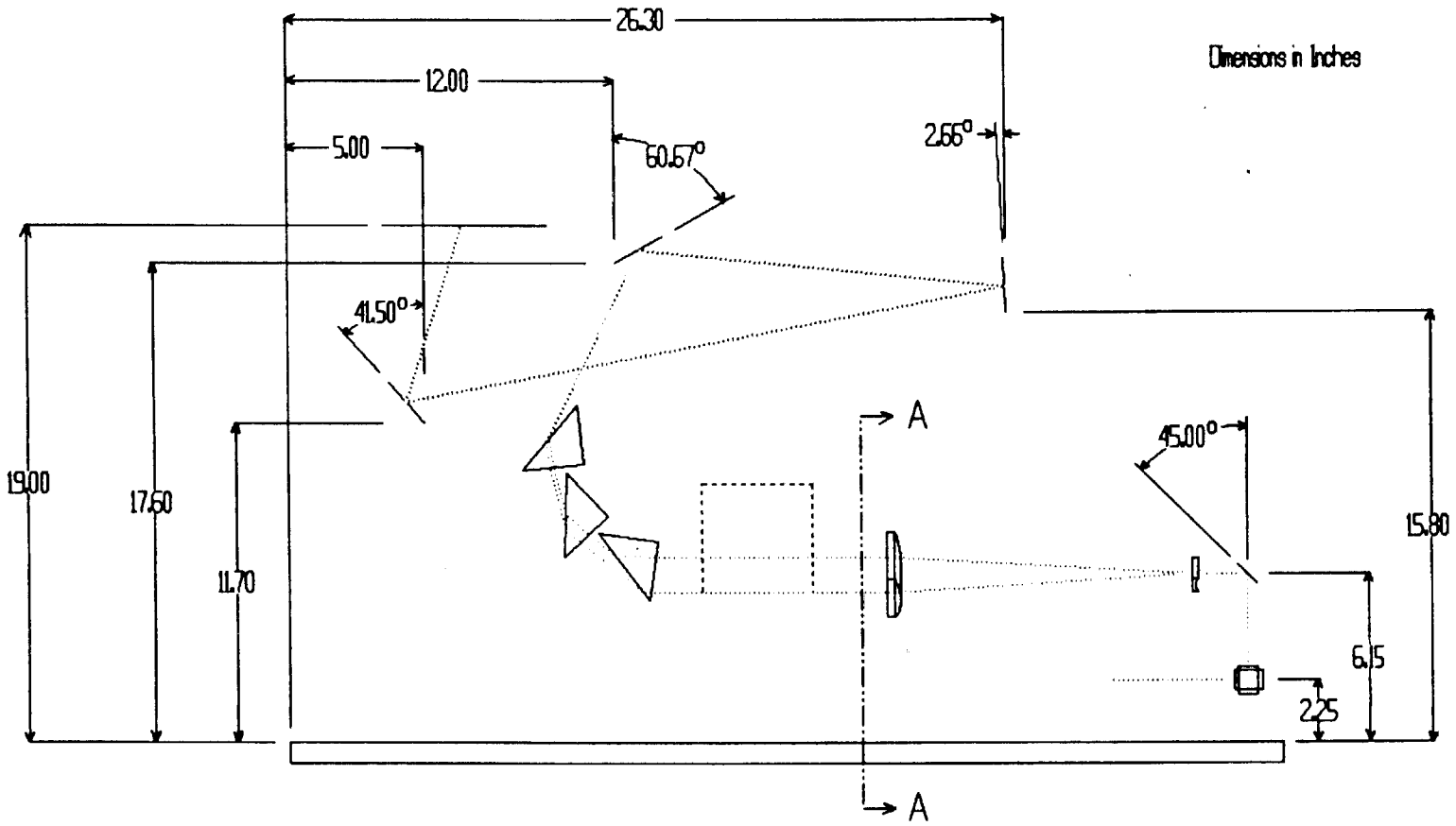

Figure A.4 - Optical System Design, Front View

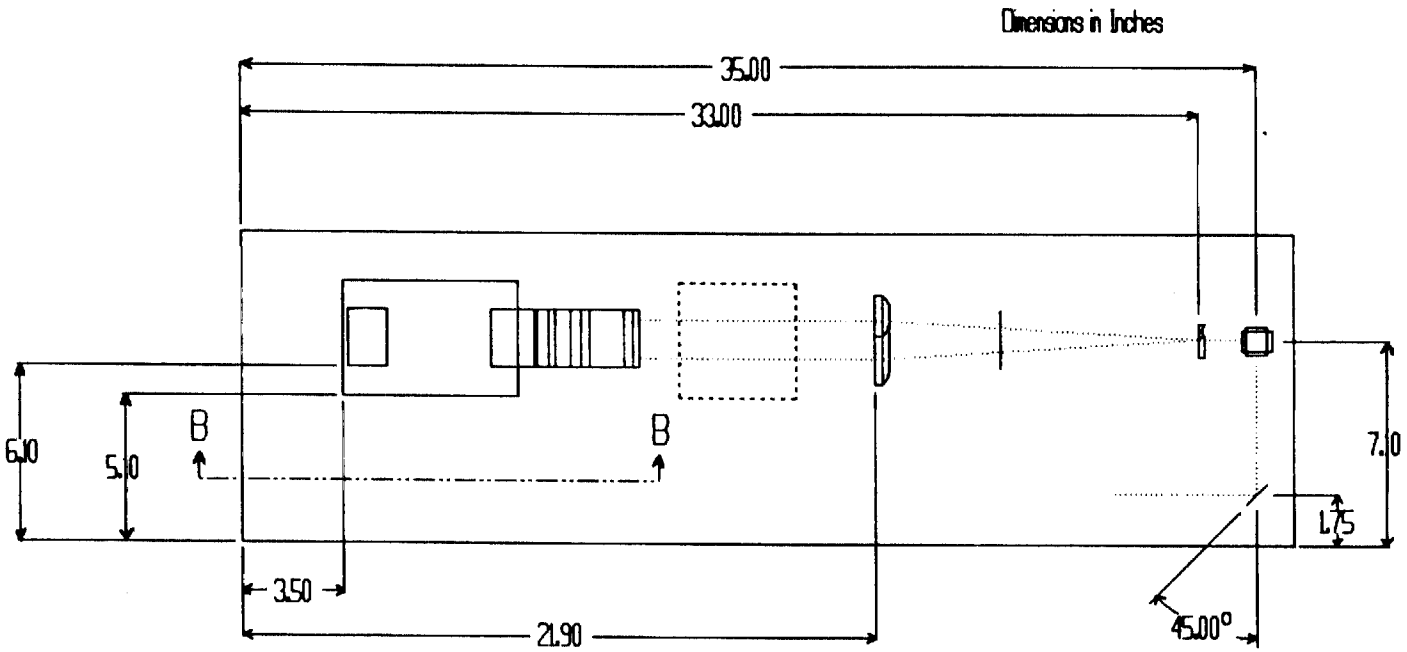

Figure A.5 - Optical System Design, Top View

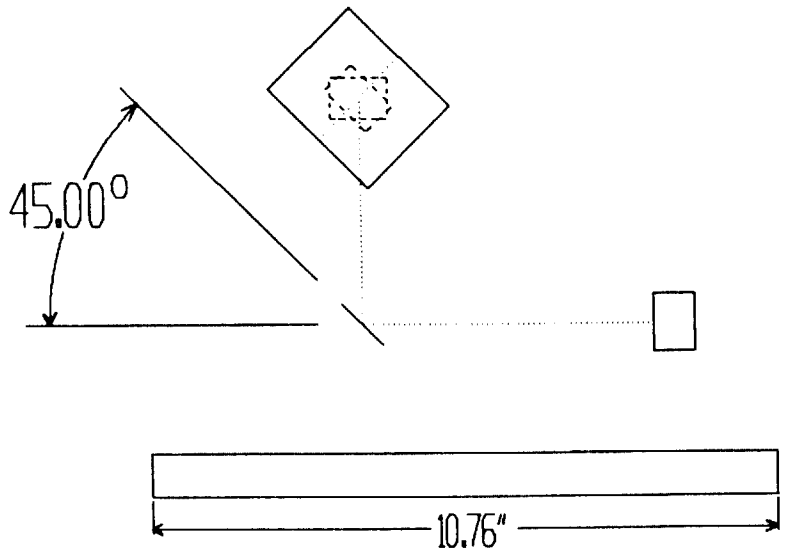

Section A–A

Figure A.6 - Optical System Design, Section A-A

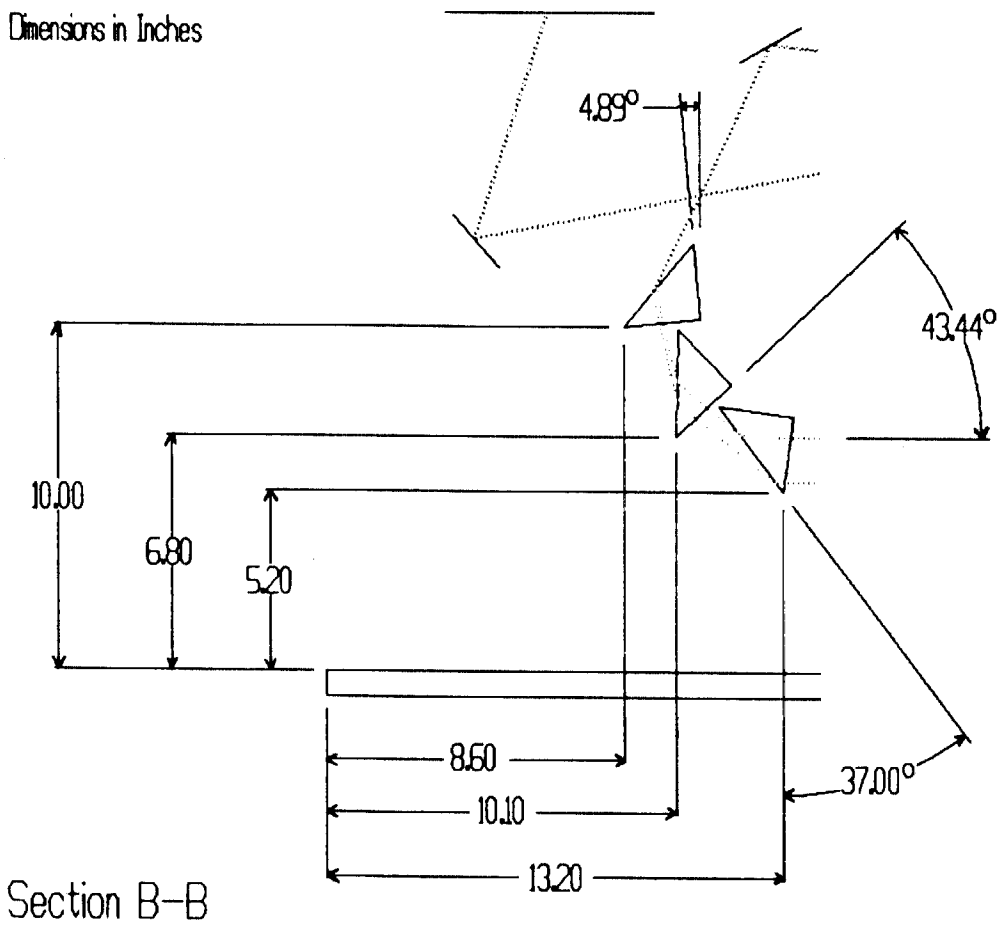

Figure A.7 - Optical System Design, Section B-B

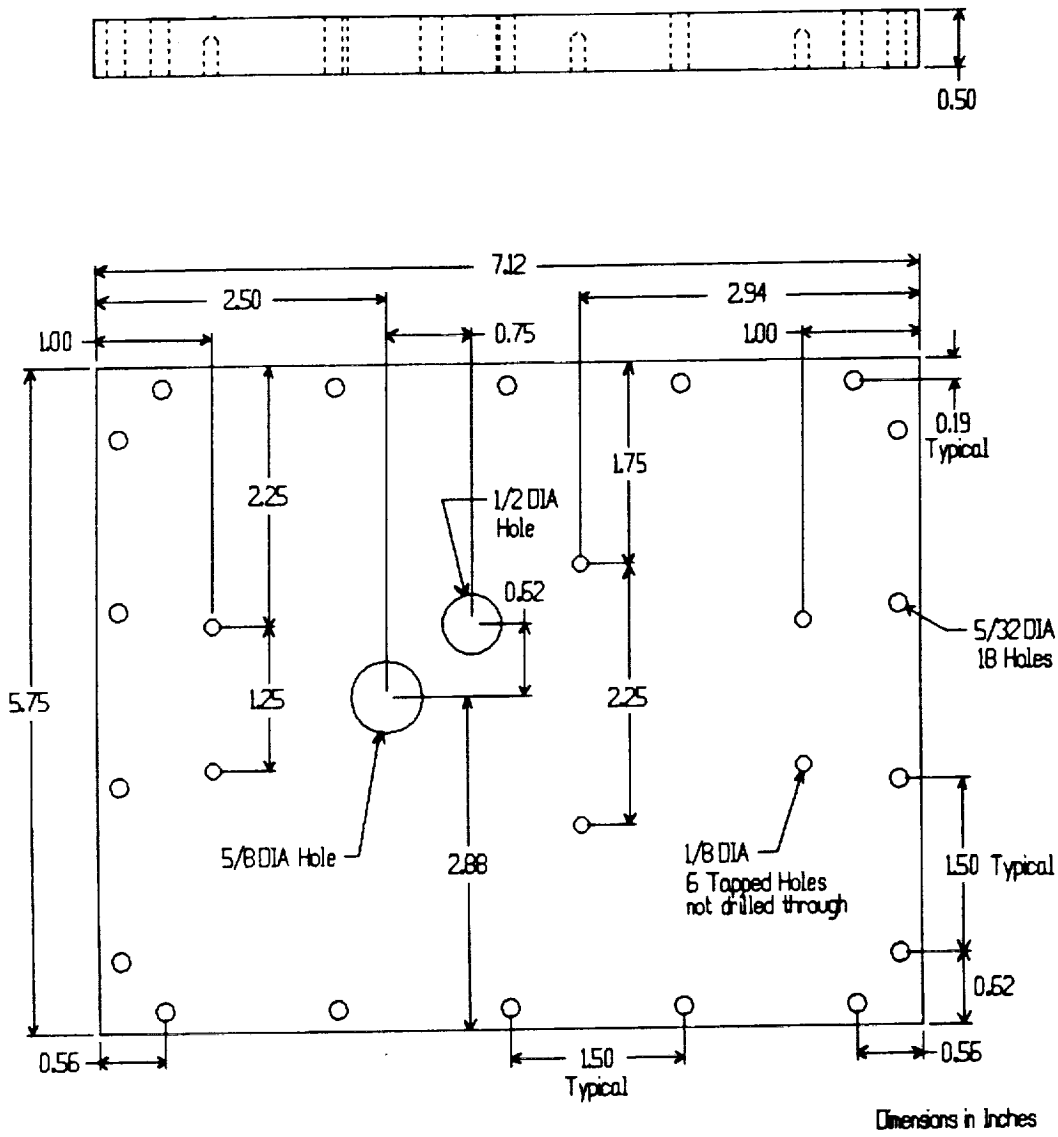

Figure A.8 - Heated Cavity Apparatus, Top Wall

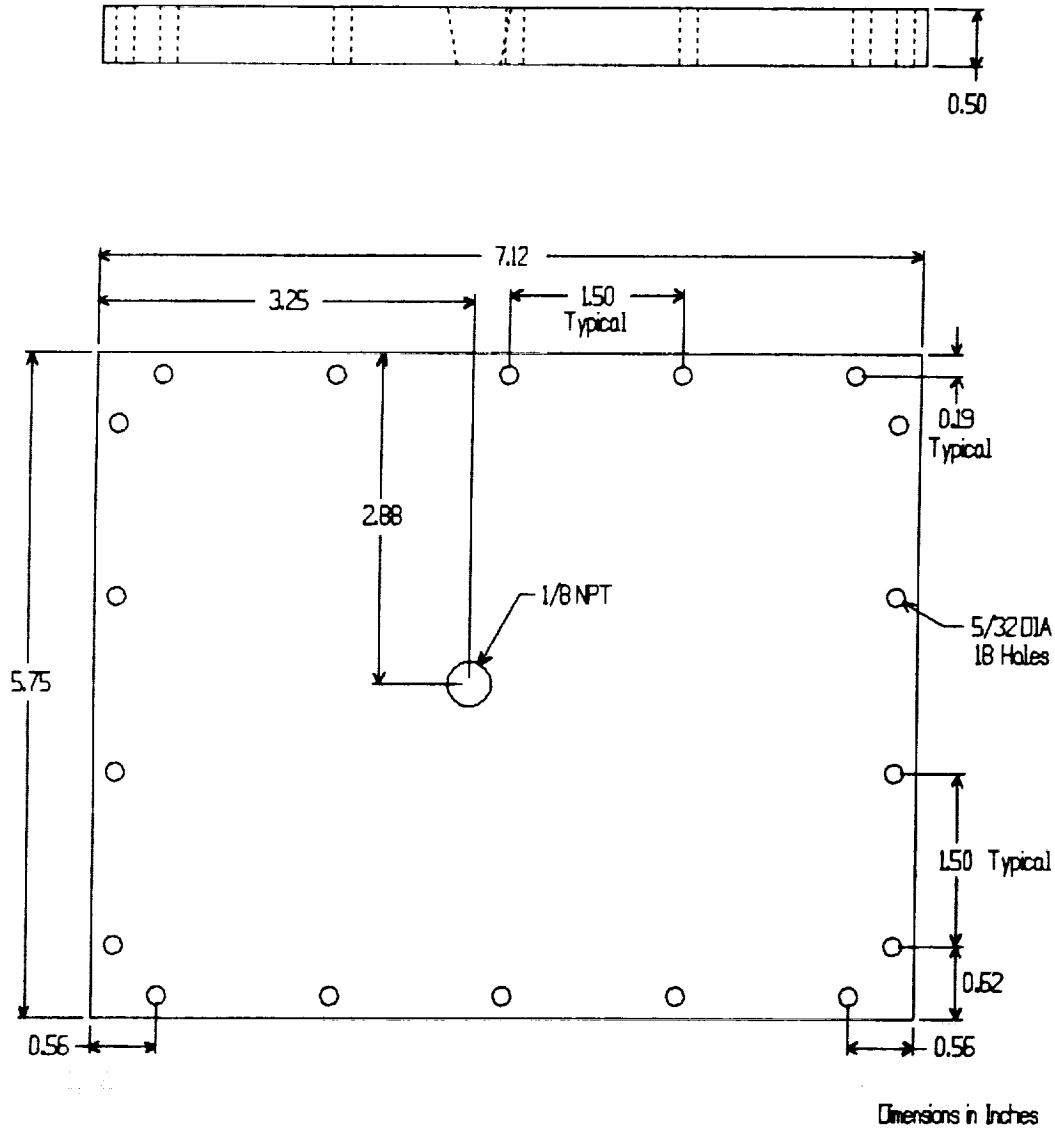

Figure A.9 - Heated Cavity Apparatus, Bottom Wall

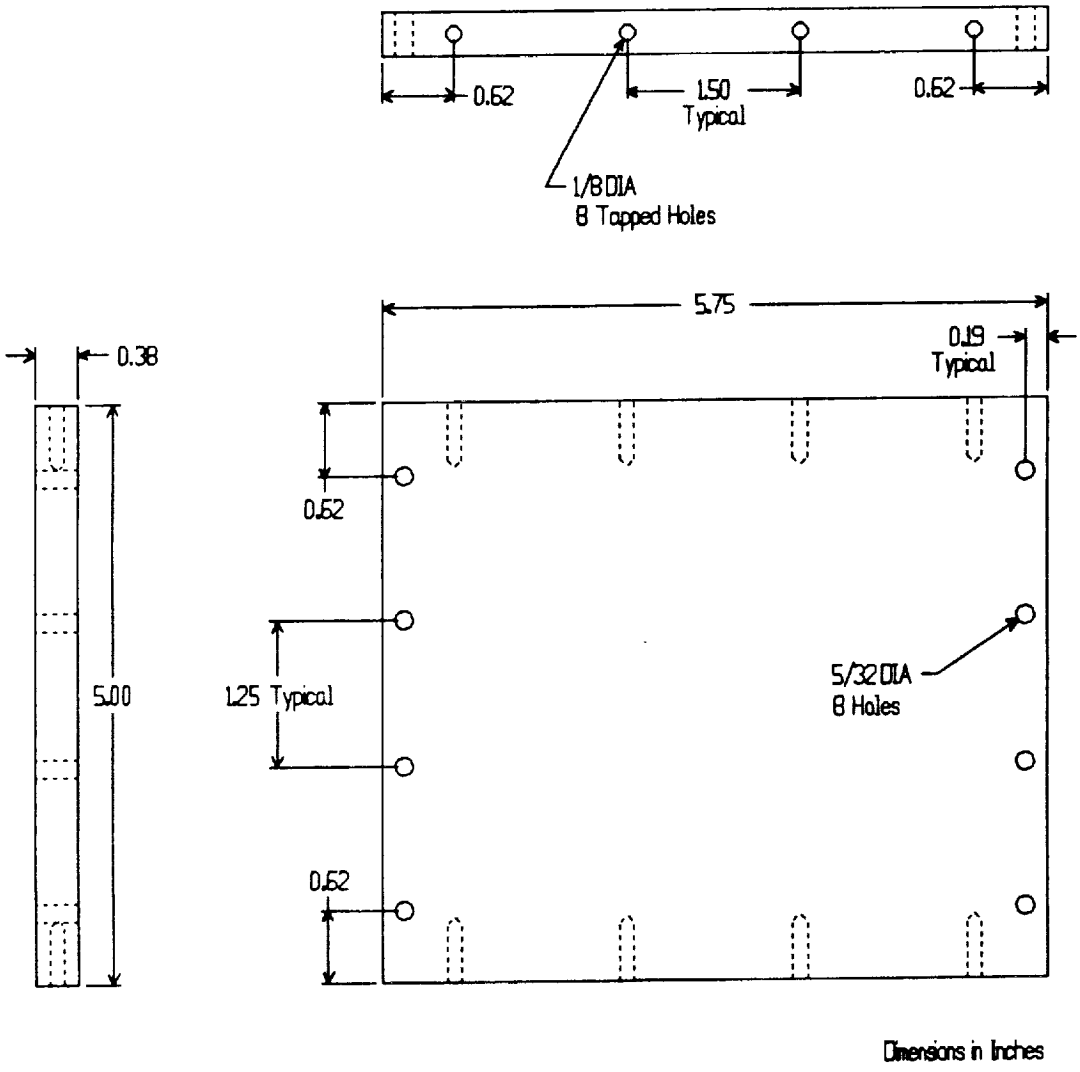

Figure A.10- Heated Cavity Apparatus, Side Wall

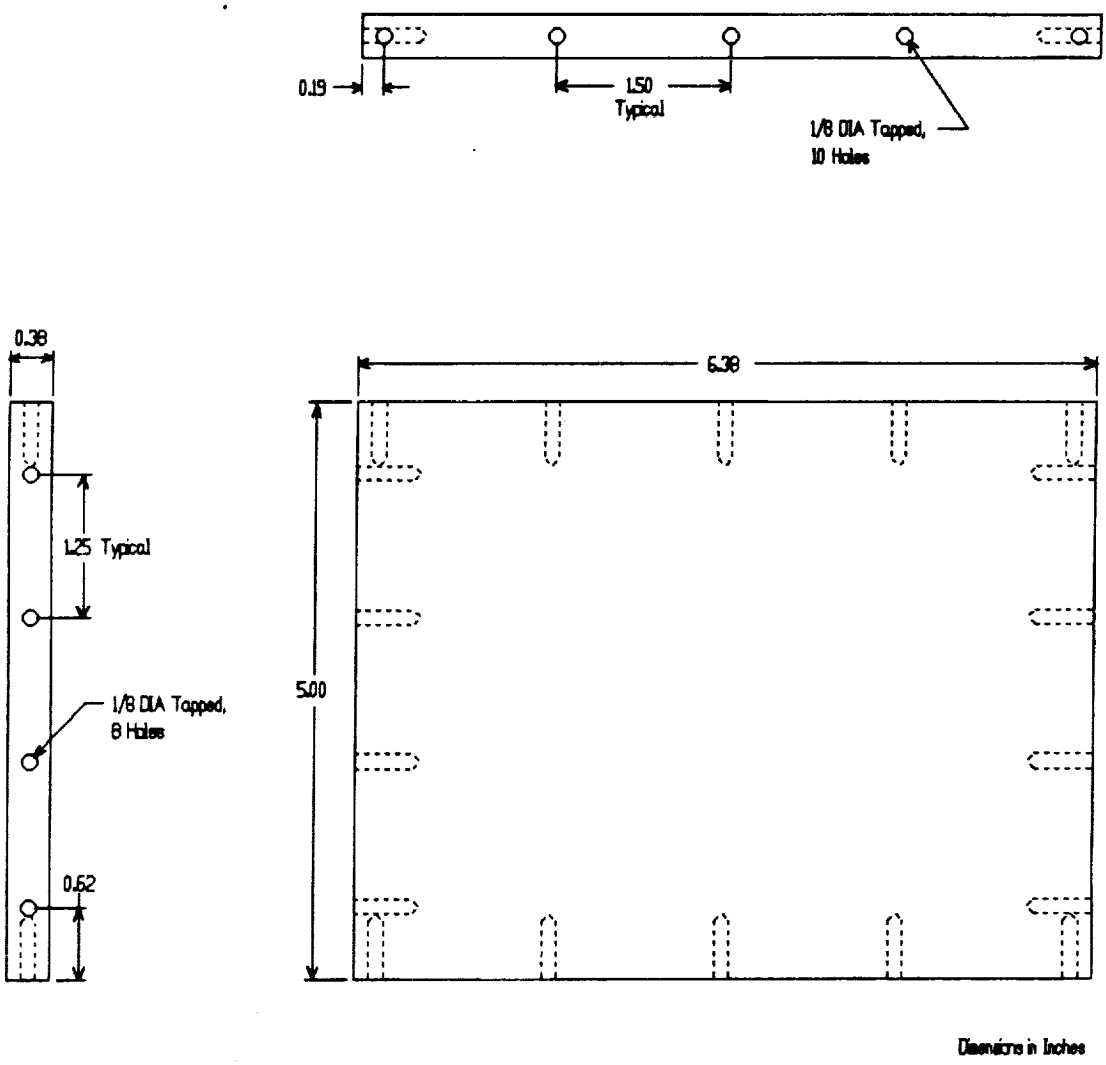

Figure A.11- Heated Cavity Apparatus, Plexiglass Wall

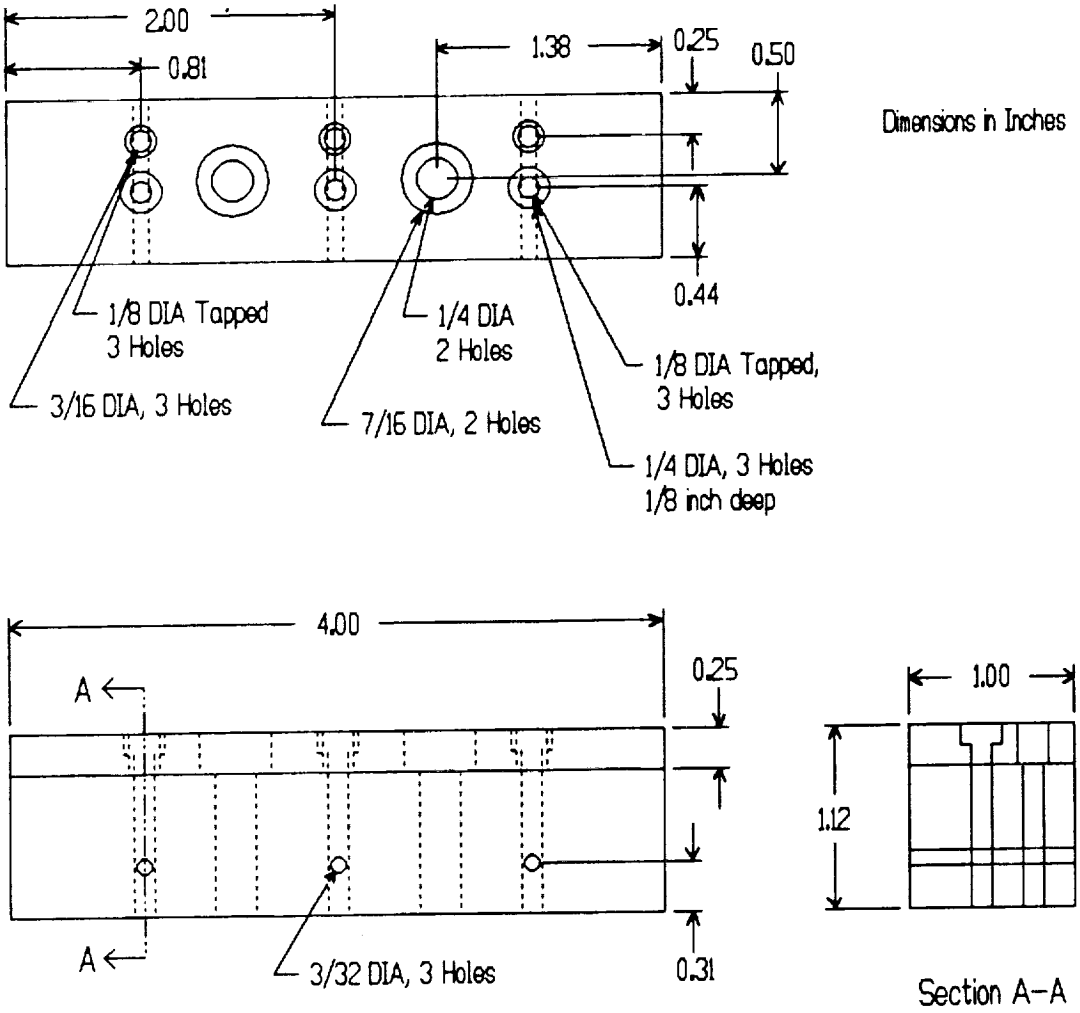

Figure A.12- Heated Cavity Apparatus, Left Busbar

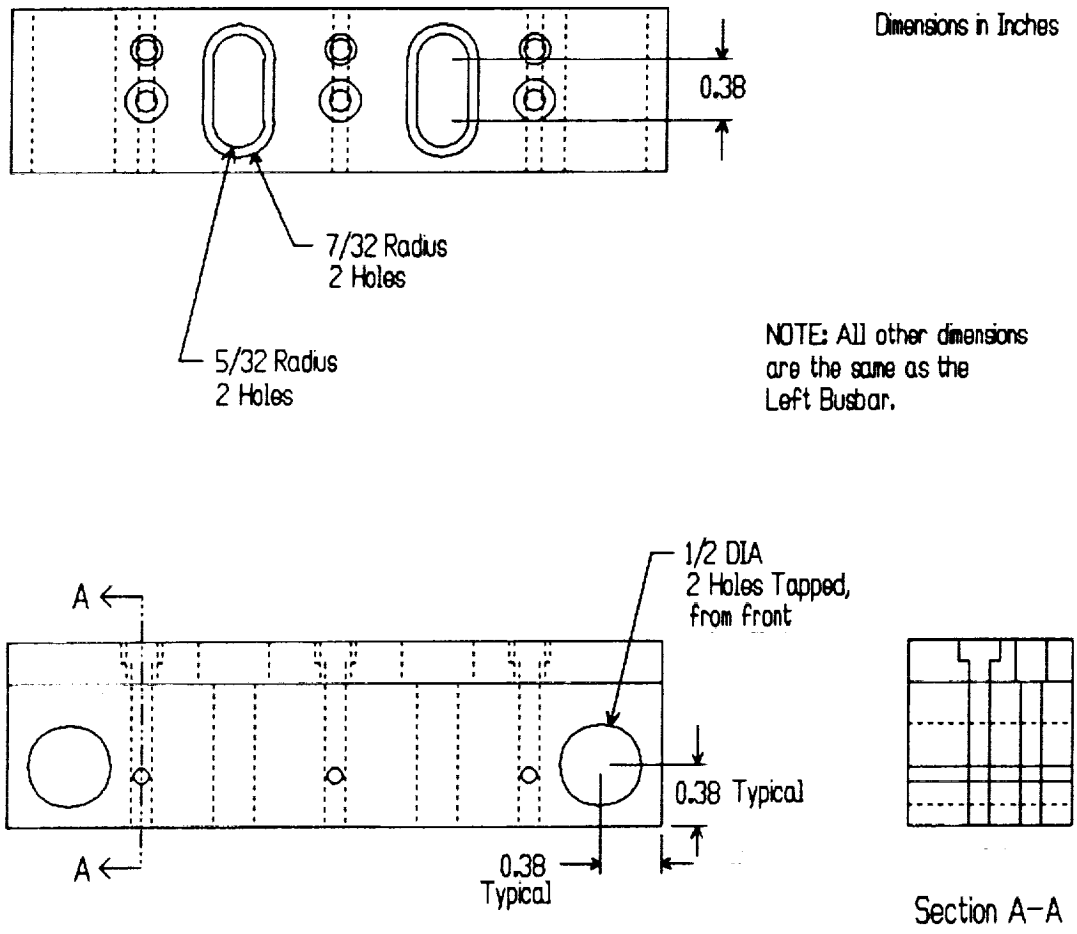

Figure A.13- Heated Cavity Apparatus, Right Busbar

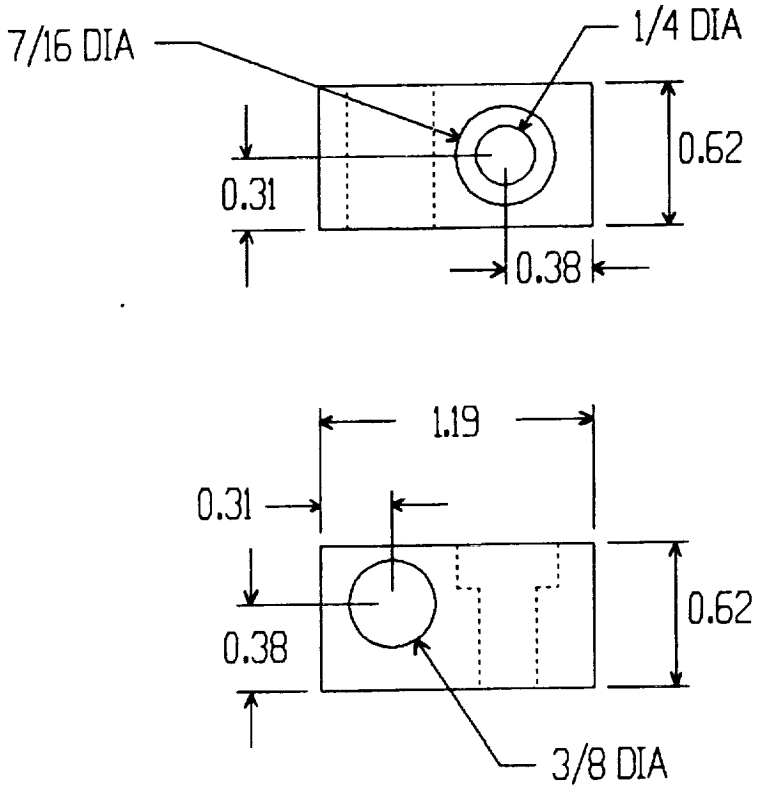

Dimensions in Inches

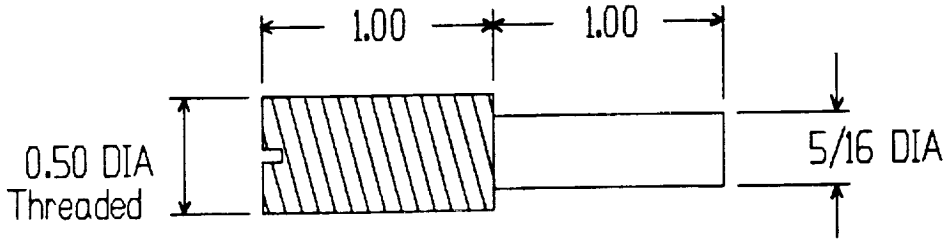

Figure A.14- Heated Cavity Apparatus,Spring Mechanism

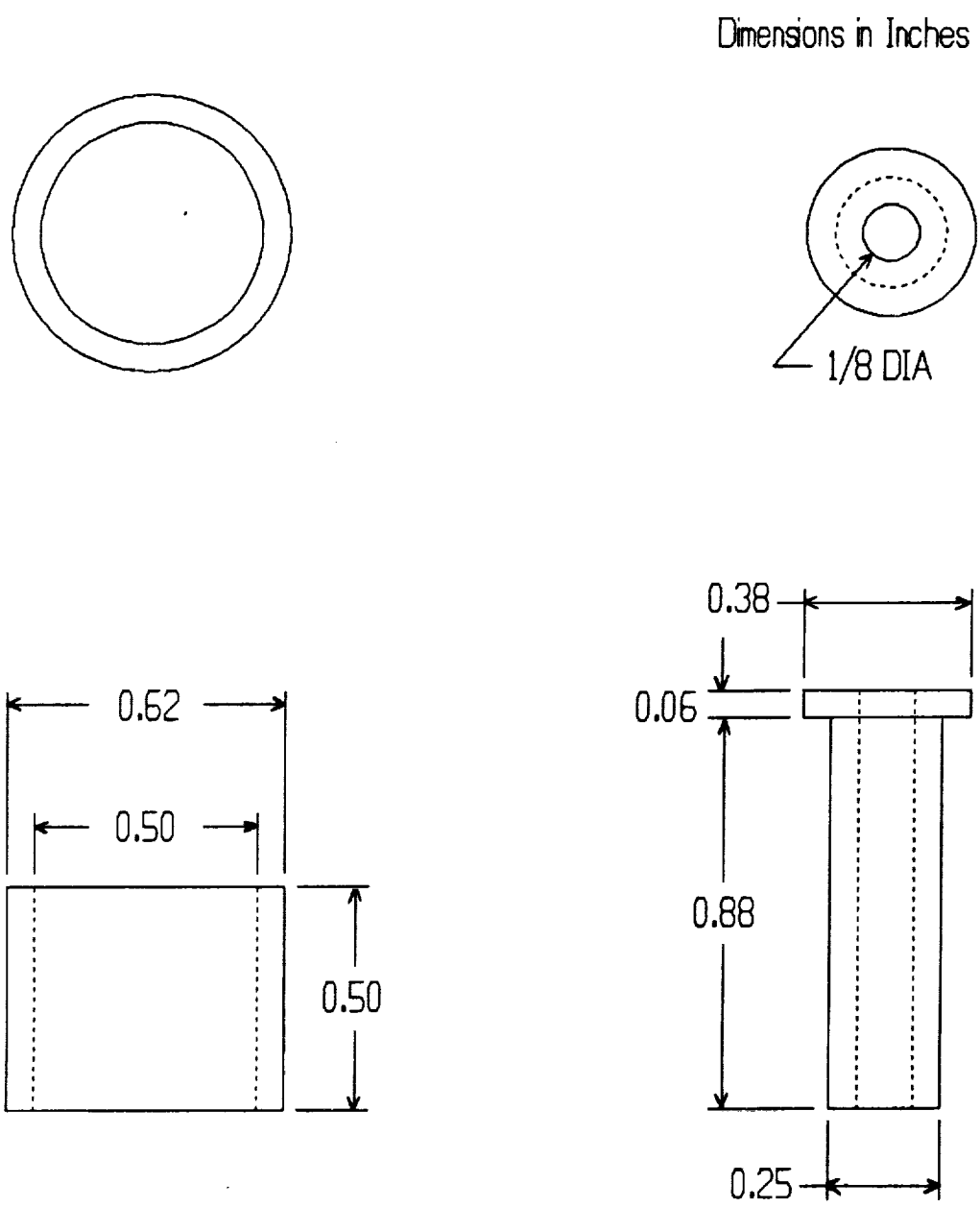

Figure A.15- Heated Cavity Apparatus, Isolators

APPENDIX B

The specifications for selected off-the-shelf hardware that could be used in the flight experiment are given below. These specifications were used in the baseline design.

1) Laser

Supplier: Oriel
Type: 10 mW He-Ne Laser; Model #79274; Includes power supply
Beam Diameter: 0.68 mm @ $1/e^2$
Beam Divergence: 1.2 mrad
Laser Dimensions: length=19.1 inches, diameter=1.75 inches
Power Supply Dimensions: 5.5x5.5x2.5 inches
Cost: $1180

2) Laser Holder

Supplier: Oriel
Type: Precision Vee-Block Laser Base; holds a 1.75 inch diameter laser head; beam will be 2.25 inches above laser base
Dimensions: 5.5x3.0 inch base
Cost: $236

3) Beam Expander System

Supplier: Oriel
Components:
a) Input lens model #15940, focal length=16 mm
b) Beam expander model #15900, focal length=80 mm
c) Laser Mounting Adapter #16140
Description: Provides 5x magnification
Dimension: length=4.0 inches, diameter=2.0 inches
Cost: $475

4) Optical Components

Supplier: Melles Griot
Components:
a) cylindrical lens #01LCP137, focal length=300 mm
b) cylindrical lens #01LCN125, focal length=-19 mm
c) prisms (qty 3) #01PRS037/066

Description of Prisms: Right angle prisms with 3 sides of length 55 mm and hypotenuse of length 77.8 mm. Includes MgF2 coating for hypotenuse and sides opposite hypotenuse.
Cost: a) $ 363, b) $ 210, c) $329 per prism

5) Data Logger
Supplier: Campbell Scientific
Type: Data Logger model CR10
Description: An example of capability -- can read 12 thermocouples and reference and one pressure transducer and store the values about 5 times per second.
Dimensions: 9.0x3.5x2.9 inches
Weight: 2 pounds
Cost: $1530

6) Data Storage Module
Supplier: Campbell Scientific
Type: Data Storage Module Model SM716
Description: Can store 358,000 data values
Dimensions: 7.8x3.5x1.5 inches
Weight: 2 pounds
Cost: $990

7) Video Camera
Supplier: Canon
Type: Canon E06 8 mm Video Camera
Dimensions: 3.75x9.7x3.9 inches
Weight: 2.5 pounds
Cost: $1300

APPENDIX C

The temperature profile can be adjusted by an alternative method. Here T_c is determined from an energy balance between the thermal boundary layer and the core region where it is assumed that air at the edge of the thermal boundary layer flows into the core region at the average core temperature. This yields

$$T_c = \frac{\left[\rho_0 + \frac{\gamma}{2}(\rho_c - \rho_0)\right]}{\left[\rho_c - \frac{\gamma}{2}(\rho_c - \rho_0)\right]} T_0 \qquad (C.1)$$

where ρ_c is the density of the core at the time of interest. Conservation of mass yields ρ_c as

$$\rho_c = \rho_0 + (\rho_0 - \rho_b)\frac{y_b}{(H + H_{ex} - y_b)} \qquad (C.2)$$

The average density of the thermal boundary is

$$\rho_b = \frac{1}{R}\int_0^{y_b} \frac{P}{T_a}\, dy \qquad (C.3)$$

Equation (C.3) is solved numerically using the measured pressure and the adjusted temperature profile and the gas constant, R. Equations (28), (C.1), (C.2) and (C.3) can be solved by iteration to give the adjusted temperature profiles and the core temperature. The adjusted temperature profiles, using this energy balance method, are shown in Figures C.1 through C.4.

The gauge pressure calculated from these adjusted temperature profiles is compared with the measured gauge pressure and is shown in Figures C.5 through C.8. The discrepancy between the measured and calculated pressure at times above 2 seconds may be due to the underestimation of the core temperature. Note that the temperature profiles in Figures C.1 through C.4 are only slightly different from those in Figures IV.20 through IV.23. This indicates that small changes in the core temperature result in large changes in pressure. The largest difference in the core temperature occurs at 10.0 seconds after the initiation of heating. The core

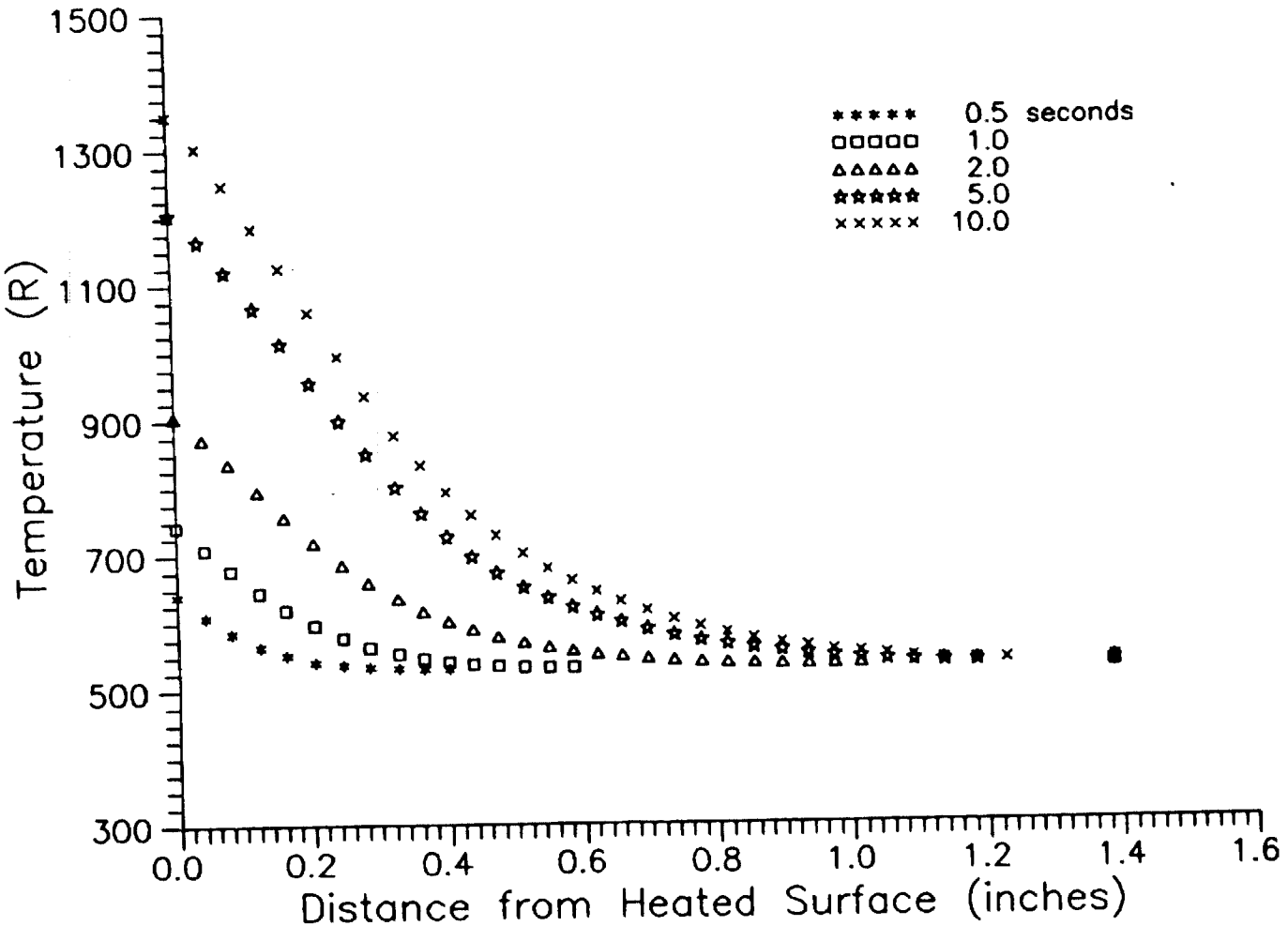

Figure C.1 - Corrected Temperature as a Function of Distance from the Heated Wall for Low Power, Energy Balance Method

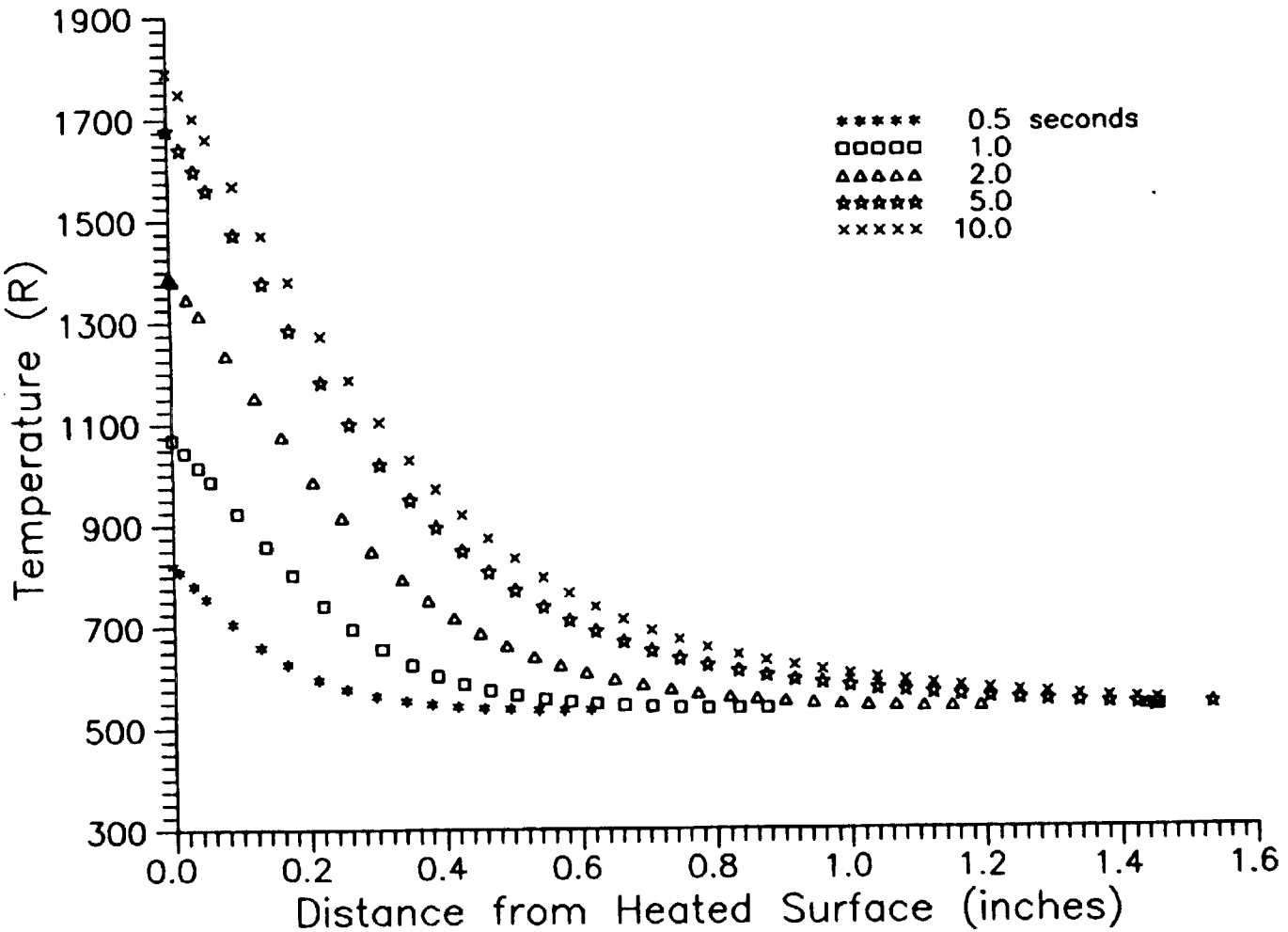

Figure C.2 - Corrected Temperature as a Function of Distance from the Heated Wall for Medium Low Power, Energy Balance Method

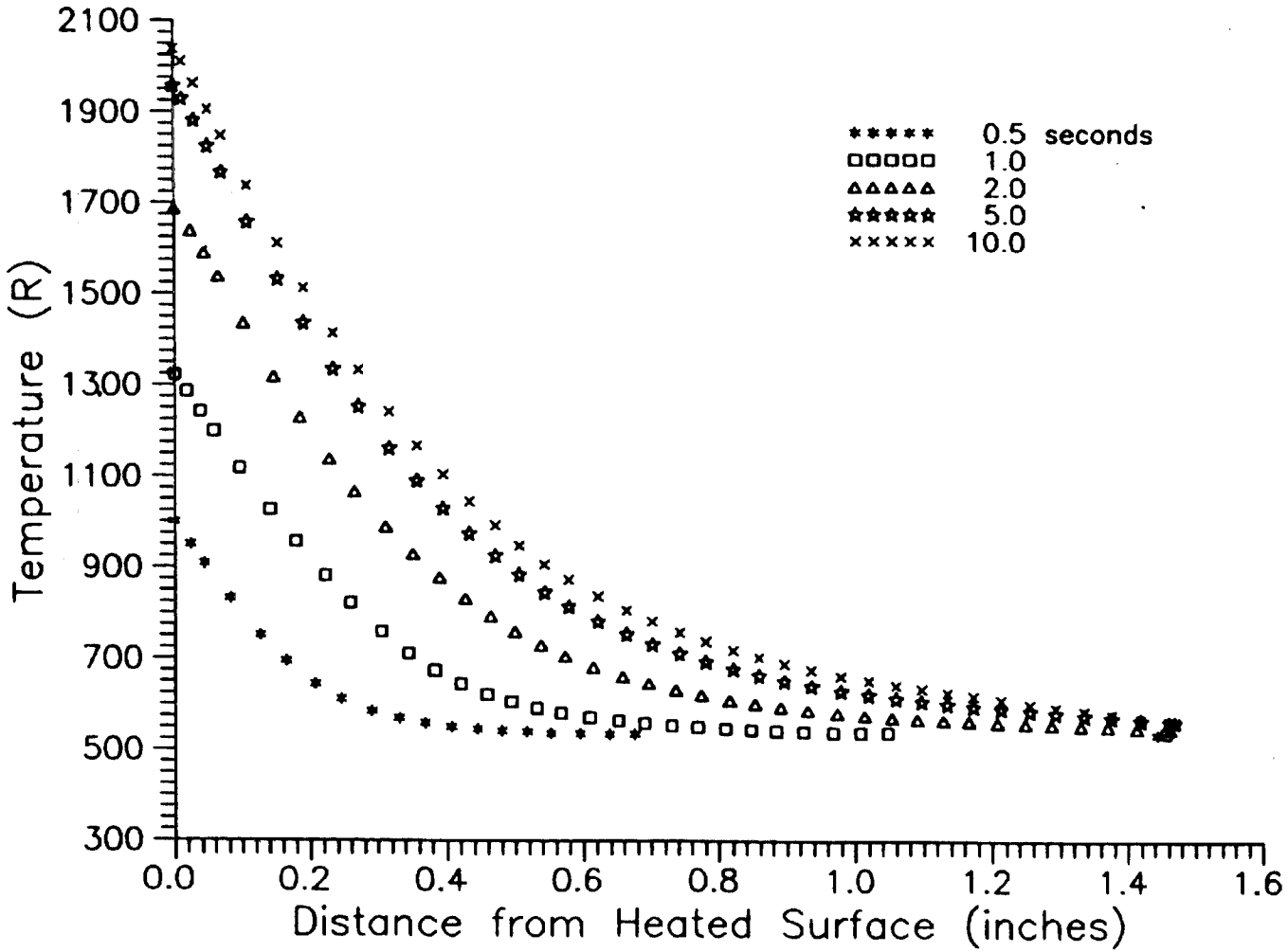

Figure C.3 - Corrected Temperature as a Function of Distance from the Heated Wall for Medium High Power, Energy Balance Method

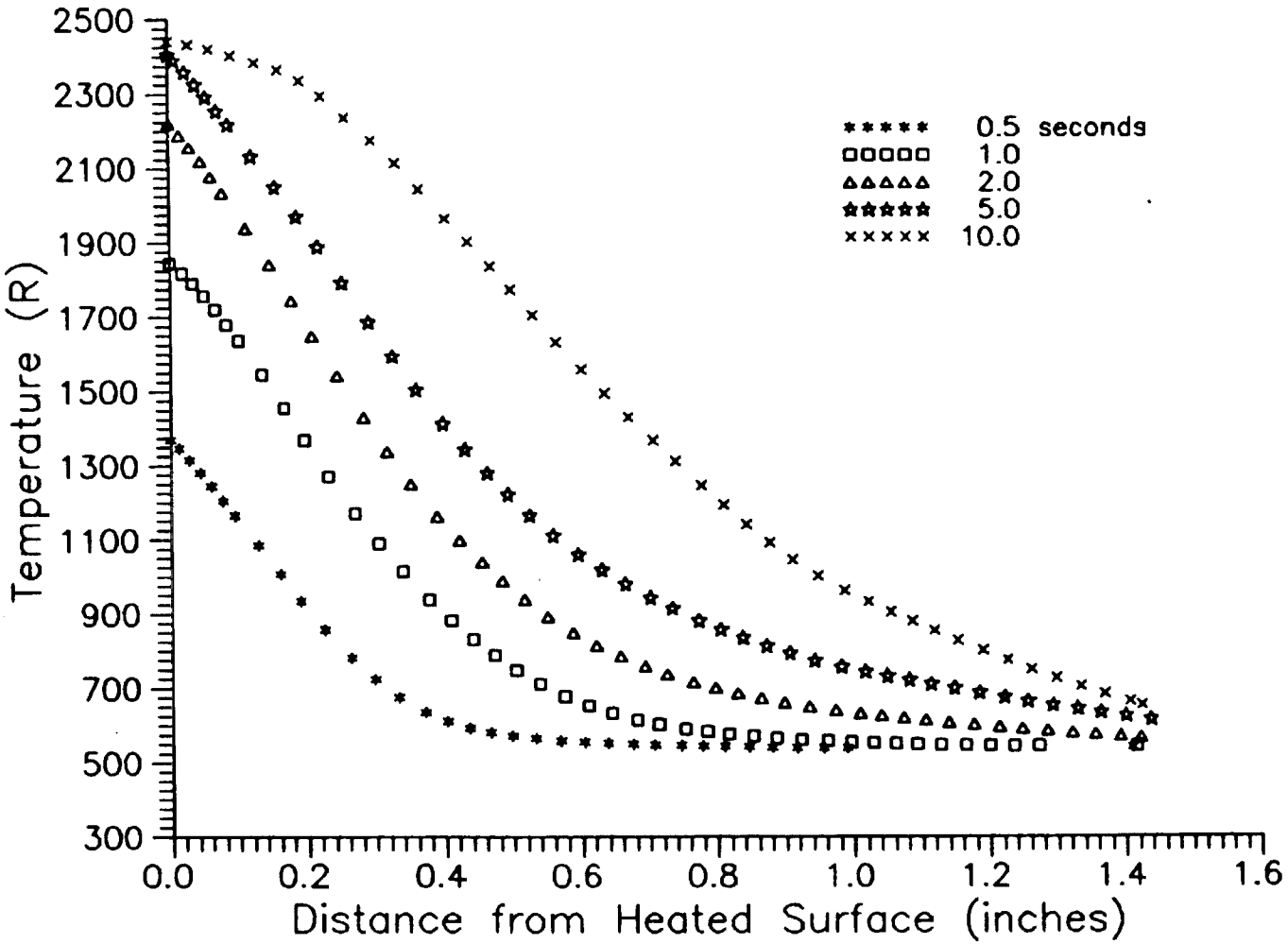

Figure C.4 - Corrected Temperature as a Function of Distance from the Heated Wall for High Power, Energy Balance Method

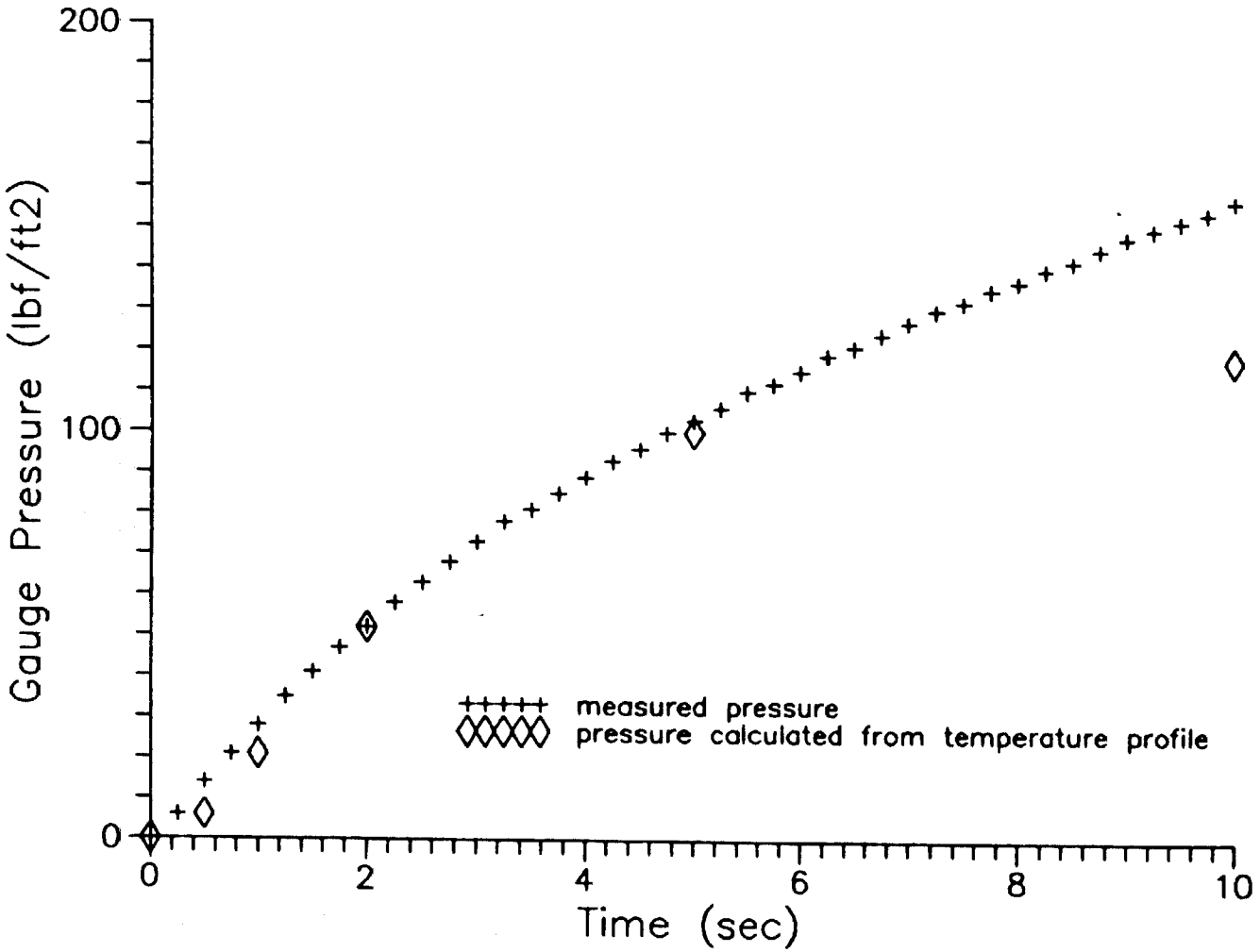

Figure C.5 - Pressure as a Function of Time for Low Power

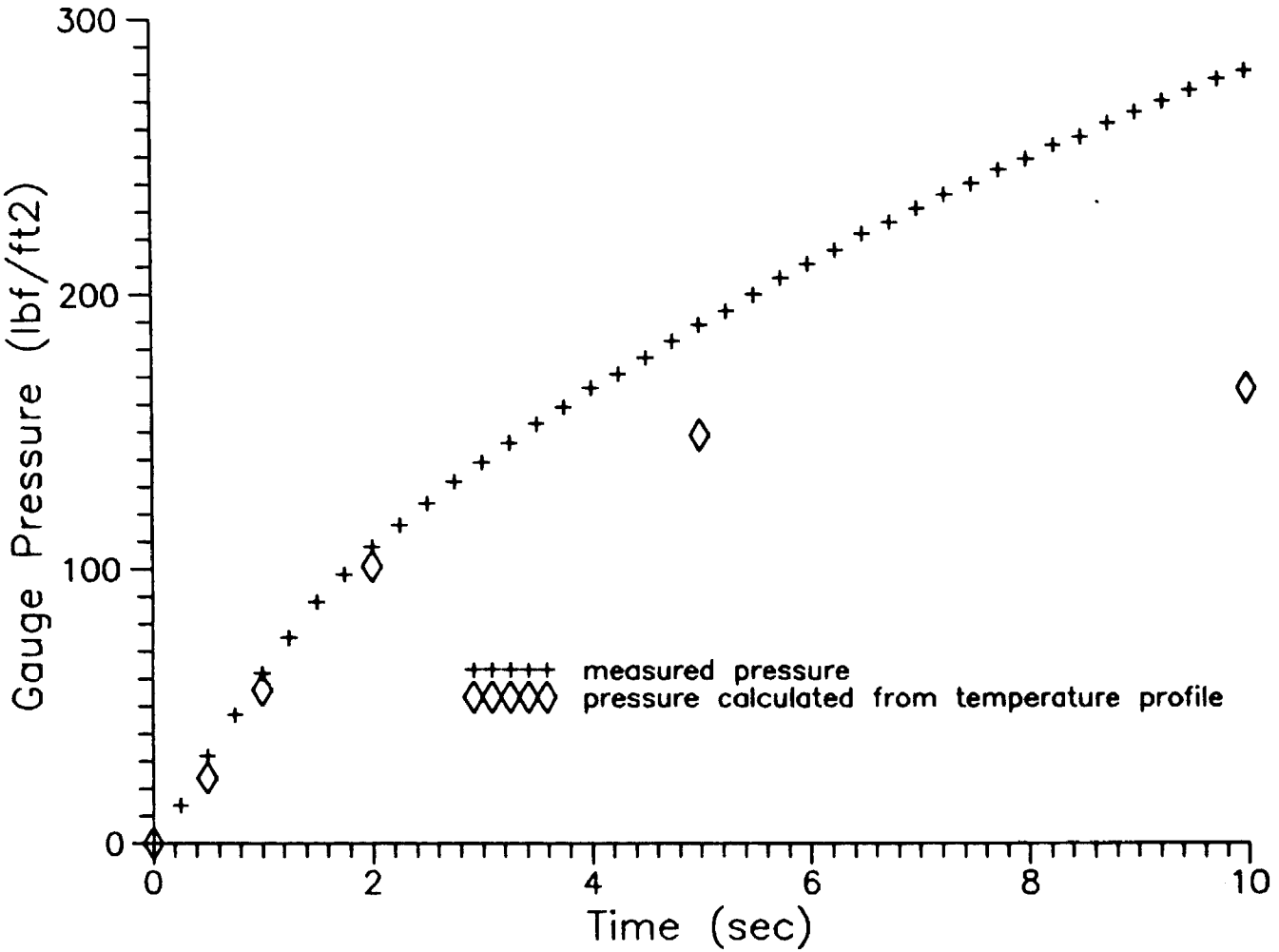

Figure C.6 - Pressure as a Function of Time for Medium Low Power

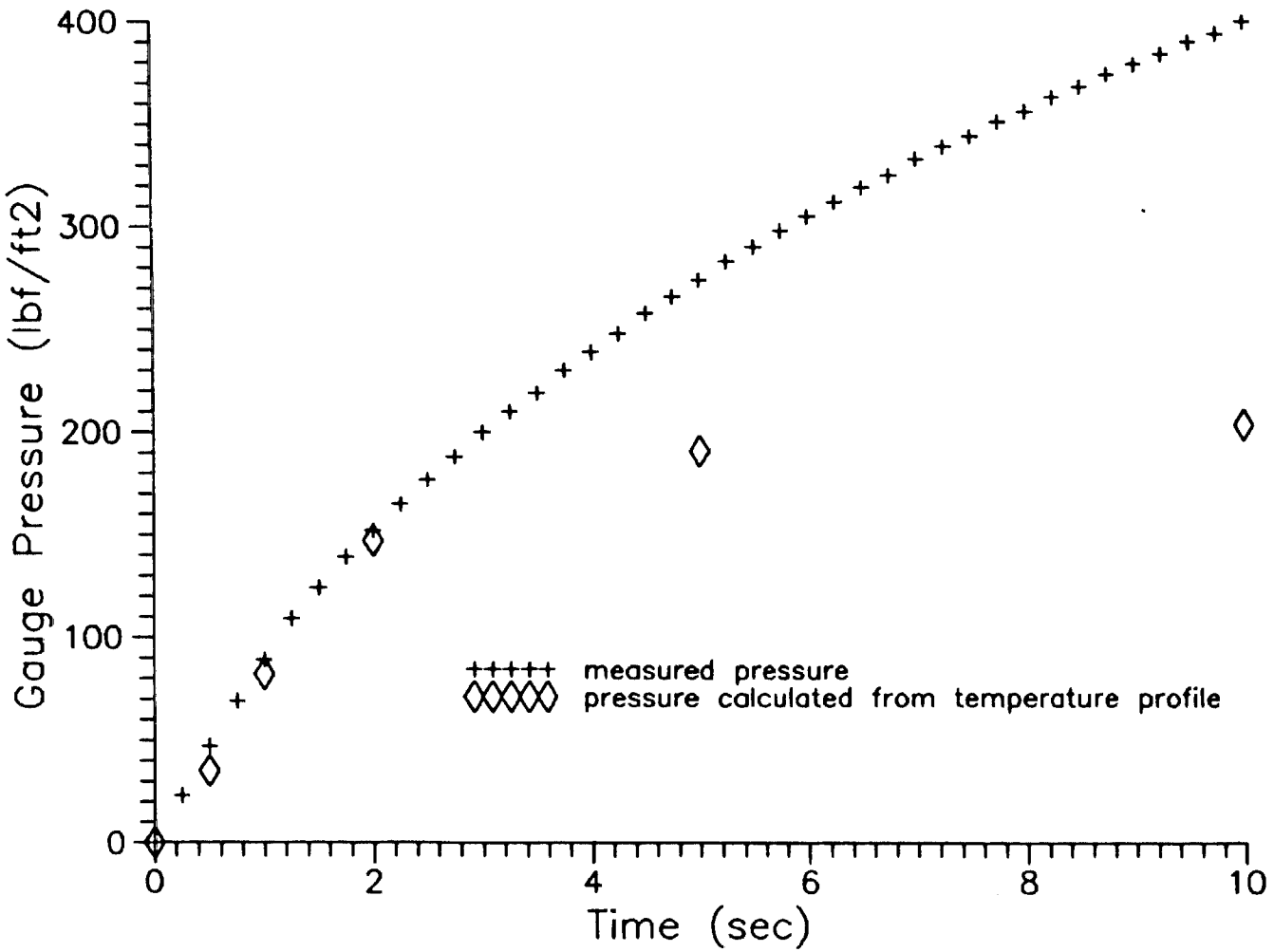

Figure C.7 - Pressure as a Function of Time for Medium High Power

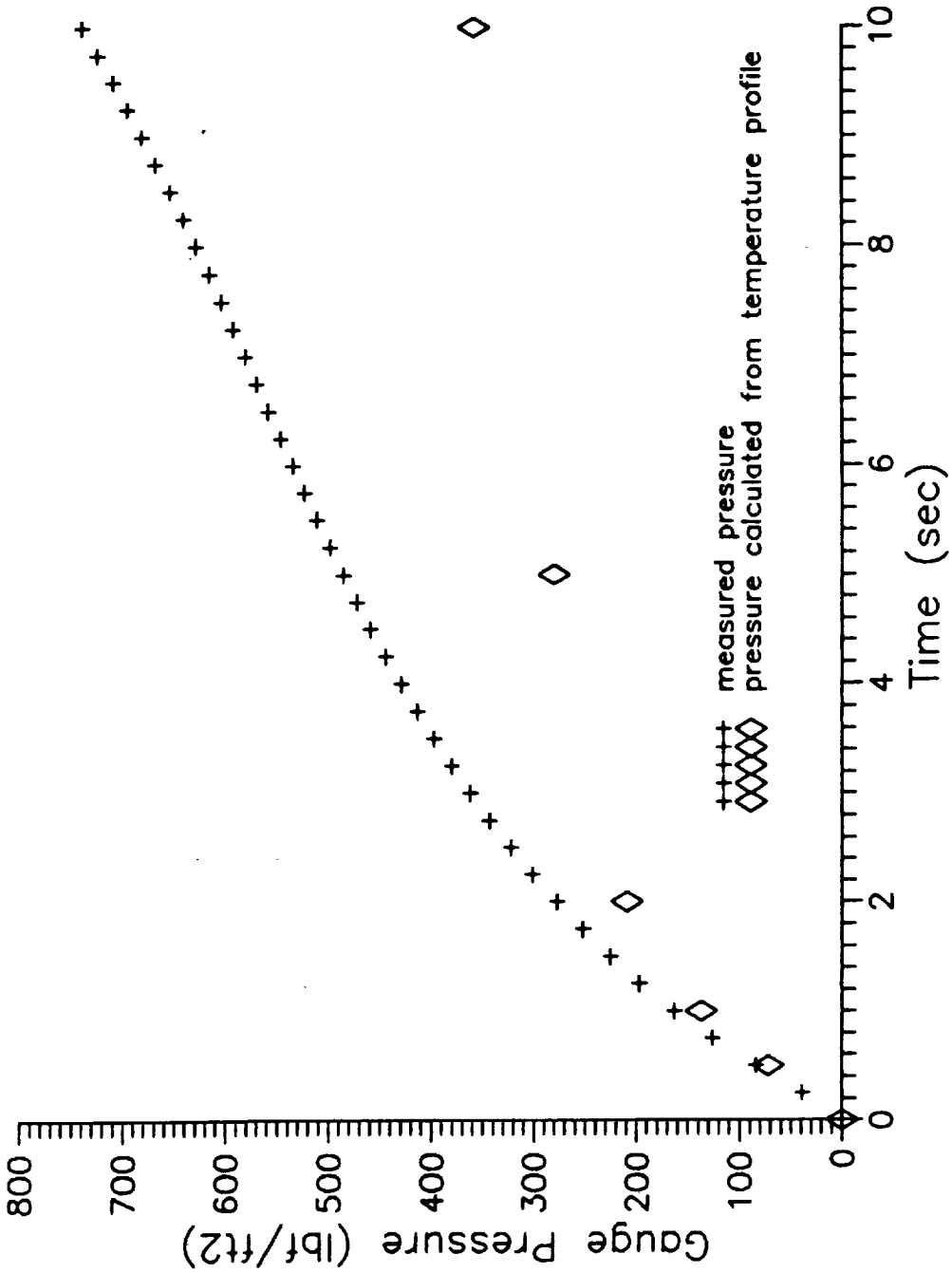

Figure C.8 - Pressure as a Function of Time for High Power

temperature difference as a percent of the total temperature rise is 1.2, 2.2, 3.3, and 4.8 percent for low, medium low, medium high and high power levels, respectively.

NASA
National Aeronautics and Space Administration

Report Documentation Page

1. Report No.	2. Government Accession No.	3. Recipient's Catalog No.
NASA CR-187070		

4. Title and Subtitle	5. Report Date
In-Space Experiment on Thermoacoustic Convection Heat Transfer Phenomenon-Experiment Definition	February 1991
	6. Performing Organization Code

7. Author(s)	8. Performing Organization Report No.
M. Parang and D.S. Crocker	None
	10. Work Unit No. 506-48-4A

9. Performing Organization Name and Address	11. Contract or Grant No.
The University of Tennessee Mechanical and Aerospace Engineering Department Knoxville, Tennessee 37996-2210	NAS3-25359
	13. Type of Report and Period Covered Contractor Report Final

12. Sponsoring Agency Name and Address	14. Sponsoring Agency Code
National Aeronautics and Space Administration Lewis Research Center Cleveland, Ohio 44135-3191	

15. Supplementary Notes

Project Manager, An-Ti Chai, Space Experiments Division, NASA Lewis Research Center. Responsible person, An-Ti Chai, (216) 433-2073.

16. Abstract

The definition phase of an in-space experiment in thermoacoustic convection (TAC) heat transfer phenomenon is completed and the results are presented and discussed in some detail in this report. Background information, application and potential importance of TAC in heat transfer processes are discussed with particular focus on application in cryogenic fluid handling and storage in microgravity space environment. This report also includes discussion on TAC space experiment objectives, results of ground support experiments, hardware information, and technical specifications and drawings. The future plans and a schedule for the development of experiment hardware (Phase B) and flight tests and post-flight analysis (Phase C/D) are also presented in the report. The specific experimental objectives are rapid heating of a compressible fluid and the measurement of fluid temperature and pressure and the recording and analysis of the experimental data for the establishment of the importance of TAC heat transfer process. The ground experiments that were completed in support of the experiment definition included fluid temperature measurement by a modified shadowgraph method, surface temperature measurement by thermocouples, and fluid pressure measurements by strain-gage pressure transducers. These experiments verified the feasibility of the TAC in-space experiment, established the relevance and accuracy of the experimental results, and specified the nature of the analysis which will be carried out in the post-flight phase of the project.

17. Key Words (Suggested by Author(s))	18. Distribution Statement
Microgravity Thermoacoustic convections Heat transfer	Unclassified – Unlimited Subject Category 34

19. Security Classif. (of this report)	20. Security Classif. (of this page)	21. No. of pages	22. Price*
Unclassified	Unclassified	110	A06

*For sale by the National Technical Information Service, Springfield, Virginia 22161